Dispersion of Fine Sediments in Tides

by

Feng Ye

Submitted to the Department of Civil and Environmental Engineering
in partial fulfillment of the requirements for the degree of

Master of Science in Civil and Environmental Engineering

at the

MASSACHUSETTS INSTITUTE OF TECHNOLOGY

June 1998

Author .....
Department of Civil and Environmental Engineering
May 8, 1998

Certified by 5/15/98
Chiang C. Mei
E. K. Turner Professor of Civil and Environmental Engineering
Thesis Supervisor

Accepted by .....
Joseph M. Sussman
Chairman, Department Committee on Graduate Students

Dispersion of Fine Sediments in Tides

by

Feng Ye

Submitted to the Department of Civil and Environmental Engineering
on May 8, 1998, in partial fulfillment of the
requirements for the degree of
Master of Science in Civil and Environmental Engineering

Abstract

A theory on the dispersion and resuspension of fine particles in the tidal wave boundary layer above the seabed is presented in Part I. The inviscid flow lying atop the bottom boundary layer is nonuniform due to the existence of a peninsula protruding out of the straight coastline. A constant eddy viscosity model is applied to achieve qualitative understanding. The length scale of the peninsula is assumed to be much smaller than the tidal wave length while much greater than the tidal excursion length. First we describe the derivations by Mei & Chian of the mean flow, effective transport equation governing the long time evolution of concentration distribution and the explicit expressions of convection velocity and dispersivity tensor in terms of the general ambient flow. A numerical scheme is developed to solve the convection diffusion equation. Two computational examples are discussed to illustrate the application of our theory: one for an initial release of particle cloud near a semicircular peninsula over a solid bed; the other for the resuspension over an erodible belt emcompassing the peninsula. It is discovered that nonuniformity of the ambient flow and earth rotation play the dominant role in determining the evolution of particle concentration.

In Part II we examine the flow field in a shallow lake forced by a low-frequency wind. Depth variation over space is allowed and a general depth-dependent eddy viscosity considered. Since the lake is quite shallow and wind period very long, it is found that the vertical structure of flow field forms a lot faster than any change of forcing takes place. For this quasi-steady problem we develop a perturbation theory to describe the free surface displacement and the velocity field. It is shown analytically that the leading order flow and the steady streaming do not depend on the horizontal extensions of a constant-depth basin under a uniform wind. Finally, the response in a rectangular lake of flat bottom is discussed in detail. It is seen that the transient effect of surface oscillation overplays the Coriolis effect for the second order flow and the mass transport results from the interaction between the leading order surface motion and oscillatory velocity.

Thesis Supervisor: Chiang C. Mei
Title: E. K. Turner Professor of Civil and Environmental Engineering

Acknowledgement

I take this opportunity to express my gratitude to my advisor, Professor Chiang C. Mei, from whom I have learned not only a lot of knowledge in hydrodynamics, but also the approach and attitude to conduct scientific research. I extremely admire his drive and devotion to engineering science. The door of his office opens towards me whenever I want to have a discussion on my research. Without his guidance and encouragement, this research could never have been done.

I gratefully acknowledge my friends in our group who discussed with me about the contents of the thesis, especially Jie Yu and Zhao Cheng. I would like to thank the professors and other graduate students at the Parsons Lab from whom I have learned a lot and with whom I have had these past three years of happy time.

I am also grateful for the financial support by the US Office of Naval Research through Grant N00014-89-J-3128 and National Science Foundation through Grant CTS 9634120.

Last but not least, my parents and sister's love has always been the source of strength with which I am confident to face any challenge.

Contents

List of Figures

List of Tables

Part I

Dispersion of Fine Particles near a Small Peninsula

Chapter 1

Introduction

Sediment transport has been one of the major topics of coastal engineering for a long time due to its signifance to human life. Under the combined action of coastal waves and currents, particles of various sizes are stirred up from the seabed and then carried around. The accumulative effect of this process results in the evolution of the coastline over time. One problem associated with the adverse influence of the coastal sediment transport is beach erosion; structures and facilities installed on the beach are threatened. Another important issue has been brought up by the marine disposal practices of the coastal cities. Where are we supposed to set up the outfall diffusers so that what we want to dispose of can really be disposed without being flushed back to the beach where people live? The flow field must be first investigated prior to any prediction of the spreading of the suspended particles can be made. It is well known that dispersion are more prominent in a shear flow than in a uniform flow with the same discharge. Since shear is significant inside boundary layer and tides are just common phenomena as a driving agent in the coastal flows, we want to study the transport process of fine particles in a tidal boundary layer above the bottom.

Transport of suspended sediments has been investigated for decades. Following the pioneering work by Taylor (1953) on dispersion in pipe flows, a number of authors have explored dispersion of a neutrally buoyant cloud in a horizontally uniform but oscillatory current. Bowden (1965) studied the horizontal mixing in a tidal current. Holly & Harleman (1965) conducted dye-release experiments in oscillatory pipe flow.

Okubo (1967) then pointed out the dependency of diffusivity on the oscillatory period of the flow. For suspended fine particles, Yasuda (1989) discovered that the dispersion coefficient of particles at the stationary stages is dependent on the settling velocity of the sediments and reaches a maximum value corresponding to a critical fall velocity.

Despite their success in showing many interesting physical courses, these uniform-tide theories are not adequate in predicting the long time evolution of a particulate cloud with a size comparable to the length scale of a coastline feature, in that case the nonuniformity of the ambient flow becomes prominent.

For the mixing and flushing of tidal embayments in the Dutch Wadden Sea, Zimmerman (1976, 1977) argued that that the large diffusivity ($100 - 1000\,\mathrm{m}^2/\mathrm{s}$) is due to horizontal mixing in a spatially nonuniform flow. His work caused scientists' attention upon the effect of horizontal variation of topography (shore configuration) on mass transport. Two approaches have been adopted to model dispersion in nonuniform tides: 1) Based on the estimated depth-averaged flow, the trajectories of a large number of marked fluid particles are computed numerically. A few works followed this Euler-Lagrangian method (Zimmerman, 1986; Awaji *et al*, 1980; and Signell & Geyer, 1990). 2) The second approach is an Eulerian approach. Young *et al* (1982) studied an idealized flow field with simple dependence on spatial coordinates and sinusoidal dependence in time. The three dimensional convective diffusion problem was solved to enable the calculation of the effective horizontal diffusivity. In our research we will take the Eulerian approach.

As for the proper form of the eddy vicosity, Sleath (1990) reviewed many depth-dependent models for gravity waves and Soulsby (1990) for tidal currents. In addition, the latter (see Soulsby, 1990, p 531) provided sketches showing that despite the varieties (constant, linear, parabolic, exponential), the resulting first-order velocity profiles do not differ qualitatively. To achieve physical understanding with simple algebra, we shall follow Sverdrup (1927), Mofjeld (1980), Kundu *et al* (1981) and Fang and Ichiye (1983) and choose the simplest model of constant eddy with no-slip boundary at the seabed.

It is our goal here to examine dispersion of fine sediments in tidal flows affected

strongly by nonuniformities due to coastline feature. In Chian (1993) and in an unpublished paper by Mei & Chian (1994) an analytical theory has been worked out for the mean flow and the dispersion equation for suspended sediments. After some revisions of their formulas, an effective numerical scheme is developed here for guantitative computations. The length scale of the peninsula is assumed to be much smaller than the tidal wave length while much greater than the tidal excursion length. In Chapter 2 we first present the solutions of the leading order oscillatory boundary layer flow and the mean flow at the second order, and then effective transport equation governing the long time evolution of concentration distribution with the explicit expressions of convection velocity and the spartially dependent dispersivity tensor in terms of the general ambient flow. A numerical scheme is developed in Chapter 3 to solve the convection diffusion equation. ADI method is applied along with boundary conditions of second order accuracy with respect to the time step and mesh density. Two computational examples are discussed in Chapter 4 and 5, respectively, to illustrate the application of our theory: one for an initial release of particle cloud near a semicircular peninsula over a solid bed; the other for the resuspension over an erodible belt emcompassing the peninsula. It is discovered through this research that nonuniformity of the ambient flow and earth rotation play the dominant role in determining the evolution of particle concentration. The analysis is an extension to our earlier works on gravity waves over a nonerodible seabed (Mei & Chian, 1994) and an erodible seabed (Mei , Fan & Jin 1997), without Coriolis effects.

Chapter 2

Mathematical Formulation

Transport of suspended sediments in coastal waters near a small peninsula is considered. The Eulerian approach is used to study dispersion in tidal flows affected strongly by nonuniformities due to coastal topography. We first find the flow field in order to study the transport of particles in the tidal wave boundary layer. Besides the obvious periodic tidal wave oscillation, a steady streaming is generated as a result of nonlinear terms.

2.1 Tidal wave boundary layer flow

Our main assumptions are as follows. The topographical length scale is assumed to be greater than the tidal excursion length, so that flow separation is not important. Let h denote the sea depth, r_o the horizontal size of the coastal topography, A the typical tide amplituide, ω the tidal frequency, and $\mathcal{U} \sim A\sqrt{gh}/h$ the typical horizontal flow velocity. Just above the sea bed, an oscillatory Ekman boundary layer of the thickness $\delta = O(\sqrt{\nu_e/\omega})$ is expected to develop, where ν_e denotes the eddy viscosity of momentum. The various scales involved in this problem are assumed to satisfy the following constraints:

$$\epsilon \equiv \frac{\mathcal{U}}{\omega r_o} \ll 1, \quad \frac{\delta}{h} \ll 1, \quad \frac{h}{r_o} \ll 1, \quad kr_o \ll 1 \tag{I.2.1}$$

They mean, respectively, that the tidal excursion is small compared to the island size, the Ekman layer is totally submerged near the sea bottom beneath the inviscid zone, the sea is shallow, and the topographical length scale is small relative to the tidal wave length $2\pi/k$. Resuspension of fine particle from the seabed is modelled by the usual empirical formula that the erosion rate is a function of the shear stress at the seabed (Krone, 1962; Patheniades, 1965).

The conditions of (1.1) are easily met. Taking for estimate the tidal amplitude $A = 1.75$ m, average depth $h = 30$ m then $\mathcal{U} = A\sqrt{gh}/h = 1$ m/s. Let the tidal period be 12 hours so that $\omega = 2\pi/12$ (1/hr)$= 1.45 \times 10^{-4}$ (1/s), and the radius be $r_o = 50$ km, then $\epsilon = \mathcal{U}/(\omega r_o) = 0.138$ and is small.

To help guide the estimate of order of magnitude of the eddy viscosity we use the usual assumption (Soulsby, 1983)

$$\nu_e = \kappa u_* z \tag{I.2.2}$$

where $\kappa = 0.4$ is the Karman constant and $u_* = \sqrt{\tau_b/\rho}$ is the friction velocity which depends on the local shear stress at the bed. Taking the typical value $u* = 2.5$ cm/s as an estimate (Soulsby, 1983, p 196) we then get for a tidal boundary layer of depth 10 m, $\nu_e = 0.05$ m^2/s which is much greater than that of the molecular viscosity of water.

Let us set up the coordinates with the vertical axis fixed on the sea bottom and pointing upward. Using the external inviscid flow equation to eliminate the pressure, with the second assumption in (I.2.1), the boundary layer equations can be written:

$$\begin{aligned} \frac{\partial \mathbf{u}}{\partial t} &+ \mathbf{u}\cdot\nabla\mathbf{u} + w\frac{\partial \mathbf{u}}{\partial z} + \mathbf{f}\times\mathbf{u} - \nu_e\frac{\partial^2\mathbf{u}}{\partial z^2} \\ &= \frac{\partial \mathbf{U}_I}{\partial t} + \mathbf{U}_I\cdot\nabla\mathbf{U}_I + \mathbf{f}\times\mathbf{U}_I, \end{aligned} \tag{I.2.3}$$

where $\mathbf{u} = (u, v)$ denotes the horizontal velocity vector, w the vertical velocity component, ν_e the eddy viscosity, and $\mathbf{f} = 2\Omega\sin\phi\mathbf{k}$ is the local angular velocity of the earth rotation, with $\Omega = 2\pi/\text{day}$ and ϕ being the local latitude. $\mathbf{U}_I$ denotes the

horizontal velocty of the inviscid flow field just outside the boundary layer,

$$\mathbf{U}_I = \mathrm{Re}[\mathbf{U}_0(x,y)e^{-i\omega t}] \;=\; \frac{1}{2}(\mathbf{U}_0 e^{-i\omega t} + \mathbf{U}_0^* e^{i\omega t}) \tag{I.2.4}$$

where asteriks signify complex conjugates.

The first assumption in (I.2.1) permits one to expand the velocity in the boundary layer as

$$\mathbf{u} = \mathbf{u}^{(1)} + \mathbf{u}^{(2)} + \cdots$$

where the superscripts indicate the order of magnitude in powers of ϵ. At the leading order the horizontal momentum equation reads

$$\frac{\partial \mathbf{u}^{(1)}}{\partial t} + \mathbf{f} \times \mathbf{u}^{(1)} - \nu_e \frac{\partial^2 \mathbf{u}^{(1)}}{\partial z^2} = \frac{\partial \mathbf{U}_I}{\partial t} + \mathbf{f} \times \mathbf{U_I} \tag{I.2.5}$$

Boundary conditions:

$$\mathbf{u}^{(1)} = \mathbf{U}_I \qquad\qquad z \to \infty, \tag{I.2.6}$$

$$\mathbf{u}^{(1)} = 0 \qquad\qquad z = 0. \tag{I.2.7}$$

In complex form, with overbars denoting the complex variables,

$$\overline{U}_I = U_I + iV_I = Be^{-i\omega t} + Ce^{i\omega t}, \tag{I.2.8}$$

in which

$$\begin{aligned} B &= \frac{1}{2}(U_0 + iV_0) \\ C &= \frac{1}{2}(U_0^* + iV_0^*). \end{aligned} \tag{I.2.9}$$

Due to linearity, we may split the solution into two components, namely,

$$\overline{u}^{(1)} = u^{(1)} + iv^{(1)} = \overline{u}_{1B} + \overline{u}_{1C}, \tag{I.2.10}$$

$$\frac{\partial \overline{u}_{1B}}{\partial t} + 2i\Omega \sin\phi \overline{u}_{1B} - \nu_e \frac{\partial^2 \overline{u}_{1B}}{\partial z^2} = i\omega(f-1)Be^{-i\omega t}, \tag{I.2.11}$$

$$\frac{\partial \overline{u}_{1C}}{\partial t} + 2i\Omega \sin\phi \overline{u}_{1C} - \nu_e \frac{\partial^2 \overline{u}_{1C}}{\partial z^2} = i\omega(f+1)Ce^{i\omega t}. \tag{I.2.12}$$

Note that on the right-hand side of Equation I.2.11 the factor $f-1$ with

$$f \equiv 2\Omega \sin\phi/\omega = \text{Coriolis factor}. \tag{I.2.13}$$

will change sign when f varies accross unity. This further causes the direction of the forcing to turn opposite and the magnitude of the forcing stops increasing and begins decreasing or verse vice. The linear response to this variation of forcing is still smooth. But due to nonlinearity, we can expect a discontinuity accross $f = 1$ in the f-derivatives in both second order streaming and transport parameters. Let

$$\begin{aligned} \overline{u}_{1B} &= \Gamma_B(\xi)Be^{-i\omega t}, \\ \overline{u}_{1C} &= \Gamma_C(\xi)Be^{i\omega t}, \end{aligned} \tag{I.2.14}$$

with

$$\xi = \frac{z}{\delta}, \qquad \delta = \sqrt{2\nu_e/\omega}. \tag{I.2.15}$$

Then,

$$[\frac{\partial^2}{\partial \xi^2} + 2i(1-f)](\Gamma_B - 1) = 0, \tag{I.2.16}$$

$$[\frac{\partial^2}{\partial \xi^2} - 2i(1+f)](\Gamma_C - 1) = 0, \tag{I.2.17}$$

we get

$$\Gamma_B = 1 - e^{-s\xi}, \qquad \Gamma_C = 1 - e^{-(1+i)\alpha\xi} \tag{I.2.18}$$

where

$$\alpha = \sqrt{1+f}, \qquad \beta = \sqrt{|1-f|} \tag{I.2.19}$$

$$s = (1-i)\beta, \qquad \text{if } f < 1,$$

$$s = (1+i)\beta, \qquad \text{if } f > 1, \tag{I.2.20}$$

Therefore, The first order horizontal velocity in the bottom boundary layer is given as follows

$$u^{(1)} = \mathrm{Re}[(U_0 F_1 - V_0 F_2)e^{-i\omega t}], \tag{I.2.21}$$

$$v^{(1)} = \mathrm{Re}[(U_0 F_2 + V_0 F_1)e^{-i\omega t}], \tag{I.2.22}$$

in which

$$F_1 = 1 - \frac{1}{2}(e^{-s\xi} + e^{-q\xi}), \tag{I.2.23}$$

$$F_2 = \frac{i}{2}(e^{-s\xi} - e^{-q\xi}), \tag{I.2.24}$$

where

$$q = (1-i)\alpha. \tag{I.2.25}$$

As has been shown by Buchwald (1971) that under the last two assumptions in (I.2.1), the inviscid tidal flow (U_I, V_I) can be described essentially by a two-dimensional, quasi-steady velocity potential, while the vertical velocity component is negligible. In particular,

$$\frac{\partial U_I}{\partial x} + \frac{\partial V_I}{\partial y} = O(kr_o)^2 \left(\frac{\mathcal{U}}{r_o}\right), \quad \frac{\partial U_I}{\partial y} - \frac{\partial V_I}{\partial x} = O(kr_o)^2 \left(\frac{\mathcal{U}}{r_o}\right) \tag{I.2.26}$$

It follows readily from continuity that the vertical velocity in the boundary layer is of the order

$$\frac{\delta}{r_o}(kr_o)^2 \frac{\mathcal{U}}{r_o} \tag{I.2.27}$$

and negligible (Lamoure & Mei, 1977). As a further consequence the spatial factors U_0 and V_0 are in phase and may be taken as real quantities with respect to i. Based on these Lamoure & Mei (1977) have solved the approximate momentum equation at the second order, $O(\epsilon)$,

$$\frac{\partial \mathbf{u}^{(2)}}{\partial t} + \mathbf{f} \times \mathbf{u}^{(2)} - \nu_e \frac{\partial^2 \mathbf{u}^{(2)}}{\partial z^2} = \mathbf{U}_I \cdot \nabla \mathbf{U}_I - \mathbf{u}^{(1)} \cdot \nabla \mathbf{u}^{(1)} = \frac{1}{2}\nabla(\mathbf{U}_I^2 - \mathbf{u}^{(1)^2}). \tag{I.2.28}$$

The period-average of $\mathbf{u}_2$ gives the Eulerian streaming induced by Reynolds stresses in the tidal boundary layer. Using real notation, the second order induced streaming is given by

$$\langle u^{(2)} \rangle = \frac{1}{2\omega} \left\{ \mathrm{Re}\, H_E(\xi) \frac{\partial}{\partial x} |\mathbf{U}_0|^2 - \mathrm{Im}\, H_E(\xi) \frac{\partial}{\partial y} |\mathbf{U}_0|^2 \right\} \tag{I.2.29}$$

$$\langle v^{(2)} \rangle = \frac{1}{2\omega} \left\{ \mathrm{Im}\, H_E(\xi) \frac{\partial}{\partial x} |\mathbf{U}_0|^2 + \mathrm{Re}\, H_E(\xi) \frac{\partial}{\partial y} |\mathbf{U}_0|^2 \right\}, \tag{I.2.30}$$

where

$$|\mathbf{U}_0| = (|U_0|^2 + |V_0|^2)^{1/2}, \tag{I.2.31}$$

angle brackets denote time averages over a tidal period, and $H_E(\xi)$ marks the vertical variation of Eulerian streaming in the boundary layer

$$\begin{aligned} H_E &= \frac{1}{2} \left\{ \left(\frac{1}{q^2 - c^2} + \frac{1}{q^{*2} - c^2} - \frac{1}{4\alpha^2 - c^2} \right) e^{-c\xi} \right. \\ &- \left. \frac{1}{q^2 - c^2} e^{-q\xi} - \frac{1}{q^{*2} - c^2} e^{-q^*\xi} + \frac{1}{4\alpha^2 - c^2} e^{-2\alpha\xi} \right\} \\ &+ \frac{1}{2} \{ \alpha \to \beta,\ q \to s \} \end{aligned} \tag{I.2.32}$$

The expression in the second pair of braces is obtained from the first pair by the indicated change of parameters. This result has been derived and discussed by Lamoure & Mei (1977).

2.2 Particle transport

A dilute cloud of fine particles in the tidal wave is considered. It can be either released from a dredge boat or resuspended locally from an erodible bed. In general the sediment size is distributed over certain range. Since for a dilute cloud, interaction among particles is negligible, one can divide the size distribution into a discrete set of particle sizes, each of which is characterized by a fall velocity w_o. After analyzing the concentration of each size, the evolution of the entire cloud can be obtained by linear superposition. In the sequel only one size is considered.

2.2.1 Governing equation and normalization

We first give reasons that the inertia of sufficiently small particles can be ignored. The ratio of the relaxation time τ for a particle to adjust to the ambient mean flow to that of the tidal wave period can be estimated by

$$\omega\tau = \frac{4d\rho_p g\omega}{3C_D\Delta u} \tag{I.2.33}$$

(Bagnold, 1957) with d, ρ_p, C_D and Δu being respectively the diameter and density of the particle, the drag coefficient and the representative initial velocity difference between a particle and the ambient fluid. With $C_D = O(1)$ and $\Delta u = O(1)$ m/s, this ratio is about $O(10^{-5})$ for $d = O(0.1)$ mm $= 100\mu$m (fine sand), and is very small so that the particles are essentally inertia-free. In a turbulent field, fine particles can also be considered inertia-free relative to turbulent fluctuations if they are small compared to the Kolmogorov length, $\ell_k = (\nu^3\ell/u'^3)^{1/4}$, which is the smallest length scale of viscous eddies, *i.e.*

$$\frac{d}{\ell_k} < O(1) \tag{I.2.34}$$

where where ℓ is the eddy size and u' the velocity scale of turbulent fluctuations scaled by the boundary layer thickness δ and friction velocity $u_* = \tau_b/\rho$ respectively, where τ_b stands for the bed shear stress. Estimating with $\nu_e = 0.001$ m^2/s and thus a tidal boundary layer thickness of $\ell = O(3)$ m and $u_* = O(0.01)$ m/s, we have $\ell_k = O(1)$ mm which is also much greater than the particle radius $O(0.1)$ mm. We shall, therefore, ignore the velocity difference between the particle and its surrounding fluid.

Let D and D_h be the vertical and horizontal eddy mass diffusivities respectively. The convection-diffusion equation for the concentration C of a dilute particle cloud can be approximated by

$$\frac{\partial C}{\partial t} + \frac{\partial u_i C}{\partial x_i} + \frac{\partial (w - w_o)C}{\partial z} = D_h \frac{\partial^2 C}{\partial x_i \partial x_i} + D\frac{\partial^2 C}{\partial z^2}, \tag{I.2.35}$$

where $i = 1, 2$ corresponding to the two horizontal coordinates.

From the experiments by Krone (1962) and Patheniades (1965) for steady flow

over an erodible bed, the net rate of erosion or deposition of cohesive sediments is related to the excess of bed shear stress above a threshold stress. In its simplest form it reads

$$-w_0 C - D\frac{\partial C}{\partial z} = \left\{ \begin{array}{c} -\mathcal{D} \\ \mathcal{E} \end{array} \right\} \quad \text{if} \quad \left\{ \begin{array}{l} |\tau_b| < \tau_d \\ |\tau_b| > \tau_c \end{array} \right\} \tag{I.2.36}$$

where $\tau_c > \tau_d$ and

$$\mathcal{D} = \alpha_d w_d C \tag{I.2.37}$$

represents the rate of deposition, w_d is the deposition velocity, α_d is an empirical coefficient no greater than unity, and

$$\mathcal{E} = E(|\tau_b| - \tau_c) \tag{I.2.38}$$

represents the rate of erosion while E is another empirical coefficient. Normally τ_d ranges from $0.03 \sim 0.15\,\mathrm{N/m^2}$ for various types of sediments while τ_c lies between 0.15 $\mathrm{N/m^2}$ and 1 $\mathrm{N/m^2}$, see Tables 11.3, 11.7 and 11.8 in Van Rijn (1994). The surface layer of the sea bed is usually covered with partially consolidated or unconsolidated particles for which τ_c is considerably less than the bed shear stress in the tidal wave boundary layer, namely, $|\tau_b| \gg \tau_c$. Thus we shall neglect τ_c as well as $\tau_d (< \tau_c)$. Consequently we shall ignore deposition and approximate (I.2.36) by

$$-(w_0 C + D\frac{\partial C}{\partial z}) = \mathcal{E} \approx E|\tau_b|, \qquad z = 0. \tag{I.2.39}$$

It should be stressed that inculsion of the small effects of deposition is only cumbersome but not difficult. In a steady turbulent flow, the condition for particles remaining in suspension without deposition is $w_0/\kappa u_* < O(1)$ (Batchelor, 1965) where u_* and κ are the bottom shear velocity and the Kármán constant, respectively. As an estimate let us take $u_* = O(0.01)$ m/s, then the above condition by Batchelor is satisfied for $w_o < O(0.004)$ m/s which corresponds to a sand size $d = O(0.1)$ mm or finer.

Because the particles are heavier than water, siediment concentration is expected to be localized boundary layer where the particles are kept in suspension by the flow

turbulence. Hence we assume that C vanishes at the upper edge of the boundary layer,

$$C = 0, \qquad z \to \infty. \tag{I.2.40}$$

There are three vertical length scales pertinent to the boundary layer,

$$\delta_s = D/w_0, \quad \delta_u = \sqrt{2\nu_e/\omega}, \quad \delta_c = \sqrt{2D/\omega}. \tag{I.2.41}$$

Here δ_s denotes the thickness of a steady concentration layer resulting from the settling of particles and the upward turbulent diffusion, and δ_u and δ_c are the boundary layer thicknesses corresponding to momentum and mass transport, respectively. For generality we shall assume that all three scales are comparable to one another and therefore characterized by a single scale δ, *i.e.*,

$$O(\delta) = O(\delta_s) = O(\delta_u) = O(\delta_c), \tag{I.2.42}$$

and thus the Schmidt number is of order unity,

$$Sc = \nu_e/D = (\delta_u/\delta_c)^2 = O(1). \tag{I.2.43}$$

Two small length ratios are crucial in this study. Compared to the horizontal dimension of the peninsula,

$$\epsilon = \frac{\mathcal{U}}{\omega r_0} = \frac{A\sqrt{gh}}{r_o}, \tag{I.2.44}$$

is a measure of the tidal excursion length, and

$$\beta = \frac{\delta}{r_0}\sqrt{\frac{D_h}{D}}, \tag{I.2.45}$$

where β is a measure of the boundary layer thickness. We shall make a generous assumption that the boundary layer thickness is as large as the tidal excursion, i.e., $O(\beta) = O(\epsilon)$, the consequence of which is that horizontal turbulent diffusion will remain effective in the long-term transport of sediment concentration.

Let us introduce the normalized variables as follows

$$x_i = r_o x_i^*, \quad z = \delta z^*, \quad t = \frac{t^*}{\omega}, \quad C = C_0 C^*, \quad u_i = \mathcal{U} u_i^*, \quad w = \frac{\delta}{r_0}\mathcal{U} w^*. \tag{I.2.46}$$

In dimensionless form, the governing equation reads, with the asterisks omitted for brevity,

$$\frac{\partial C}{\partial t} + \epsilon \frac{\partial (u_i C)}{\partial x_i} + \frac{\partial}{\partial z}[(-Pe + \epsilon w)C] = \frac{\partial^2 C}{\partial z^2} + \beta^2 \frac{\partial^2 C}{\partial x_i \partial x_i}, \tag{I.2.47}$$

where $Pe = w_0 \delta / D$ is the particle Péclet number.

As shown by Mei, Fan & Jin (1997), the characteristic concentration C_0 can be estimated by balancing the rate of erosion and the net horizontal flux by Eulerian streaming within the boundary layer, namely,

$$\mathcal{U}_E \, \delta \frac{\partial C}{\partial x} \sim E \tau_b, \tag{I.2.48}$$

where $\mathcal{U}_E$ denotes the scale of the Eulerian steady streaming. From (2.15) and (2.16) we can estimate

$$\mathcal{U}_E = O\left(\frac{\mathcal{U}^2}{\omega r_0}\right), \tag{I.2.49}$$

where $\mathcal{U} = A\sqrt{gh}/h$ for long waves in shallow seas, hence,

$$E\tau_0 \sim \frac{\delta A^2 g C_0}{\omega h r_0^2}. \tag{I.2.50}$$

The shear stress on the sea bottom can be estimated from the boundary layer theory as

$$\tau_0 = \frac{\sqrt{2}\rho D \mathcal{U}}{\delta} = \frac{\sqrt{2g}\rho D A}{\delta \sqrt{h}}, \tag{I.2.51}$$

therefore

$$C_0 \sim \frac{\sqrt{2}\rho E D \omega r_0^2 \sqrt{h}}{A\delta^2 \sqrt{g}} \sim \frac{\sqrt{2}\rho D E \omega r_0^2}{\delta^2 \mathcal{U}}. \tag{I.2.52}$$

Using this, the normalized boundary condition at the seabed reads

$$-Pe\,C-\frac{\partial C}{\partial z}=\frac{\mathcal{U}^2\delta^2}{\omega D r_0^2}|\tau_b|, \tag{I.2.53}$$

where

$$\frac{\mathcal{U}^2\delta^2}{\omega D r_0^2}\sim\frac{A^2}{r_o}\frac{\delta^2\omega}{D}=O(\epsilon^2). \tag{I.2.54}$$

This scale estimate is consistent with field observations by Huhe & Yang (1996), Yu *et al* (1995), and cited by Mei, Fan & Jin (1997).

In the present problem there are two time scales: One is $\omega^{-1}=T/2\pi=O(\delta^2/D)$, which characterizes the vertical diffusion across the boundary layer . The other is the time scale for horizontal diffusion or convection across the peninsula, $O(r_0^2/D_h)$. The ratio between these two time scales is $O(\beta^2)=O(\epsilon^2)$. Accordingly we may introduce a slow time variable $T=\epsilon^2 t$.

2.2.2 Effective equation for horizontal particle transport

After those scaling and order estimates then we return to physical coordinates by keeping the order symbols in order to mark the relative magnitudes. Thus we have

$$\frac{\partial C}{\partial t}+\epsilon\frac{\partial(u_i C)}{\partial x_i}+\frac{\partial}{\partial z}[(-w_o+\epsilon\, w)C]=D\frac{\partial^2 C}{\partial z^2}+\epsilon^2 D_h\frac{\partial^2 C}{\partial x_i\partial x_i}, \tag{I.2.55}$$

$$-(w_0 C+D\frac{\partial C}{\partial z})=\epsilon^2 E|\tau_b|, \qquad z=0, \tag{I.2.56}$$

$$C\to 0, \quad z\gg\delta. \tag{I.2.57}$$

As in Mei & Chian (1994) and Mei *et al* (1997), we employ multiple-scale expansions

$$C=C^{(0)}(x_i,z,T)+\epsilon C^{(1)}(x_i,z,t,T)+\epsilon^2 C^{(2)}(x_i,z,t,T)+O(\epsilon^3), \tag{I.2.58}$$

At the leading order $O(1)$, the equation is quasi-steady and homogeneous,

$$\frac{\partial}{\partial z}\left(w_0 C^{(0)} + D\frac{\partial C^{(0)}}{\partial z}\right) = 0. \tag{I.2.59}$$

subject to the homogeneous boundary conditions

$$w_0 C^{(0)} + D\frac{\partial C^{(0)}}{\partial z} = 0 \tag{I.2.60}$$

$$C^{(0)} = 0 \quad z = \infty \tag{I.2.61}$$

Thus, the solution is

$$C^{(0)} = \hat{C}(x_i, T)e^{-Pe\xi}. \tag{I.2.62}$$

represents the time averaged concentration whose dependence on x_i, T through the factor $\hat{C}(x_i, T)$ is yet unknown.

At $O(\epsilon)$, we have the equation for the concentration fluctuation $C^{(1)}$ from the mean,

$$\frac{\partial C^{(1)}}{\partial t} - \frac{\partial}{\partial z}\left(w_0 C^{(1)} + D\frac{\partial C^{(1)}}{\partial z}\right) = -u_i^{(1)}\frac{\partial C^{(0)}}{\partial x_i}, \tag{I.2.63}$$

subject to the same boundary conditions (I.2.60) and (I.2.61). In Equation (I.2.63) we have dropped the term $w_1 \partial C^{(0)}/\partial z$ because w_1 is negligible near a small peninsula, as pointed out before in Section 2.1. Let

$$C^{(1)} = \mathrm{Re}\, C_{11} e^{-i\omega t}, \tag{I.2.64}$$

Using the solutions for u_{1i} as given in Equations (I.2.21) and (I.2.22) , the formal solution for $C^{(0)}$ and the boundary conditions for $C^{(1)}$, we obtain

$$\begin{aligned} C_{11} &= \frac{1}{\omega}\left[(R_1 U_0 - R_2 V_0)e^{A_1 Pe\xi} + R_3 U_0 e^{-Pe\xi}\right. \\ &+ \left. R_\alpha(U_0 - iV_0)e^{-A_\alpha Pe\xi} + R_\beta(U_0 + iV_0)e^{-A_\beta Pe\xi}\right]\frac{\partial \hat{C}}{\partial x} \\ &+ \frac{1}{\omega}[U_0 \to V_0, V_0 \to -U_0]\frac{\partial \hat{C}}{\partial y}, \end{aligned} \tag{I.2.65}$$

with

$$R_1 = -\frac{Sc}{Pe^2(A_1+1)}\left[\frac{A_\beta - 1}{(A_1+A_\beta)(A_2+A_\beta)} + \frac{A_\alpha - 1}{(A_1+A_\alpha)(A_2+A_\alpha)}\right], \tag{I.2.66}$$

$$\begin{aligned} R_2 &= \frac{iSc(A_\alpha - A_\beta)}{Pe^2(A_1 - A_2)}\left[-\frac{1}{(A_1+A_\alpha)(A_1+A_\beta)}\right. \\ &+ \left.\frac{A_2+1}{(A_2+A_\alpha)(A_2+A_\beta)(A_1+1)}\right], \end{aligned} \tag{I.2.67}$$

$$R_3 = -i = \frac{2Sc}{Pe^2(1+A_1)(1+A_2)}, \tag{I.2.68}$$

$$R_{\alpha,\beta} = -\frac{Sc}{Pe^2(A_1+A_{\alpha,\beta})(A_2+A_{\alpha,\beta})}, \tag{I.2.69}$$

$$A_\alpha = (1-i)\alpha/Pe + 1, \quad A_\beta = (1-i)\beta/Pe + 1, \tag{I.2.70}$$

$$A_{1,2} = -\frac{1}{2}(1 \pm \Gamma_1) \pm \frac{1}{2}i\Gamma_2, \tag{I.2.71}$$

$$\Gamma_{1,2} = [\frac{\sqrt{(1+N^4)} \pm 1}{2}]^{\frac{1}{2}}, \tag{I.2.72}$$

$$N = \frac{2\sqrt{2Sc}}{Pe}, \quad Pe = \frac{w_0\delta}{D}, \quad Sc = \frac{\nu_e}{D}, \tag{I.2.73}$$

Note that Pe is the particle Péclet number which increases with the particle fall velcoity, hence its diameter. Sc is the Schmitt number measuring the ratio of momentum and mass diffusivities.

At $O(\epsilon^2)$, $C^{(2)}$ is governed by

$$\begin{aligned} \frac{\partial C^{(2)}}{\partial t} &+ \frac{\partial}{\partial z}(-w_0 C^{(2)} - D\frac{\partial C^{(2)}}{\partial z} + w^{(1)}C^{(1)} + w^{(2)}C^{(0)}) \\ &= -u_i^{(1)}\frac{\partial C^{(1)}}{\partial x_i} - \frac{\partial C^{(0)}}{\partial T} - u_i^{(2)}\frac{\partial C^{(0)}}{\partial x_i} + D_h\frac{\partial^2 C^{(0)}}{\partial x_i \partial x_i}. \end{aligned} \tag{I.2.74}$$

Taking time average and integrating across the boundary layer, and noting that the concentration vanishes at the top of the layer and that the vertical velocity must be

zero at the bottom, we get the effective transport equation for $\hat{C}$:

$$\frac{\partial \hat{C}}{\partial T}\overline{F} + \frac{\partial}{\partial x_i}\left[\overline{\langle u_i^{(2)}\rangle F}\hat{C}\right] = -\frac{\partial}{\partial x_i}\overline{\langle u_i^{(1)} C^{(1)}\rangle} + D_h \overline{F}\frac{\partial^2 \hat{C}}{\partial x_i \partial x_i} + E\langle|\tau_b|\rangle. \tag{I.2.75}$$

where overbars denote vertical integration across the boundary layer and $F = e^{-Pe\xi}$. Using the results (I.2.21), (I.2.22), (I.2.65), and (I.2.29), we finally have the following effective transport equation:

$$\frac{\partial \hat{C}}{\partial T} + \frac{\partial}{\partial x_i}(U_{Ei}\hat{C}) = \frac{\partial}{\partial x_i}[(E_{ij} + D_h\delta_{ij})\frac{\partial \hat{C}}{\partial x_j}] + \frac{EPe\langle|\tau_b|\rangle}{\delta}, \tag{I.2.76}$$

The effective convection velocity $\mathbf{U}_E$ has the components

$$\begin{aligned}\begin{Bmatrix} U_{E1} \\ U_{E2} \end{Bmatrix} &= \frac{1}{2\omega}[\begin{Bmatrix} \frac{\partial}{\partial x} \\ \frac{\partial}{\partial y} \end{Bmatrix}(|U_0|^2 + |V_0|^2)\mathrm{Re}(H_1) \\ &+ \begin{Bmatrix} -\frac{\partial}{\partial y} \\ \frac{\partial}{\partial x} \end{Bmatrix}(|U_0|^2 + |V_0|^2)\mathrm{Im}(H_1)],\end{aligned} \tag{I.2.77}$$

where

$$H_1 = G(\alpha) + G(\beta) \tag{I.2.78}$$

with

$$G(\alpha) = Pe\left[\frac{I_1(\alpha)}{c + Pe} + \frac{I_2(\alpha)}{q + Pe} + \frac{I_3(\alpha)}{q^* + Pe} + \frac{I_4(\alpha)}{2\alpha + Pe}\right], \tag{I.2.79}$$

and

$$I_1(\alpha) = \frac{1}{4(\alpha^2 + f)i} - \frac{1}{4(\alpha^2 - f)i} + \frac{1}{8\alpha^2 - 4fi}, \tag{I.2.80}$$

$$I_2(\alpha) = -\frac{1}{4(\alpha^2 + f)i}, \tag{I.2.81}$$

$$I_3(\alpha) = \frac{1}{4(\alpha^2 - f)i}, \tag{I.2.82}$$

$$I_4(\alpha) = -\frac{1}{8\alpha^2 - 4fi}, \tag{I.2.83}$$

The polar plot of complex coefficient H_1 is presented in figure I-2-1 for a wide range

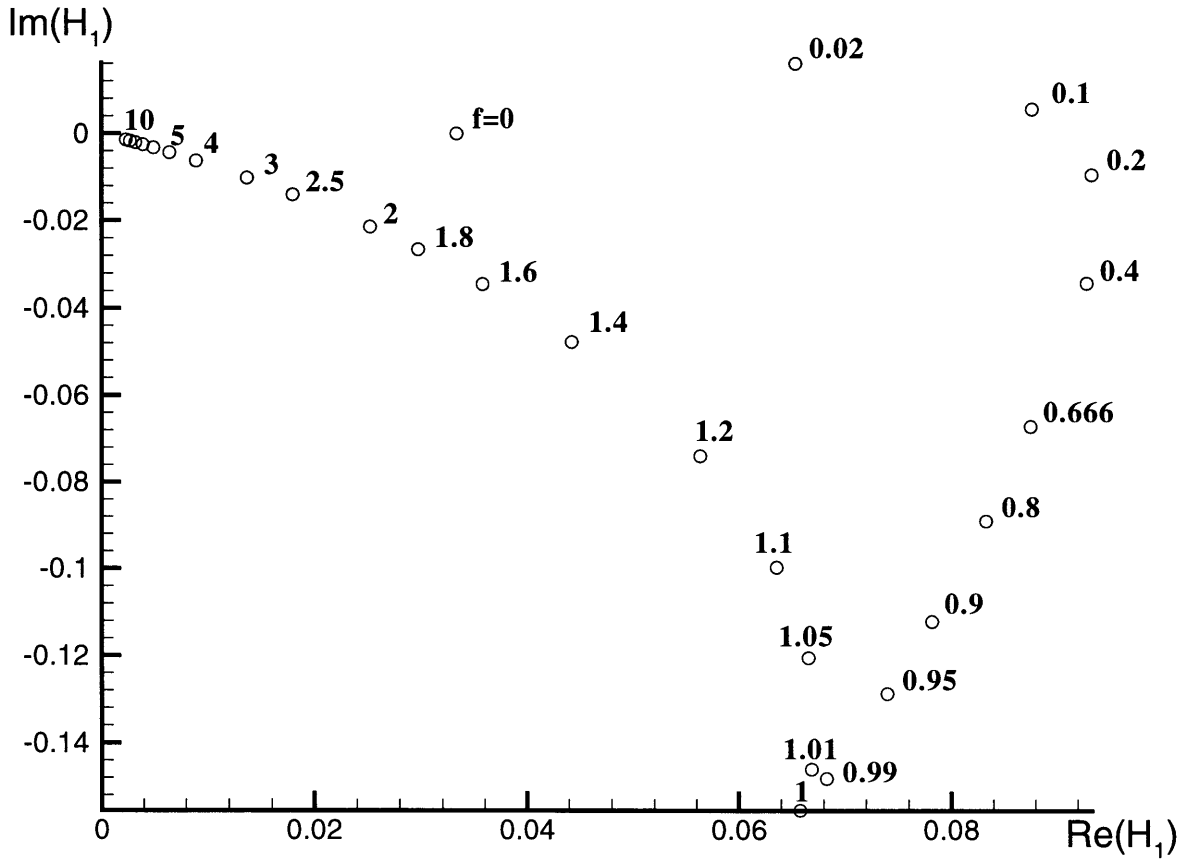

Figure I-2-1: Dimensionless complex coefficient $H_1(f, Pe)$ for the mean convection velocity, as a function of Coriolis number $f = 2\Omega \sin\phi/\omega$, for $Pe = 1$.

of f.

Referring to (I.2.77), the effecive convection velocity field is the weighted depth-average of the Eulerian streaming velocity, proportional to the Reynolds stress imposed by convective inertia in the inviscid flow above the boundary layer. The complex factor H_1 combines the effects of shear and the concentration variation F inside the boundary layer. The ratio $\mathrm{Im}\, H_1/\mathrm{Re}\, H_1 = \tan^{-1}\theta_H$ gives the angle θ_H between the driving external Reynolds stress and the convection current, as a result of earth rotation. Thus for $f = 0$, $\mathrm{Im}H_1 = 0$ so that the angle is zero. But as f increases to 1, the convection velocity is inclined at 67° clockwise from the external Reynolds stress. For f increasing past unity, the angle θ_H decreases again.

The dispersion tensor is in general non-symmetric and has the components :

$$E_{xx} = \frac{1}{\omega}\mathrm{Re}[H_{41}|U_0|^2 + H_{42}|V_0|^2 + H_{43}U_0^*V_0 + H_{44}V_0^*U_0], \tag{I.2.84}$$

$$E_{yy} = \frac{1}{\omega}\mathrm{Re}[H_{41}|V_0|^2 + H_{42}|U_0|^2 - H_{44}U_0^*V_0 - H_{43}V_0^*U_0], \tag{I.2.85}$$

$$E_{xy} = \frac{1}{\omega}\mathrm{Re}[-H_{43}|U_0|^2 + H_{44}|V_0|^2 + H_{41}U_0^*V_0 - H_{42}U_0V_0^*], \tag{I.2.86}$$

$$E_{yx} = \frac{1}{\omega}\mathrm{Re}[H_{43}|V_0|^2 - H_{44}|U_0|^2 + H_{41}U_0V_0^* - H_{42}U_0^*V_0], \tag{I.2.87}$$

Note that all components of the dispersion tensor depends quadratically on the ambient velocity components. Moreover the coefficients

$$H_{41} = -\frac{1}{2}[R_1S_1(A_1) + R_3S_1(-1) + R_\alpha S_1(-A_\alpha) + R_\beta S_1(-A_\beta)], \tag{I.2.88}$$

$$H_{42} = -\frac{1}{2}[R_2S_2(A_1) + iR_\alpha S_2(-A_\alpha) - iR_\beta S_2(-A_\beta)], \tag{I.2.89}$$

$$H_{43} = \frac{1}{2}[R_2S_1(A_1) + iR_\alpha S_1(-A_\alpha) - iR_\beta S_1(-A_\beta)], \tag{I.2.90}$$

$$H_{44} = \frac{1}{2}[R_1S_2(A_1) + R_3S_2(-1) + R_\alpha S_2(-A_\alpha) + R_\beta S_2(-A_\beta)], \tag{I.2.91}$$

$$S_1(a_i) = Pe\frac{2a_iPe - (s^* + q^*)}{2(a_iPe - q^*)(a_iPe - s^*)} - \frac{1}{a_i}, \tag{I.2.92}$$

$$S_2(a_i) = Pe\frac{i(s^* - q^*)}{2(a_iPe - q^*)(a_iPe - s^*)}, \tag{I.2.93}$$

in which $\{a_1, a_2, a_3, a_4\} = \{A_1, -1, -A_\alpha, -A_\beta\}$. represent the integrated effects of the vertical variation of the fluctuating velocity and concentration inside the Ekman boundary layer, hence they are functions of f, Sc and Pe. Since U_0, V_0 are in phase and can be taken as real numbers, only the real parts of H_{4i} are needed, and are plotted in figure I-2-2 as functions of the Péclet number Pe for $f = 0.8$ and three different values of Sc.

In the northern hemisphere, this correspond to the latitude of 53°. All of these coefficients except $\mathrm{Re}\, H_{44}$ achieve their greatest values near $Pe \approx 1$. Dependence of

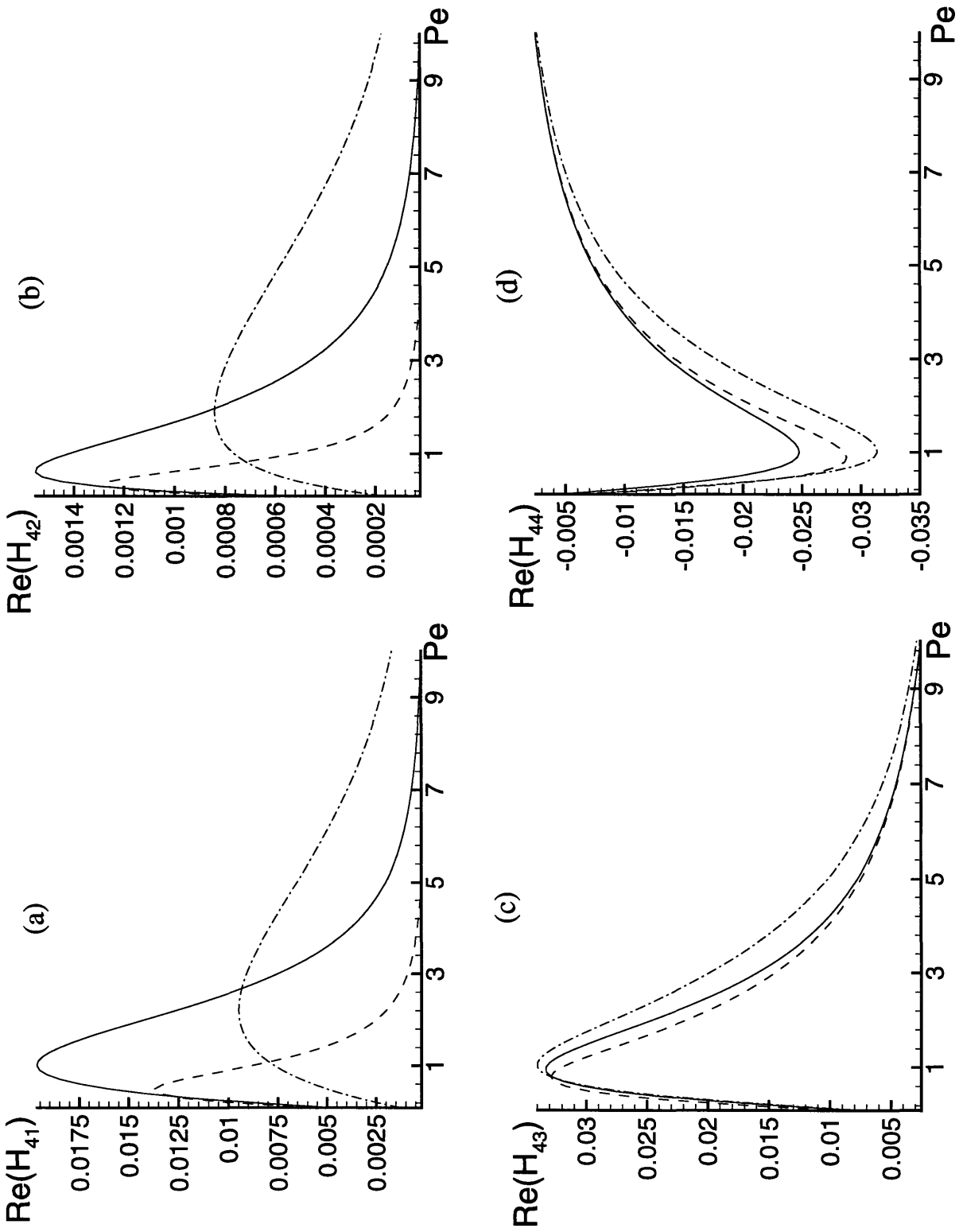

Figure I-2-2: Dimensionless dispersivity coefficients as functions of Pe for $f = 0.666$. Dashed: $Sc = 0.1$, solid: $Sc = 1$, dashdot: $Sc = 10$.

these coefficients on f is plotted in figures I-2-3 for $Pe = 1$ and three values of Sc. Discontinuity in slope at $f = 1$, i.e., $\omega = 2\Omega \sin\phi$ is a common feature which is caused by the change of sign in (I.2.93).

The effective convection-dispersion equation can be written in conservation form

$$\frac{\partial \hat{C}}{\partial T} + \frac{\partial \mathcal{F}_i}{\partial x_i} = 0, \tag{I.2.94}$$

where

$$\mathcal{F}_i = U_{Ei}\hat{C} - (E_{ij} + D\delta_{ij})\frac{\partial \hat{C}}{\partial x_j} \tag{I.2.95}$$

is the particle flux vector.

Under the present assumption of constant depth, the shore must be a vertical cliff normal to which there is no horizontal flux i.e.,

$$\mathcal{F}_i n_i = \left[U_{Ei}\hat{C} - (E_{ij} + D\delta_{ij})\frac{\partial \hat{C}}{\partial x_j}\right] n_i = 0 \tag{I.2.96}$$

For presentation of numerical results, it is convenient to renormalize the variables as follows

$$\begin{aligned} t = T'\frac{r_o^2\omega}{\mathcal{U}^2}\ ,\ x_i = r_o x_i',\ \hat{C} = C'C_0 \\ U_{Ei} = U'_{Ei}\frac{\mathcal{U}^2}{\omega r_o}\ ,\ (D,\ E_{ij}) = \frac{\mathcal{U}^2}{\omega}\left(D', E'_{ij}\right) \end{aligned} \tag{I.2.97}$$

where the concentration scale depends on the problem to be specified later. The effective convection-diffusion equation then becomes

$$\frac{\partial \hat{C}'}{\partial T'} + \frac{\partial (U'_{Ei}C')}{\partial x_i'} = \frac{\partial}{\partial x_i'}\left((E'_{ij} + D'_h)\frac{\partial C}{\partial x_i'}\right) + \mathcal{E}'. \tag{I.2.98}$$

In the following sections we shall limit our discussion to a semicircular peninsula. The first order spatial dependence of the inviscid velocity field is then simple and is

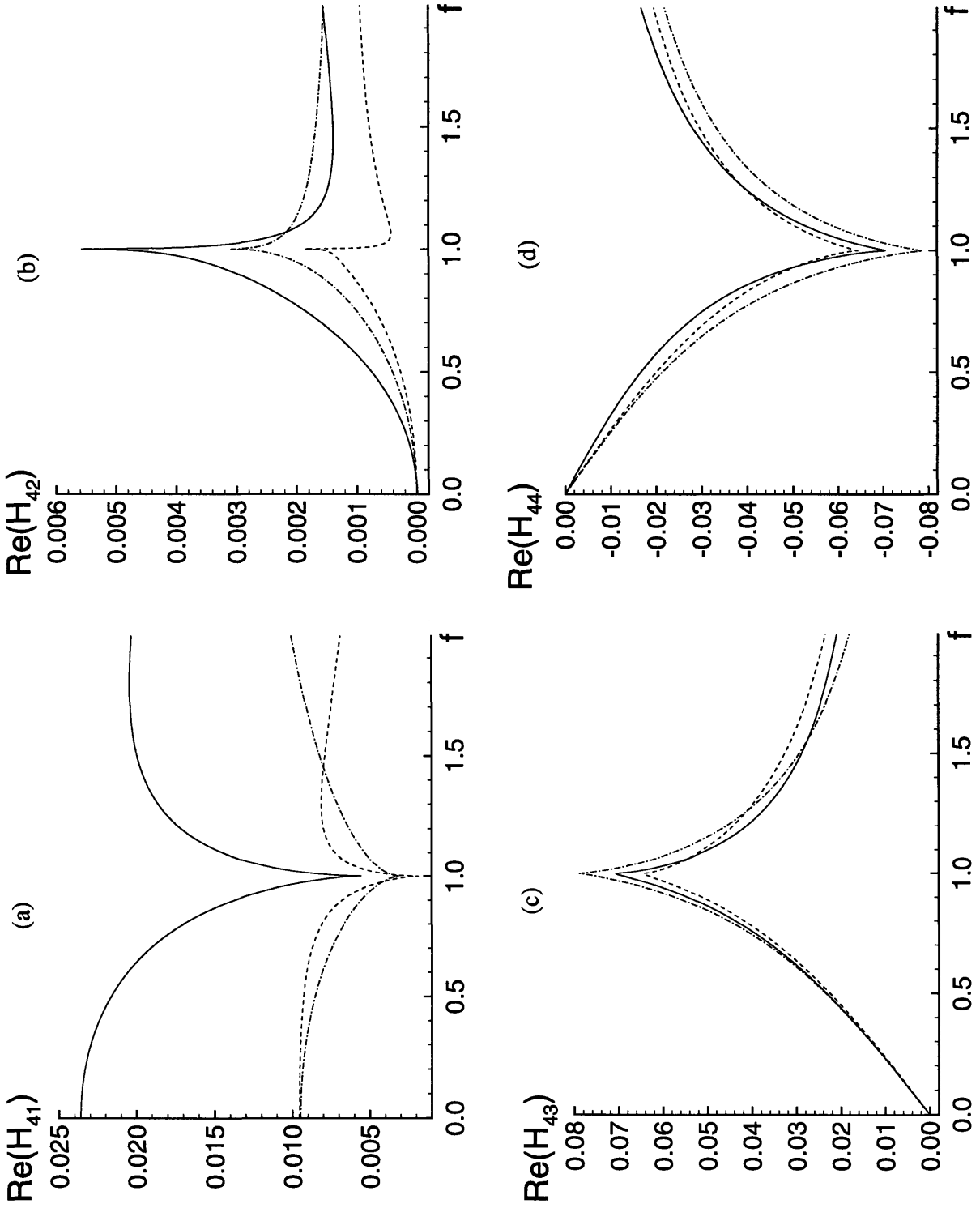

Figure I-2-3: Dimensionless dispersivity coefficients as functions of f for $f = 0.666$. Dashed: $Sc = 0.1$, solid: $Sc = 1$, dashdot: $Sc = 10$.

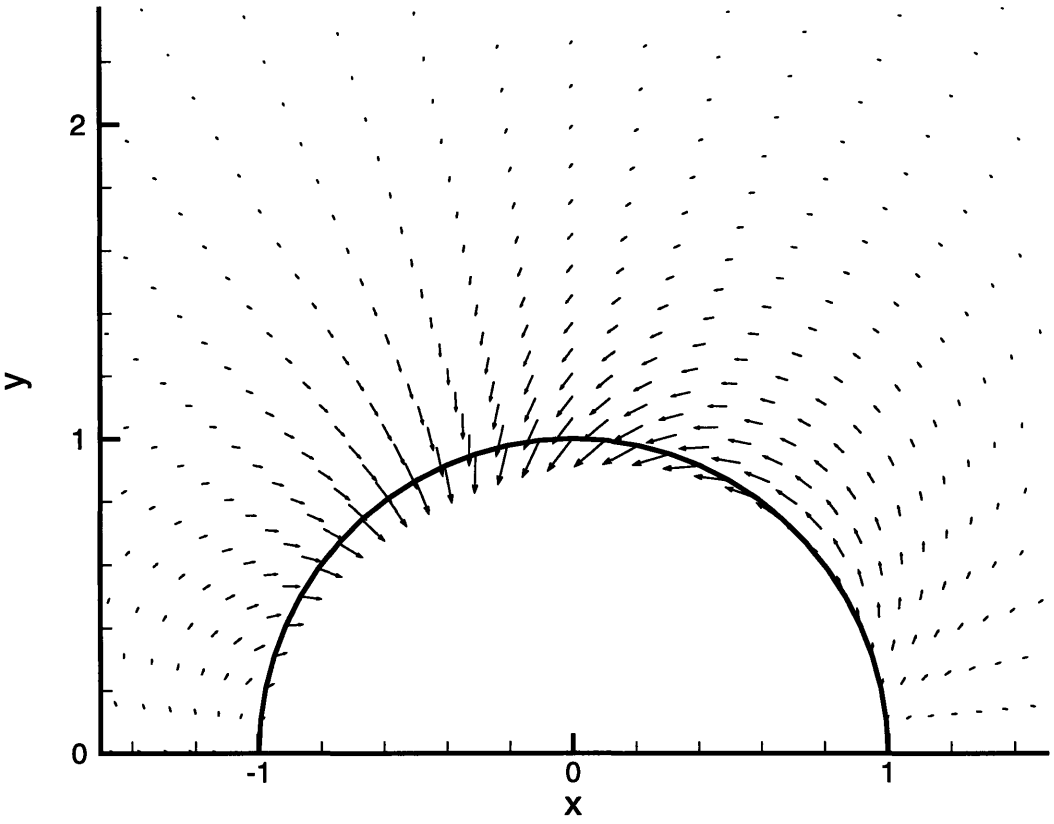

Figure I-2-4: Weighted depth-average of convection velocity $\mathbf{U}_E$ in the tidal boundary layer for $f = 0.666$ and $Pe = 1$.

identical to that for uniform flow passing a circular cylinder

$$U_0 = \mathcal{U}U_0' = \mathcal{U}\left(1 - \frac{\cos 2\theta}{r'^2}\right), \qquad V_0 = \mathcal{U}V_0' = -\mathcal{U}\left(\frac{\sin 2\theta}{r'^2}\right), \tag{I.2.99}$$

where $r' = r/r_o$. The mean velocity of Eulerian streaming is shown for $f = 0.8$ in figure I-2-4, showing a distinct assymmetry due to earth rotation and a convergence to a coastal region near $\theta = 135°$. In contrast the mean streaming field in a nonrotating sea would be symmetical with respect to the offshore (y) axis of the peninsula, with convergence toward the offshore tip of the peninsula (Lamoure & Mei, 1977).

In figure I-2-5 we display the cartesian components of the dispersion tensor E_{ij} for the semi cirular peninsula, for $f = 0.8, Pe = Sc = 1$. Again the asymmetry is notable.

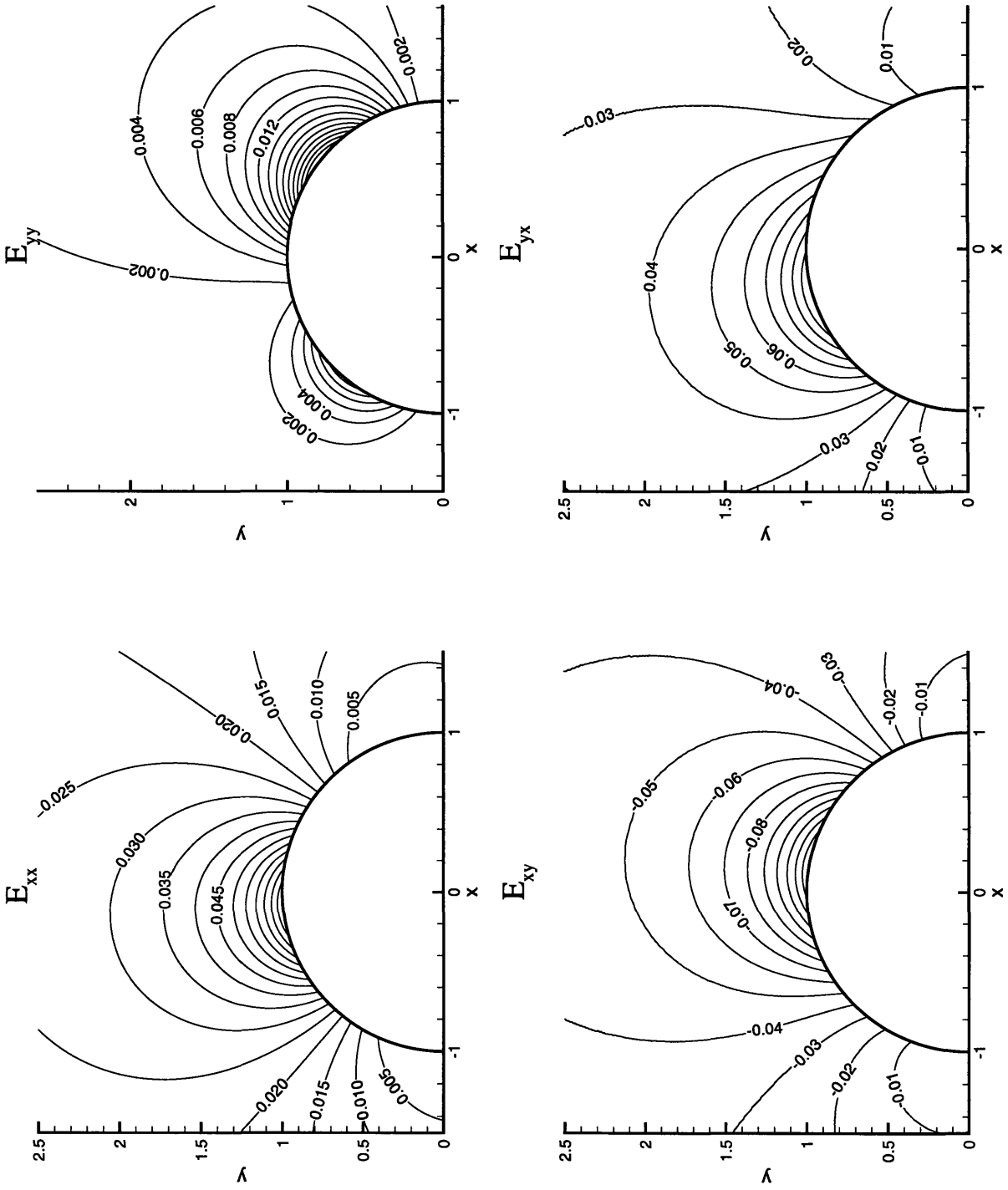

Figure I-2-5: Dispersivity tensor components around a circular peninsula for $f = 0.666$, $Pe = 1$ and $Sc = 1$

For $f = 0$ these components are symmetrical with respect to the y axis, as shown in figure I-2-6. For rough estimate let us take again $\mathcal{U} = 1$ m/s and $\omega = 1.45 \times 10^{-4}$ 1/s. From figure I-2-2 the typical value of E_{ij} near the peninsula is 0.05, therefore the dispersivity is of the order $E_{ij} \sim 0.05\mathcal{U}^2/\omega = 345$ m^2/s which is consistent with the data cited by Zimmerman (1976) and far greater than the eddy diffusivity.

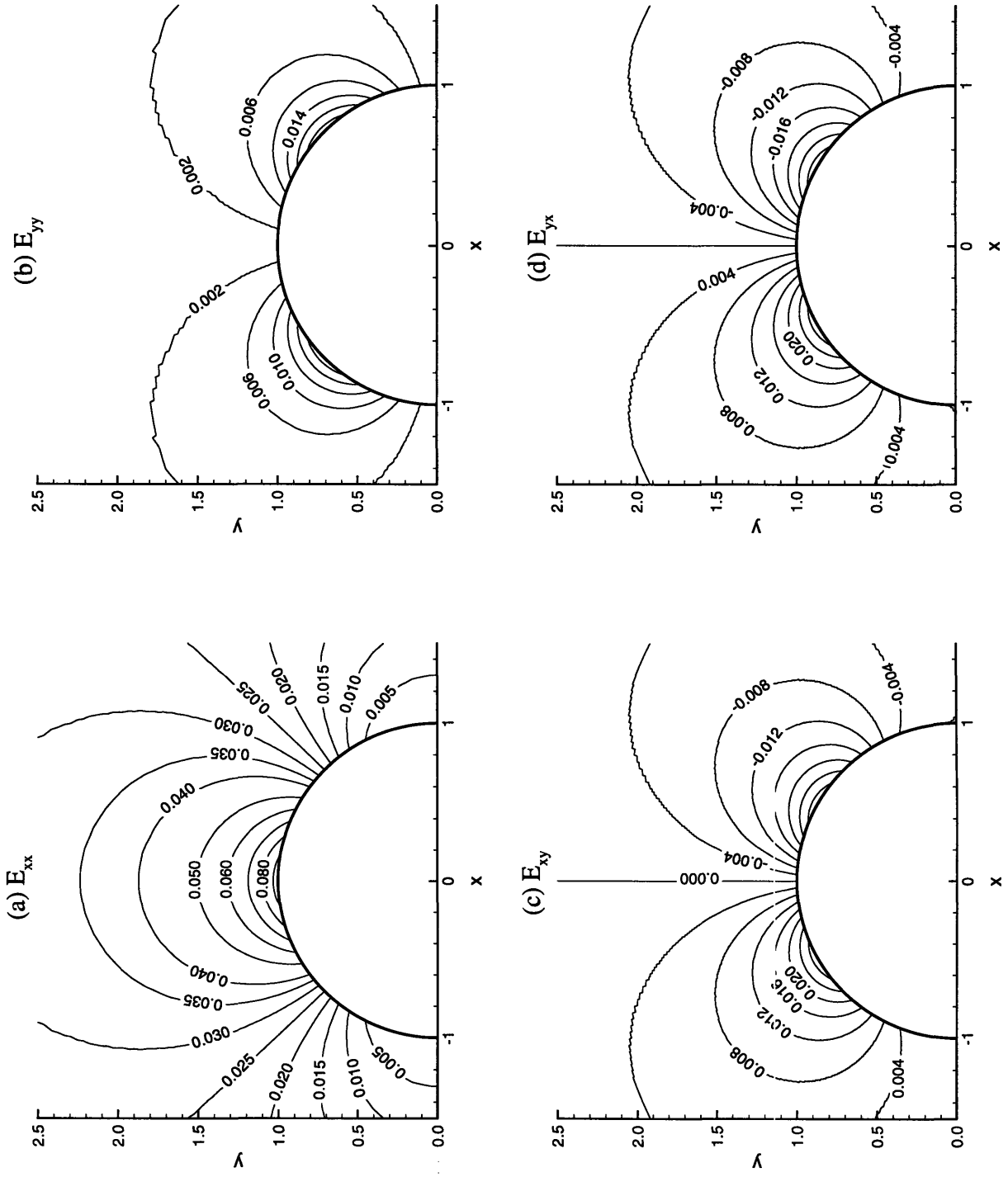

Figure I-2-6: Dispersivity tensor components around a circular peninsula for $f = 0$, $Pe = 1$ and $Sc = 1$

Chapter 3

Numerical scheme

For computational convenience, we first split the dispersion tensor E_{ij} into symmetric D_{ij} and antisymmetric A_{ij} parts and rewrite the governing equation (I.2.98), with primes omitted, in the following form:

$$\frac{\partial C}{\partial t} + u'\frac{\partial C}{\partial x} + v'\frac{\partial C}{\partial y} + \gamma C = D_{xx}\frac{\partial^2 C}{\partial x^2} + D_{yy}\frac{\partial^2 C}{\partial y^2} + 2D_{xy}\frac{\partial^2 C}{\partial x \partial y} + \mathcal{E}, \tag{I.3.1}$$

where

$$u' = U_{E1} + \frac{\partial A_{xy}}{\partial y} - \frac{\partial D_{xx}}{\partial x} - \frac{\partial D_{xy}}{\partial y}, \tag{I.3.2}$$

$$v' = U_{E2} - \frac{\partial A_{xy}}{\partial x} - \frac{\partial D_{xy}}{\partial x} - \frac{\partial D_{yy}}{\partial y}, \tag{I.3.3}$$

$$\gamma = \frac{\partial U_{E1}}{\partial x} + \frac{\partial U_{E2}}{\partial y}, \tag{I.3.4}$$

and $D_{xx} = E_{xx}$, $D_{yy} = E_{yy}$,

$$\begin{aligned} D_{xy} &= D_{yx} = \frac{1}{2}(E_{xy} + E_{yx}) \\ &= \frac{1}{2}[Re(H_{43}) + Re(H_{44})](|V_0|^2 - |U_0|^2) \\ &\quad + Re(U_0 V_0^*)[Re(H_{41} - Re(H_{42})], \end{aligned} \tag{I.3.5}$$

$$
\begin{aligned}
A_{xy} &= -A_{yx} = \frac{1}{2}(E_{xy} + E_{yx}) \\
&= \frac{1}{2}[\mathrm{Re}(H_{44}) - \mathrm{Re}(H_{43})](|V_0|^2 + |U_0|^2) \\
&\quad -\mathrm{Im}(U_0^* V_0)[\mathrm{Im}(H_{41}) + \mathrm{Im}(H_{42})]. \qquad \text{(I.3.6)}
\end{aligned}
$$

Equation (I.3.1) is then transformed in polar coordinates, handy for our circular peninsula,

$$
\begin{aligned}
\frac{\partial C}{\partial t} &+ u'_r \frac{\partial C}{\partial r} + u'_\theta \frac{\partial C}{r \partial \theta} + \gamma C \\
&= D_{rr} \frac{\partial^2 C}{\partial r^2} + D_{\theta\theta} \frac{\partial^2 C}{r^2 \partial \theta^2} + 2 D_{\theta r} \frac{\partial^2 C}{r \partial \theta \partial r} + \mathcal{E}, \qquad \text{(I.3.7)}
\end{aligned}
$$

with

$$
u'_r = u' \cos\theta + v' \sin\theta - \frac{D_{xx}}{r} \sin^2\theta - \frac{D_{yy}}{r} \cos^2\theta + \frac{D_{xy}}{r} \sin 2\theta, \qquad \text{(I.3.8)}
$$

$$
u'_\theta = -u' \sin\theta + v' \cos\theta - \frac{1}{r}(D_{xx} \sin 2\theta + D_{yy} \sin 2\theta + 2 D_{xy} \cos 2\theta), \qquad \text{(I.3.9)}
$$

$$
D_{rr} = D_{xx} \cos^2\theta + D_{yy} \sin^2\theta + D_{xy} \sin 2\theta, \qquad \text{(I.3.10)}
$$

$$
D_{\theta\theta} = D_{xx} \sin^2\theta + D_{yy} \cos^2\theta - D_{xy} \sin 2\theta, \qquad \text{(I.3.11)}
$$

$$
D_{\theta r} = \frac{1}{2} \sin 2\theta (D_{yy} - D_{xx}) + D_{xy} \cos 2\theta. \qquad \text{(I.3.12)}
$$

As the radial variation near the peninsula is expected to be very rapid, we introduce the stretching: $r = \exp(2\pi\zeta)$, and $\eta = \theta/\pi$ so that Equation (I.3.7) becomes

$$
\frac{\partial C}{\partial T} + u_\zeta \frac{\partial C}{\partial \zeta} + u_\eta \frac{\partial C}{\partial \eta} + \gamma C = D_{\zeta\zeta} \frac{\partial^2 C}{\partial \zeta^2} + D_{\eta\eta} \frac{\partial^2 C}{\partial \eta^2} + 2 D_{\zeta\eta} \frac{\partial^2 C}{\partial \zeta \partial \eta} + \mathcal{E}, \qquad \text{(I.3.13)}
$$

where

$$
u_\zeta = u'_r s_0 + 2\pi s_0^2 D_{rr}, \quad u_\eta = 2 u'_\theta s_0, \qquad \text{(I.3.14)}
$$

$$
D_{\zeta\zeta} = s_0^2 D_{rr}, \quad D_{\eta\eta} = 4 s_0^2 D_{\theta\theta}, \quad D_{\zeta\eta} = 2 s_0^2 D_{r\theta}, \qquad \text{(I.3.15)}
$$

$$
s_0 = \frac{1}{2\pi r}, \qquad \text{(I.3.16)}
$$

For this initial value two dimensional convection-dispersion equaiton, we adopt the ADI Method (Alternating Direction Implicit Scheme) which is unconditionally stable and thus allows us to use reasonably large time steps, with second order accuracy, $O(\Delta t^2, \Delta\zeta^2, \Delta\eta^2)$. With each time step Δt, we solve implicit one-dimensional problem for ζ and η alternately.

ζ-sweep:

$$\begin{aligned}
&\frac{C_{ij}^{n+1/2} - C_{ij}^{n}}{\Delta t/2} + u_{\zeta,ij}\frac{C_{i+1,j}^{n+1/2} - C_{i-1,j}^{n+1/2}}{2\Delta\zeta} + u_{\eta,ij}\frac{C_{i,j+1}^{n} - C_{i,j-1}^{n}}{2\Delta\eta} + \gamma_{ij}\frac{C_{ij}^{n+1/2} + C_{ij}^{n}}{2} \\
= \;& D_{\zeta\zeta,ij}\left(\frac{C_{i+1,j}^{n+1/2} + C_{i-1,j}^{n+1/2} - 2C_{ij}^{n+1/2})}{\Delta\zeta^2} + D_{\eta\eta,ij}\left(\frac{C_{i,j+1}^{n} + C_{i,j-1}^{n} - 2C_{ij}^{n})}{\Delta\eta^2}\right.\right. \\
&+2D_{\zeta\eta,ij}\frac{(C_{i+1,j+1}^{n} + C_{i+1,j-1}^{n})/2\Delta\eta - (C_{i-1,j+1}^{n} + C_{i-1,j-1}^{n})/2\Delta\eta}{2\Delta\zeta} + \mathcal{E}_{ij}, \qquad \text{(I.3.17)}
\end{aligned}$$

and η-sweep:

$$\begin{aligned}
&\frac{C_{ij}^{n+1} - C_{ij}^{n+1/2}}{\Delta t/2} + u_{\zeta,ij}\frac{C_{i+1,j}^{n+1/2} - C_{i-1,j}^{n+1/2}}{2\Delta\zeta} + u_{\eta,ij}\frac{C_{i,j+1}^{n+1} - C_{i,j-1}^{n+1}}{2\Delta\eta} + \gamma_{ij}\frac{C_{ij}^{n+1/2} + C_{ij}^{n+1}}{2} \\
= \;& D_{\zeta\zeta,ij}\left(\frac{C_{i+1,j}^{n+1/2} + C_{i-1,j}^{n+1/2} - 2C_{ij}^{n+1/2})}{\Delta\zeta^2} + D_{\eta\eta,ij}\left(\frac{C_{i,j+1}^{n+1} + C_{i,j-1}^{n+1} - 2C_{ij}^{n+1})}{\Delta\eta^2}\right.\right. \\
&+2D_{\zeta\eta,ij}\frac{(C_{i+1,j+1}^{n+1/2} + C_{i+1,j-1}^{n+1/2})/2\Delta\eta - (C_{i-1,j+1}^{n+1/2} + C_{i-1,j-1}^{n+1/2})/2\Delta\eta}{2\Delta\zeta} + \mathcal{E}_{ij}. \qquad \text{(I.3.18)}
\end{aligned}$$

These, respectively, give

$$a_{1\zeta}C_{i-1,j}^{n+1/2} + a_{2\zeta}C_{ij}^{n+1/2} + a_{3\zeta}C_{i+1,j}^{n+1/2} = r_{\zeta}^{n}, \qquad \text{(I.3.19)}$$

and

$$a_{1\eta}C_{i,j-1}^{n+1} + a_{2\eta}C_{ij}^{n+1} + a_{3\eta}C_{i,j+1}^{n+1} = r_{\eta}^{n+1/2}, \qquad \text{(I.3.20)}$$

in which

$$\begin{aligned}
a_{1\zeta,\eta} &= -b_{1\zeta,\eta} - b_{3\zeta,\eta}, \\
a_{2\zeta,\eta} &= b_0 + b_2 + 2b_{2\zeta,\eta},
\end{aligned}$$

$$
\begin{aligned}
a_{3\zeta,\eta} &= b_{1\zeta,\eta} - b_{3\zeta,\eta}, \\
b_0 &= 2\Delta\zeta\Delta\eta/\Delta t \\
b_{1\zeta} &= u_\zeta \Delta\eta/2, \\
b_{1\eta} &= u_\eta \Delta\zeta/2, \\
b_2 &= \gamma\Delta\zeta\Delta\eta/2, \\
b_{3\zeta} &= D_{\zeta\zeta}\Delta\eta/\zeta, \\
b_{3\eta} &= D_{\eta\eta}\Delta\zeta/\eta, \\
b_{3\zeta\eta} &= D_{\zeta\eta}/2,
\end{aligned} \tag{I.3.21}
$$

$$
\begin{aligned}
r_\zeta^n &= (b_0 - b_2 - 2b_{3\eta})C_{ij}^n + (b_{3\eta} - b_{1\eta})C_{i,j+1}^n \\
&+ (b_{3\eta} + b_{1\eta})C_{i,j-1}^n + \mathcal{E}_{ij} + \alpha^n, \\
r_\eta^{n+1/2} &= (b_0 - b_2 - 2b_{3\zeta})C_{ij}^{n+1/2} + (b_{3\zeta} - b_{1\zeta})C_{i+1,j}^{n+1/2} \\
&+ (b_{3\zeta} + b_{1\zeta})C_{i-1,j}^{n+1/2} + \mathcal{E}_{ij} + \alpha^{n+1/2}, \\
\alpha^{n,n+1/2} &= b_{3\zeta\eta}(C_{i+1,j+1}^{n,n+1/2} - C_{i+1,j-1}^{n,n+1/2} - C_{i-1,j+1}^{n,n+1/2} + C_{i-1,j-1}^{n,n+1/2}).
\end{aligned} \tag{I.3.22}
$$

Now let us consider the boundary conditions. At the open sea ($i = mm$), assuming that the computational domain is sufficiently large given that the convection transports particles toward the peninsula, and therefore, the concentration vanishes practically, namely,

$$
C_{mm,j} = 0. \tag{I.3.23}
$$

At the rim of the peninsula, $r = 1$, it follows from (I.2.95)

$$
\mathcal{F}_r = U_{Er}C - (E_{rr} + D)\frac{\partial C}{\partial r} - E_{r\theta}\frac{\partial C}{r\partial\theta} = 0, \tag{I.3.24}
$$

where

$$
U_{Er} = U_{E1}\cos\theta + U_{E2}\sin\theta, \tag{I.3.25}
$$

$$
E_{rr} = E_{xx}\cos^2\theta + (E_{xy} + E_{yx})\cos\theta\sin\theta + E_{yy}\sin^2\theta, \tag{I.3.26}
$$

and

$$E_{r\theta} = (E_{yy} - E_{xx}) \cos\theta \sin\theta + E_{xy} \cos^2\theta - E_{yx} \sin^2\theta. \tag{I.3.27}$$

Written in stretched coordinates we have

$$U_{Er} C - (E_{rr} + D) \frac{\partial C}{2\pi r \partial r} - E_{r\theta} \frac{\partial C}{r\pi \partial \theta} = 0. \tag{I.3.28}$$

To be consistent in accuracy with the ADI scheme for the governing equation, we adopt the second order approximation for the normal derivatives. By Taylor expansion,

$$C_{2j} = C_{1j} + \frac{\partial C}{\partial \xi}_{1j} \Delta\xi + \frac{\partial^2 C}{\partial \xi^2}_{1j} \frac{\Delta\xi^2}{2} + O(\Delta\xi)^3, \tag{I.3.29}$$

and

$$C_{3j} = C_{1j} + \frac{\partial C}{\partial \xi}_{1j} 2\Delta\xi + \frac{\partial^2 C}{\partial \xi^2}_{1j} \frac{4\Delta\xi^2}{2} + O(\Delta\xi)^3. \tag{I.3.30}$$

Eliminating the second derivative terms the above two equation give

$$\frac{\partial C}{\partial \xi}_{1j} = \frac{-3C_{1j} + 4C_{2j} - C_{3j}}{2\Delta\xi} + O(\Delta\xi)^2. \tag{I.3.31}$$

For $\partial C/\partial\theta$ we simply apply the common central differencing

$$\frac{\partial C}{\partial \theta} = \frac{C_{1,j+1} - C_{1,j-1}}{2\Delta\eta} + O(\Delta\eta)^2. \tag{I.3.32}$$

We then get a tridiagonal difference equation,

$$a_{1\eta} C_{1,j-1} + a_{2\eta} C_{1j} + a_{3\eta} C_{1,j+1} = R_\eta, \tag{I.3.33}$$

in which

$$\begin{aligned} a_{1\eta} &= 2E_{r\theta}\Delta\xi, \\ a_{2\eta} &= 4\pi r_0 U_{Er,1j} \Delta\xi\Delta\eta + 3(E_{rr,1j} + D)\Delta\eta \\ a_{3\eta} &= -a_{1\eta}, \end{aligned}$$

$$R_\eta = (E_{rr,1j} + D)\Delta\eta(4C_{2j} - C_{3j}). \tag{I.3.34}$$

At $\theta = 0$,

$$\mathcal{F}_\theta = U_{E\theta}C - E_{\theta r}\frac{\partial C}{\partial r} - \frac{(E_{\theta\theta} + D)}{r}\frac{\partial C}{\partial \theta} = 0, \tag{I.3.35}$$

where

$$U_{E\theta} = -U_{E1}\sin\theta + U_{E2}\cos\theta, \tag{I.3.36}$$

$$E_{\theta r} = (E_{yy} - E_{xx})\cos\theta\sin\theta - E_{xy}\sin^2\theta + E_{yx}\cos^2\theta, \tag{I.3.37}$$

and

$$E_{\theta\theta} = E_{xx}\sin^2\theta - (E_{xy} + E_{yx})\cos\theta\sin\theta + E_{yy}\cos^2\theta. \tag{I.3.38}$$

In (ξ, η) domain, we get the approximate differennce equation,

$$U_{E\theta,i1}C_{i1} - \frac{E_{\theta r,i1}}{2\pi r_i}\frac{C_{i+1,1} - C_{i-1,1}}{2\Delta\xi} - \frac{E_{\theta\theta,i1}}{\pi r_i}\frac{-3C_{i1} + 4C_{i2} - C_{i3}}{\Delta\eta} = 0. \tag{I.3.39}$$

We then get the equation for solving the boundary value of C:

$$a_{1\xi,0}C_{i-1,1} + a_{2\xi,0}C_{i1} + a_{3\xi,0}C_{i+1,1} = R_{\xi,0}, \tag{I.3.40}$$

with

$$\begin{aligned} a_{1\xi,0} &= E_{\theta r}\Delta\eta, \\ a_{2\xi,0} &= 4\pi r_i U_{E\theta,i1}\Delta\xi\Delta\eta + 6(E_{\theta\theta,i1} + D)\Delta\xi \\ a_{3\xi,0} &= -a_{1\xi,0}, \\ R_{\xi,0} &= 2(E_{\theta\theta,i1} + D)\Delta\xi(4C_{i2} - C_{i3}). \end{aligned} \tag{I.3.41}$$

At $\theta = \pi$ $(j = \mathrm{nn})$,

$$\frac{\partial C}{\partial \eta} = \frac{3C_{i,nn} - 4C_{i,nn-1} + C_{i,nn-2}}{\Delta\eta} \tag{I.3.42}$$

Similar to the boundary condition at $\theta = 0$, we obtain the equation for solving the boundary value of C:

$$a_{1\xi,\pi}C_{i-1,nn} + a_{2\xi,\pi}C_{i,nn} + a_{3\xi,\pi}C_{i+1,nn} = R_{\xi,\pi}, \tag{I.3.43}$$

with

$$\begin{aligned} a_{1\xi,\pi} &= -E_{\theta r}\Delta\eta, \\ a_{2\xi,\pi} &= -4\pi r_i U_{E\theta,i,nn}\Delta\xi\Delta\eta + 6(E_{\theta\theta,i,nn} + D)\Delta\xi \\ a_{3\xi,\pi} &= -a_{1\xi,\pi}, \\ R_{\xi,\pi} &= 2(E_{\theta\theta,i,nn} + D)\Delta\xi(4C_{i,nn-1} - C_{i,nn-2}). \end{aligned} \tag{I.3.44}$$

At stagnant points $U_{Ei} = 0,\ i = 1, 2$

$$C_{1,1} = \frac{4C_{2,1} - C_{3,1}}{3}, \tag{I.3.45}$$

$$C_{1,nn} = \frac{4C_{2,nn} - C_{3,nn}}{3}, \tag{I.3.46}$$

In the following section we examine the spreading of a particle cloud for two examples. In the first a particle cloud is initially released into the bottom boundary layer near the peninsula; the surrounding seabed is nonerodible. This is to simulate the fate of particles dumped into sea. In the second we examine the transport of sediments eroded from a strip of the seabed surrounding the peninsula.

Chapter 4

Release of a particle cloud

Let the initial concentration be Gaussian and the maximum initial concentration be chosen as C_0 for the scale of normalization. If the initial cloud has the dimensionless standard deviation S and is centered at x'_c, y'_c, then

$$C'(x', y', 0) = \exp\left\{-\frac{(x' - x'_c)^2 + (y' - y'_c)^2}{S^2}\right\} \tag{I.4.1}$$

where $x'_c = r'_c \cos\theta_c, \quad y'_c = r'_c \sin\theta_c$. In all calculations we take $r'_c = 1.3$ and $S = 0.1$. The Coriolis factor is taken to be $f = 0.8$. Three locations of initial releases have been considered: $\theta_c = 45°$, $\theta_c = 90°$, and $\theta_c = 135°$. In each case the snapshots at $T' = 1$, $T' = 2$, $T' = 3$, and $T' = 4$ are plotted. Note that for $r_o = 50$ km, $\mathcal{U} = 1$ m/s, $\omega = 1.45 \times 10^{-4}$ 1/s), $T =' 1$ corresponds to 4.2 days. For comparison the tidal time scale is $1/\omega = 0.08day$. In figures I-4-1 we show the concentration contours when the inititial cloud center is at $r'_c = 1.3, \theta_c = 45°$. At $T' = 1$ the initially concentric circular contours become tilted ellipses due mainly to the off-diagonal dispersivities (E_{xy} and E_{yx}). Some particles are transported toward the coastline around the point ($r' = 1$, $\theta = 45°$) as a result of both Eulerian convection and diffusion from the cloud center. Since the normal flux vanishes at the vertical shore, particles tend to pile against the shore and the local radial gradient of the concentration reverses, i.e., $\partial C/\partial r$ changes from positive to negative. Consequently, two local concentration peaks appear, one, designated as P_1, say, corresponds to the center of the initial cloud which is affected

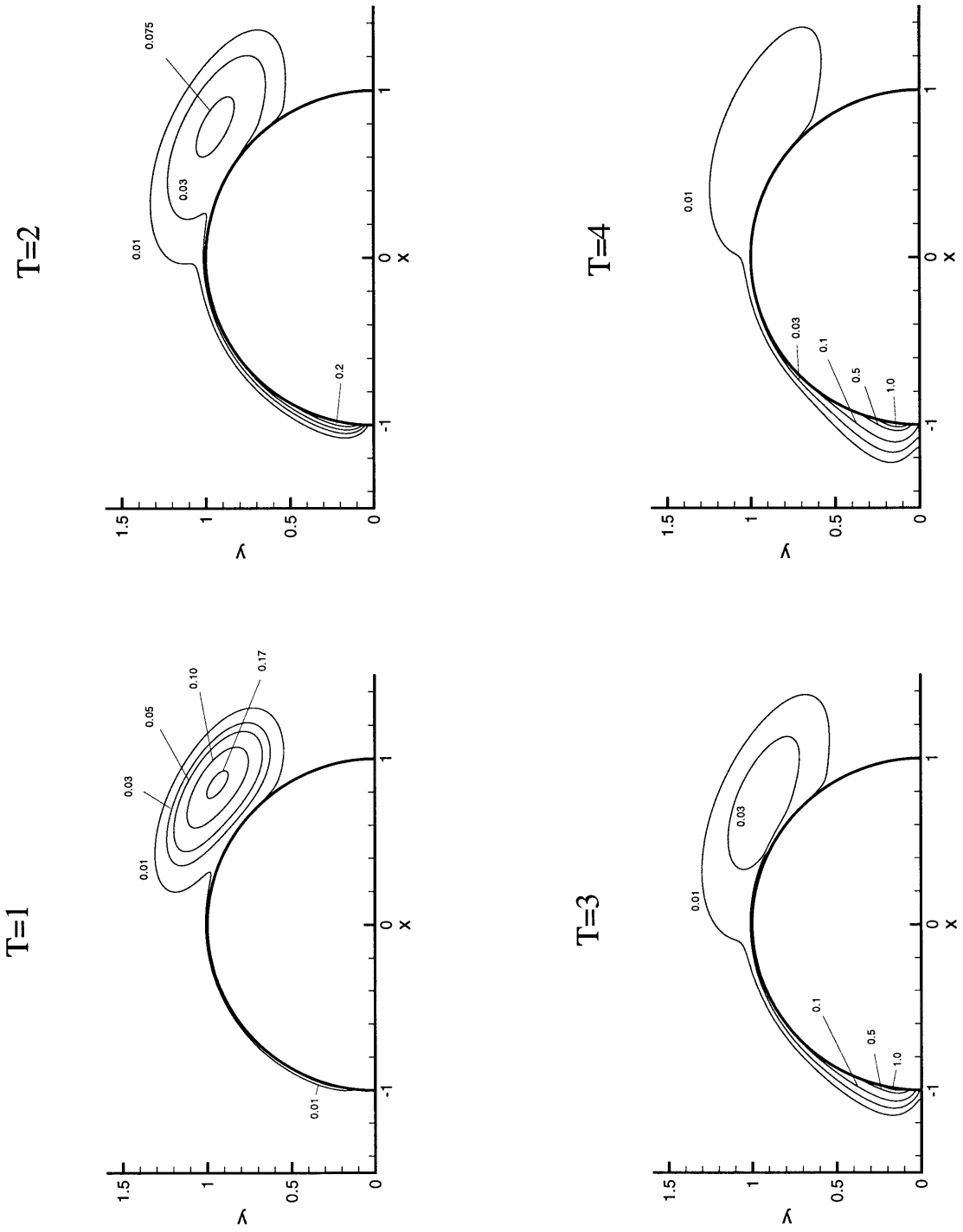

Figure I-4-1: Evolution of particle concentration. Cloud center is initially released at north-east ($r_c' = 1.3$, $\theta_c = 45°$) for $f = 0.666$, $Pe = 1$ and $Sc = 1$.

mainly by convection, since the local concentration gradient is zero. The other peak corrresponds to the accumulation along the coast, designated as P_2, say, and moves along the circular coastline. Note that at $T' = 1$, P_1 has not moved much from its original location owing to the small local convection velocity (cf. figure I-4-1.a). P_2, however, is displaced quite far from the where the particle cloud first reaches the coast. More interesting is that P_2 passes the point where the Eulerian streaming converges around ($r' = 1$, $\theta = 135°$), instead of stopping there. To understand this phenomenon we express in polar form:the component of particle flux along the circular coastline,

$$F_\theta = U_\theta C - E_{\theta r}\frac{\partial C}{\partial r} - \frac{E_{\theta\theta}}{r}\frac{\partial C}{\partial \theta}, \tag{I.4.2}$$

The last term plays a small role in displacement of P_2 where $\partial C/\partial\theta$ vanishes. The second term on the right-hand side stands for the longshore flux due to the radial gradient, a result of the off-diagonal dispersivity, $E_{\theta r}$. As shown in figure I-4-2, $E_{\theta r}$ is positive along the entire rim of the island.

Since $\partial C/\partial r$ is negative, the longshore flux is along the positive θ direction. Now the physical picture is clear:

i) When a peak is formed at the coastline due to local accumulation of particles, it is transported along the direction of increasing θ by both convection and diffusion;

ii) When the peak of accumulation P_2 reaches the converging point of the convection field, the term representing off-diagonal dispersibity $E_{\theta r}\partial C/\partial r$ dominates and tends to move the peak P_2 past the point of velocity convergence. The clockwise convection velocity is too weak to counter the trend until the peak finally is stopped by the straight coastline.

From Figure I-4-1 b-d it can be seen that P_1 moves from its original location (0.9,0.9) in x, y plane to about (0.8,1.0). The concentration at P_2 increases with time due to additional accumulation of particles.

For other locations of initial release, the results are qualitatively the same (see Figure I-4-3 a-d for initial release at ($r' = 1.3, \theta_c = 135°$)).

Thus regardless of the different locations of initial release, the peak of the concen-

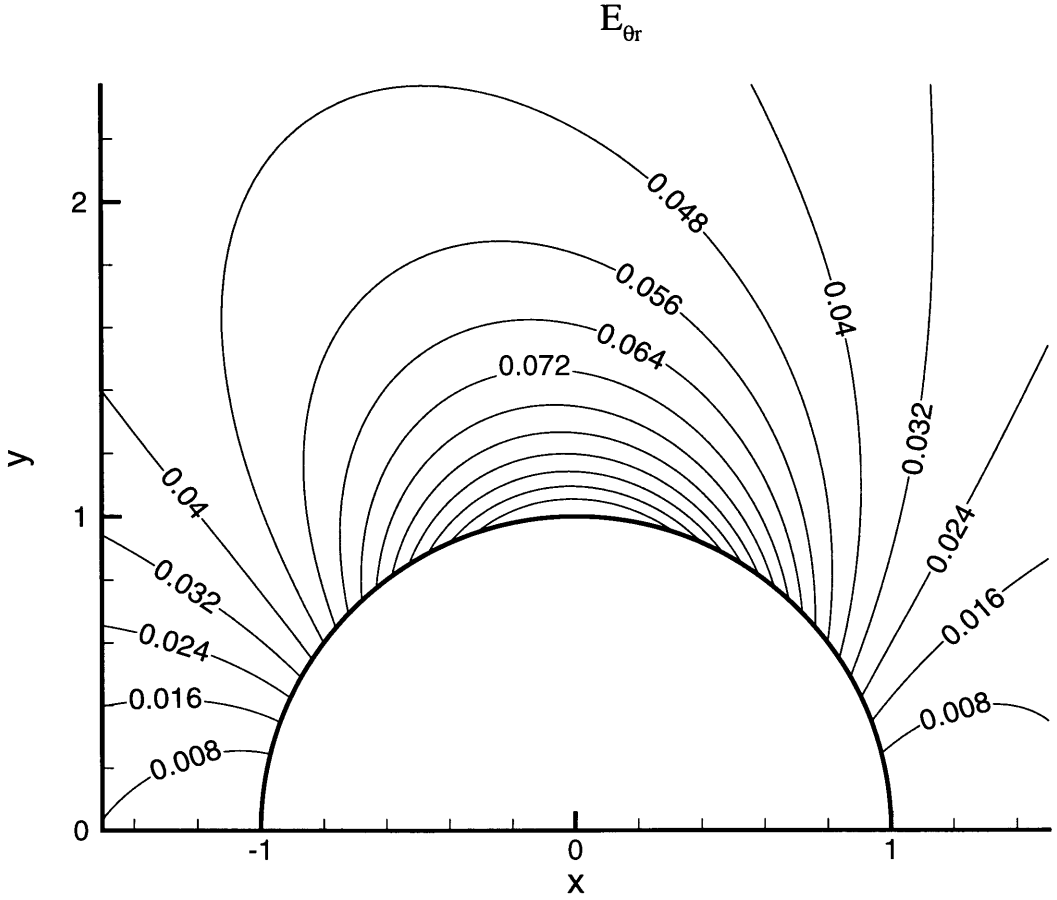

Figure I-4-2: Off-diagonal dispersivity tensor component $E_{\theta r}$ around a circular peninsula for $f = 0.666$, $Pe = 1$, and $Sc = 1$

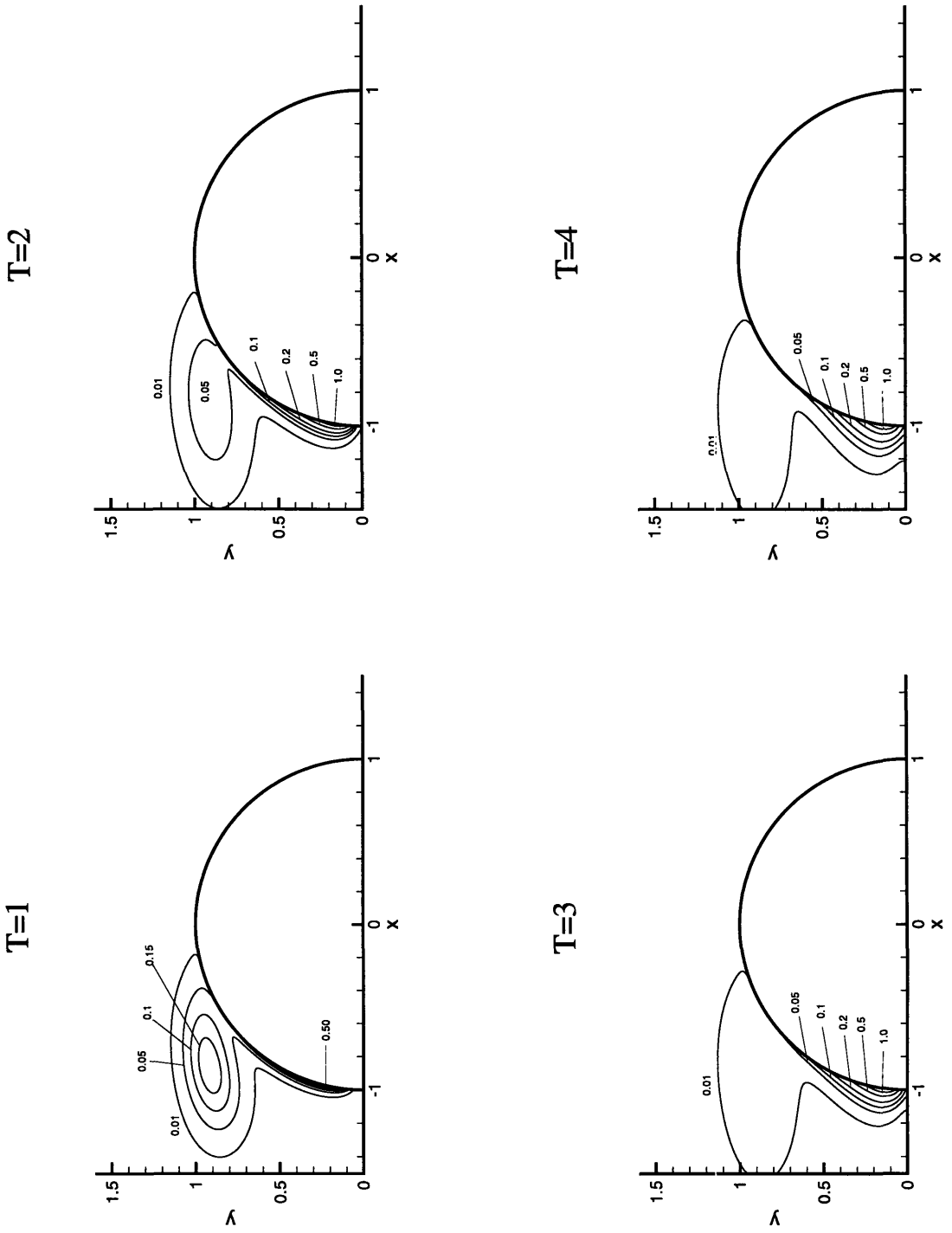

Figure I-4-3: Evolution of particle concentration. Cloud center is initially released at north-west ($r'_c = 1.3$, $\theta_c = 135°$) for $f = 0.666$, $Pe = 1$ and $Sc = 1$.

tration cloud eventually reaches and stays around the stagnation point at $r' = 1, \theta = 180°$.

Along the equator the effects of earth rotation vanish since $f = 0$; the velocity field is symmetrical with respect to the y axis. Accordingly, the convection field and the dispersivity tensor are symmetrical with respect to the y axis. No matter where it is initially released, the cloud finally moves to the coastline and converges to the offshore tip of the peninsula. We only show in figure I-4-4 the results for the case where the center is released at $r' = 1.3, \theta = 45°$.

Thus convection by Eulerian streaming, already predicted by Larmoure and Mei (1977), dominates the phenomenon, unlike the case with $f \neq 0$.

As a confirmation of numerical accuracy, we check that total mass is conserved in the non-erosion case:

$$\begin{aligned} M &= M_0 = \iint C(x,y)dxdy \\ &= \iint C(r,\theta)rdrd\theta \\ &= \iint C(\xi,\eta)e^{2\pi\xi}|J|d\xi d\eta, \end{aligned} \tag{I.4.3}$$

where the Jacobi determinant is given by

$$|J| = \frac{\partial(r,\theta)}{\partial(\zeta,\eta)} = 2\pi^2 r. \tag{I.4.4}$$

With time marching, the computed total mass however, increases slightly due mainly to the temporal accumulation of numerical errors and the inaccuracy in numerical integration for the total mass. The improvement of numerical accuracy by denser grids is shown in the following table where the relative mass increase is shown at a certain time after an initial release at a particular location.

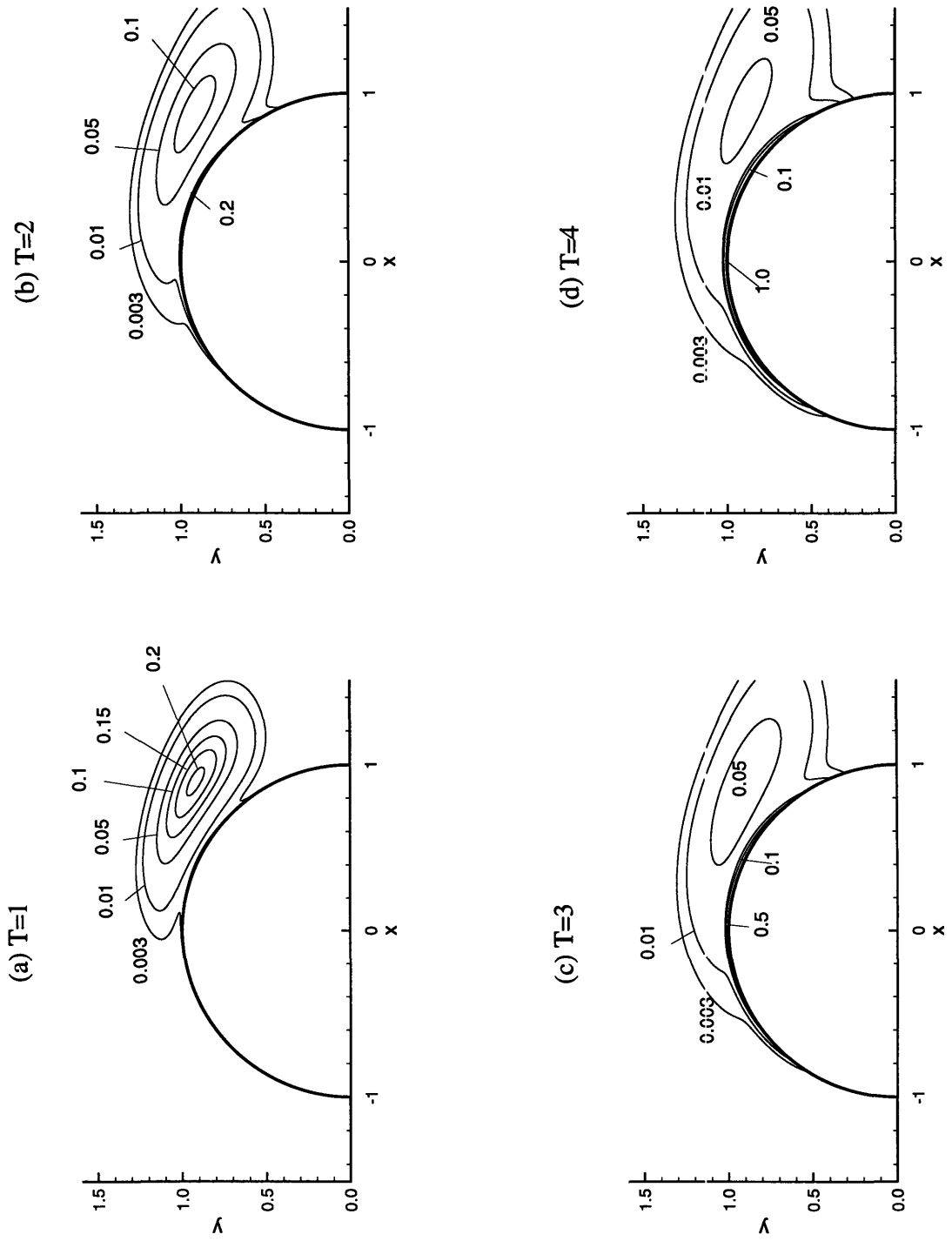

Figure I-4-4: Evolution of particle concentration. Cloud center is initially released at north-east ($r'_c = 1.3$, $\theta_c = 45°$) for $f = 0$, $Pe = 1$ and $Sc = 1$.

Mesh Density		200×200	400×200
$\theta_c = 45°$	$T = 2$	0.27%	0.34%
	$T = 4$	1.9%	1.2%
$\theta_c = 135°$	$T = 2$	1.3%	0.67%
	$T = 4$	3.0%	1.1%

Table I-1: Dependence of numerical accuracy on density of grids

Chapter 5

Resuspension and transport of bottom sediments

We consider a peninsula surrounded by a ring-like strip of erodible seabed covering the region $r_0 < r < r_1$, $0° < \theta < 180°$. The bottom shear stress is dominated by the vertical derivative of the oscillatory horizontal velocity at $z = 0$, which can be evaluated from (2.4) and (2.5),

$$\begin{pmatrix} \tau_{bx} \\ \tau_{by} \end{pmatrix} = \begin{pmatrix} \mu \frac{\partial u^{(1)}}{\partial z} \\ \mu \frac{\partial v^{(1)}}{\partial z} \end{pmatrix}_{z=0} = \frac{\mu}{2\delta} \mathrm{Re} \left\{ \begin{bmatrix} U_0(s+q) - iV_0(q-s) \\ iU_0(q-s) + V_0(s+q) \end{bmatrix} e^{-i\omega t} \right\}, \qquad \text{(I.5.1)}$$

where q and s are defined in (2.8) and (2.9). Limiting our discussion to $f = 2\Omega \sin\phi/\omega < 1$ only, it can be shown that

$$|\tau_b| = \sqrt{\tau_{bx}^2 + \tau_{by}^2} = \frac{\mu}{\delta} \sqrt{U_0^2 + V_0^2} \sqrt{1 - \sqrt{1 - f^2} \sin 2\omega t}, \qquad \text{(I.5.2)}$$

The time-average over a wave period is

$$\langle |\tau_b| \rangle = \frac{\mu I}{2\pi\delta} \sqrt{U_0^2 + V_0^2}, \qquad \text{(I.5.3)}$$

while I denotes the elliptic integral

$$I = 2\int_0^{\pi} dt' \sqrt{1 - \sqrt{1 - f^2 \sin 2t'}} \tag{I.5.4}$$

which can be evaluated numerically.

We now choose the concentration scale to be

$$C_0 = \frac{Pe\ E\mu\ I\omega}{2\pi \mathcal{U}} \frac{r_o^2}{\delta^2} \tag{I.5.5}$$

so that the normalized erosion term on the right of (I.2.98) is

$$\mathcal{E}' = \begin{cases} \sqrt{U_o'^2 +' V_o'^2}, & 1 < r' < r_1' \\ 0, & r' > r_1' \end{cases} \tag{I.5.6}$$

Using (5.39), we find for the semi circular peninsula

$$\mathcal{E}' = \begin{cases} \sqrt{1 + \frac{1}{r^4} - \frac{2\cos 2\theta}{r^2}}, & 1 < r' < r_1' \\ 0, & r' > r_1' \end{cases} \tag{I.5.7}$$

which is plotted for $r_1' = 0.5$ in figure I-5-1.

Note that this spatial variation is symmetrical with respect to the y axis, and is unaffected by earth rotation because of the small size of the peninsula.

Computed results representing the evolution of the sediment concentration are shown for both $f = 0$ and $f = 0.8$. The corrsponding elliptic integrals are $I = 5.65685$ and 6.12751 respectively.

As in the case of a nonerodible bed, once the particles are eroded from the bottom and resuspended, they drift toward the shore, resulting in a very sharp radial gradient. The concentration contours are asymmetrical with respect to y axis for $f \neq 0$, but symmetrical for $f = 0$, as expected. At large times, the peak of the resuspended sediment cloud moves past the region of velocity convergence and eventually settles around the stagnation point at $\theta = 180°$, if $f \neq 0$; see figure I-5-2 for $f = 0.8$.

Without rotation, however, the cloud settles around the point of velocity conver-

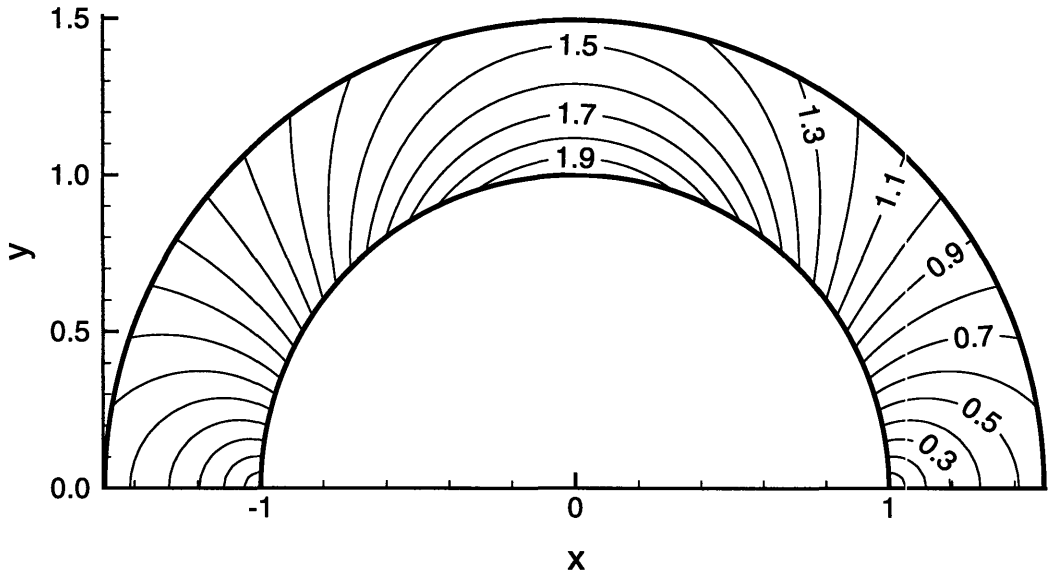

Figure I-5-1: Dimensionless erosion rate around a circular peninsula due to tidal oscillation.

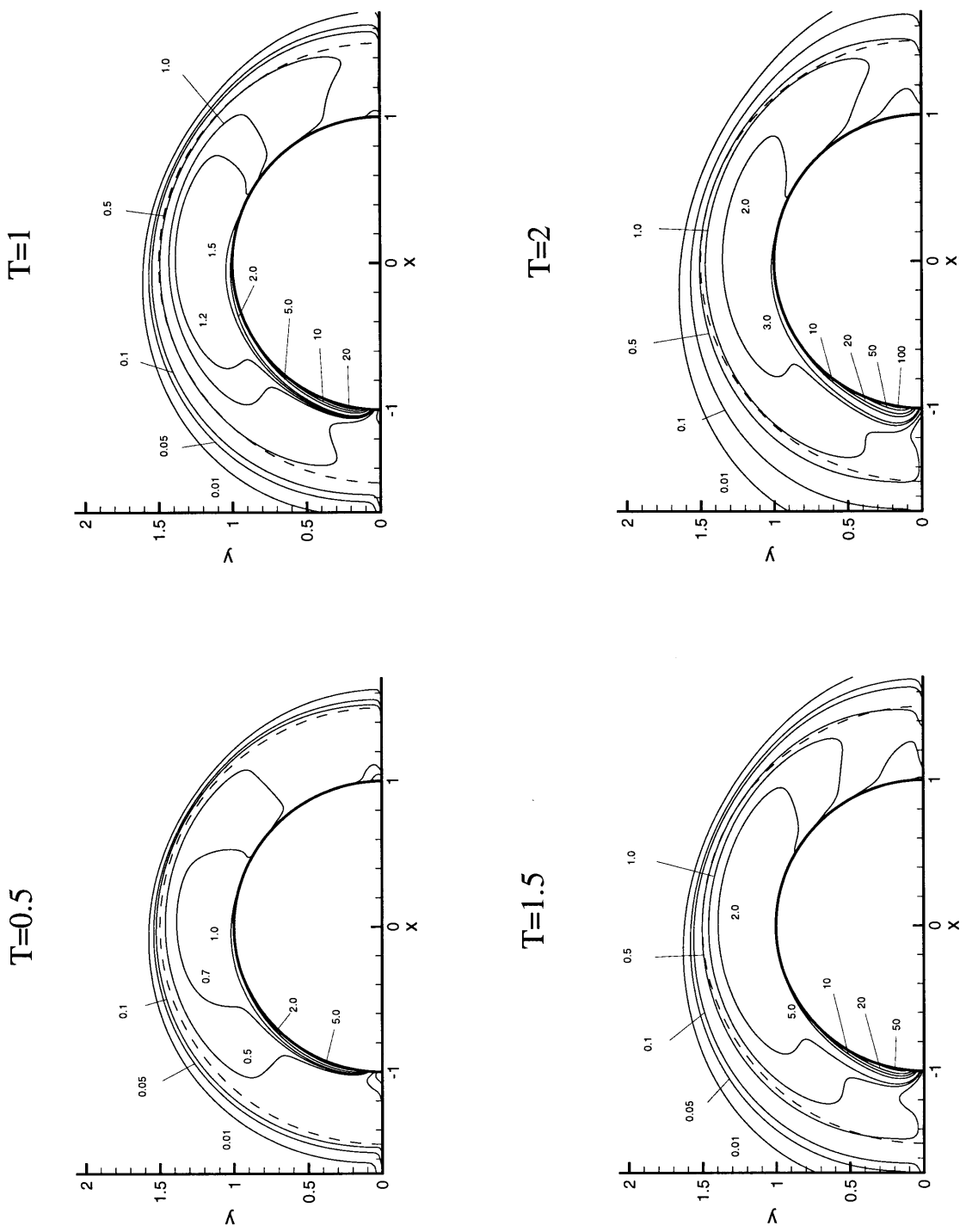

Figure I-5-2: Evolution of concentration of resuspended particles. Dashed curve indicates outer edge of the erodible belt. $f = 0.666$, $Pe = 1$ and $Sc = 1$.

gence; see figure I-5-3.

Since the source term $\mathcal{E}'$ due to erosion is independent of time in our theory, the total mass in suspension increases with time at a constant rate.

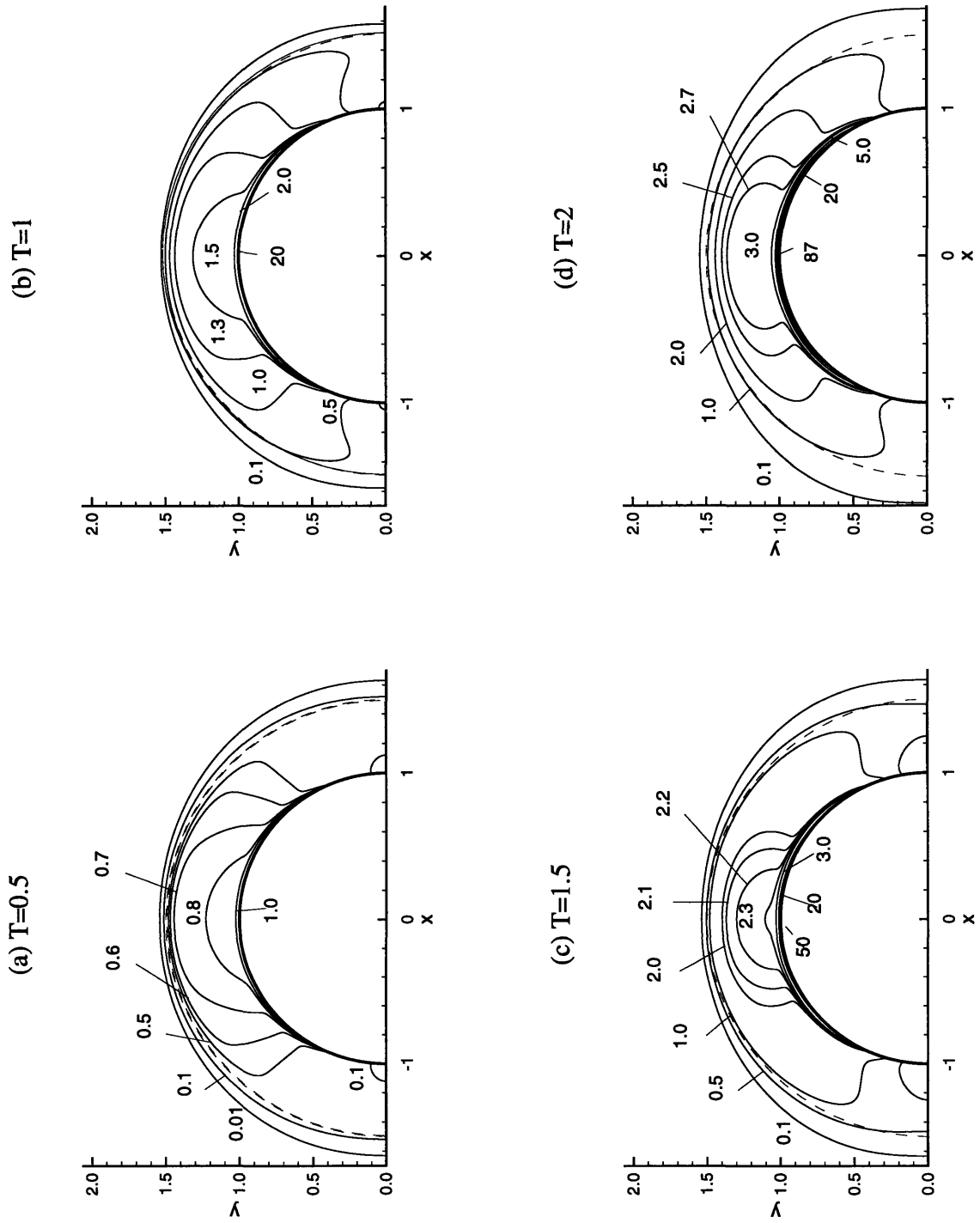

Figure I-5-3: Evolution of concentration of resuspended particles. Dashed curve indicates outer edge of the erodible belt. $f = 0$, $Pe = 1$ and $Sc = 1$.

Chapter 6

Conclusion

It has been shown that the vertical shear indeed enhances the horizontal dispersivities which is much greater than the eddy viscosity and agrees in order of magnitude with that found by Zimmerman (1976, 1977). Both the effective convection and dispersion are functions of the ambient tidal field which is in turn affected by bathymetry and shore configuration. Consequently the convection velocity and dispersion coefficients are in general varying from point to point as a result of the nonuniform ambient flow. We thus infer that in regions near a protruding coastline feature the dispersivities are spatial functions and can not be fixed through limited field data at a few locations.

From numerical simulations we see that the evolution of the concentration contours over time is determined jointly by the steady streaming field and the spatial pattern of the dispersivity tensor. In particular, the center of the particulate cloud (maximum concentration point) is driven purely by the convection prior to its arrival at the bank. With the particles piling up against the vertical wall a negative gradient of concentration in the normal direction to the coastline results and the gradient grows sharper and sharper. This causes the center to be affected by the off-diagonal dispersivity ($E_{\theta r}$ for semicircular peninsula) anywhere $f \neq 0$. Due to the sharp negative gradient this action can overplay the convection and drive the center of cloud to move counterclockwisely away from the convergent point of the convection field.

For further investigation, an extention to variable depth domain is theoretically

challenging. Inclusion of surface wind forcing will make our theory more useful in modeling real situations. The quantitative effect of different choice of eddy viscosity model is also worth further consideration.

Part II

Flow Field in a Basin Forced by a Low-Frequency Wind

Chapter 1

Introduction

A large lake can have great influence on the lives of people who live near its shore. The evaporation which occurs at the air-water interface will increase the humidity of the air and enhance rainfall within a region encompassing the lake. Some lakes serve as sources of drinking water. The large surface water body also recharges the underlying groundwater aquifer which can be a water supply for the nearby region as well. Under these circumstances, protecting the lake from being polluted becomes an important environmental issue. Since sediment particles could be vehicles to spread the contaminants adsorbed on their surfaces, the dispersion of these particles deserves careful investigation. As the first step the flow field in the lake must be determined. The effects of earth rotation and topographical variation are usually considered for the wind-driven flow in a typical natural lake.

The wind-driven circulation in a closed water body has been one of essential topics of hydrodynamics. Numerous theoretical models have been developed in the past several decades (see, for example, Pedlosky, 1979). To study the global circulation in lakes or oceans, the water bodies are normally considered shallow in a sense that the vertical dimension is much smaller than the horizontal length scale. Welander (1957) extended Ekman's pioneering theory on sea-level changes of a deep sea under a steady wind to a shallow sea and, in addition, to the transient situation. At steady state a single linear equation for the surface displacement was derived for general bathemetry and constant eddy viscosity. The water depth was assumed to comparable to

the Ekman layer thickness. It was found that the bottom topography induces surface curvature even with uniform wind. For a general transient wind an integro-differential equation was obtained to predict surface elevation in terms of the local time-histories of the forcing and the response. Numerical computation had not been conducted based on the theory. Stratification in estuarine regions and oceanic basin (with thermocline) is evident and could have a profound influence on the circulation pattern. The role of stratification interacting with depth variation was further investigated by Welander (1968) and it was discovered that essential differences exist between the homogeneous and the two-layer oceans in terms of circulation patterns or strength. The numerical efforts were made later by Liggett & Hadjitheodorou (1969) for steady circulation and Liggett (1969) for the unsteady circulation in shallow, homogeneous lakes by deriving and solving the equation for evolution of pressure distribution. In addition, Lee & Liggett (1970) investigated numerically the wind-induced steady circulation in a two-layer lake of arbitrary bottom and shore configuration. Nonlinear terms was not included for the steady-state behavior.

A two-layer wind-driven ocean model in a doubly connected domain with bottom topography was developed by Krupitsky & Cane (1997). A number of numerical experiments were done on a β plane and showed that the two layers were decoupled in most cases. Reasons for this behavior were given by comparing the relevant terms in the model under various circumstances. The depth variation was found to produce topographic pressure drag which, along with the lateral friction in the upper layer, balances the momentum input due to the wind. Yet no nonlinear effect was considered.

These previous works have indeed demonstrated many interesting features of the wind-driven circulations in closed basins. However, some of them dealt with steady state and are not applicable for predicting transient responses. More in common, these results are all linear. Consequently, steady streaming, which is an interesting response under periodic forcing and determines mean convection of particles, can not be viewed using these models.

Numerical efforts by Sheng (1991) have drawn our attention to a very shallow lake

(such as Lake Okeechobee with an average depth of 3 m) forced by low-frequency periodic wind. For these lakes both the depth and the size are small enough so that certain approximations are possible. We are interested in presenting a theory on the flow field in a shallow basin with an arbitrary bottom topography, driven by a long-period sinusoidal wind. Our approach is to conduct analytical discussion as far as possible to obtain fundamental understanding of the physics. Numerical simulations could then be done based on simplified equations resulting from the theoretical arguements.

We first examine the flow field in a shallow lake forced by a low-frequency wind. Depth variation over space is allowed and a general depth-dependent eddy viscosity is considered. Water density has been taken as a constant which is reasonable for a shallow lake (say, three meters deep for Lake Okeechobee). A constant Coriolis factor is used since the horizontal length scale is yet incomparably small ($O(10^4$ m)) with respect to the earth radius. Since the lake is quite shallow and wind period very long, it is found that the vertical structure of flow field forms a lot faster than any change of forcing takes place. For this quasi-steady problem we develop a perturbation theory to describe the free surface displacement and the velocity field in Chapter 2. It is shown analytically in Chapter 3 that the leading order flow and the steady streaming do not depend on the horizontal extensions of a constant-depth basin under a uniform wind. Finally, in Chapter 4, the response in a rectangular lake of flat bottom is discussed in detail. It is seen that the transient effect of surface oscillation overplays the Coriolis effect for the second order flow and the mass transport results from the interaction between the leading order surface motion and oscillatory velocity. No numerical simulation has been attempted so far in solving the flow over variable depth based on our theory while it is planned as the immediately next step following this research.

Chapter 2

Perturbation Theory

A water body with a small aspect ratio ($h_0/L \ll 1$, with h_0 being mean depth, L horizontal length scale) is considered as a shallow water system. A typical natural lake, like the Lake Okeechobee in Florida, falls in this category. As for the forcing of interest, we consider a sinusoidal wind with a low frequency, say, $\omega = 0.727 \cdot 10^{-4}$ s^{-1}, corresponding to a wind period of one day (Sheng et al, 1991). Under this circumstance, a small dimensionless parameter exists and thus the perturbation method is appliable to give approximate analytical solution in the constant-depth case or simple equations for numerical solution in the varying depth situation. The eddy viscosity is assumed to be independent of the horizontal variation of the flow field to avoid coping with the nonlinearilty otherwise.

2.1 Formulation

Let us set up our reference frame so that x is pointing to the east, y the north and z upward with the datum at the static water surface. The equations of motion for a shallow lake with constant water density read

$$\frac{\partial}{\partial z}(\nu\frac{\partial \mathbf{u}}{\partial z}) + \nu\nabla^2\mathbf{u} - \frac{\nabla p}{\rho} = \frac{\partial \mathbf{u}}{\partial t} + 2\Omega\cos\phi \cdot w\mathbf{i} + \mathbf{f} \times \mathbf{u} + \mathbf{u} \cdot \nabla\mathbf{u} + w\frac{\partial \mathbf{u}}{\partial z}, \quad \text{(II.2.1)}$$

and in the vertical direction,

$$\frac{\partial}{\partial z}(\nu\frac{\partial w}{\partial z}) + \nu\nabla^2 w - \frac{\partial p}{\rho\partial z} - g = \frac{\partial w}{\partial t} - 2\Omega\cos\phi\cdot u + \mathbf{u}\cdot\nabla w + w\frac{\partial w}{\partial z}, \qquad \text{(II.2.2)}$$

where $\nu = \nu(z)$ is the eddy viscosity, $\mathbf{u} = (u, v)$ the horizontal velocity vector, ρ the fluid density, p the pressure, g the gravitational acceleration, $\mathbf{f} = (0, 0, 2\Omega\sin\phi)$, $\Omega = 2\pi/\text{day} = 7.27\cdot 10^{-5}\ \text{s}^{-1}$ the angular speed of the Earth, ϕ the latitude, $\mathbf{i}$ the unit vector in x direction, w the vertical velocity component, and

$$\nabla = (\frac{\partial}{\partial x}, \frac{\partial}{\partial y}). \qquad \text{(II.2.3)}$$

Introduce the following scaling,

$$\begin{aligned}(x, y) = L(x', y'),\ z = h_0 z',\ p = Pp',\ t = t'/\omega,\\ \mathbf{u} = U\mathbf{u}',\ w = (h_0/L)Uw',\ \nu = \nu_0\nu',\end{aligned} \qquad \text{(II.2.4)}$$

where primes denote dimensionless quantities, L the typical length of the lake, $h_0 = (\iint_S h(x,y)dxdy)/S$ the average water depth with S being the total surface area of the lake, P the typical pressure, ω the wind frequency, U the typical horizontal flow speed, $\nu_0 = [\int_{-h_0}^{0}\nu(z)dz]/h_0$. Since in shallow water the net shear stress and pressure force are expected to be of comparable importance, we take

$$P \equiv \frac{\rho L\nu_0 U}{h_0^2}. \qquad \text{(II.2.5)}$$

The dimensionless momentum equations are, with primes omitted,

$$\begin{aligned}\frac{\partial}{\partial z}(\nu\frac{\partial \mathbf{u}}{\partial z}) \quad &+ \quad (h_0/L)^2\nu\nabla^2\mathbf{u} - \nabla p\\ = \epsilon[\frac{\partial \mathbf{u}}{\partial t} + (\mathbf{f}/\omega)\times\mathbf{u}] \quad &+ \quad \frac{Uh_0^2}{L\nu_0}(\mathbf{u}\cdot\nabla\mathbf{u} + w\frac{\partial \mathbf{u}}{\partial z}) + \epsilon(h_0/L)\frac{2\Omega\cos\phi}{\omega}w,\end{aligned} \qquad \text{(II.2.6)}$$

where

$$\epsilon = \frac{\omega h_0^2}{\nu_0} = \frac{h_0^2}{\delta^2} \qquad \text{(II.2.7)}$$

with

$$\delta = \sqrt{\nu_0/\omega} \tag{II.2.8}$$

being the thickness of the shear layer generated by the surface sinusoidal wind, and

$$\begin{aligned}&(h_0/L)^2\frac{\partial}{\partial z}(\nu\frac{\partial w}{\partial z}) + (h_0/L)^4\nu\nabla^2 w - \frac{\partial p}{\rho\partial z} - \frac{gh_0^3}{L\nu_0 U}\\ &= \epsilon(h_0/L)^2\frac{\partial w}{\partial t} - \frac{2\Omega}{\omega}\epsilon(h_0/L)\cos\phi\cdot u + (h_0/L)^2\frac{Uh_0^2}{L\nu_0}(\mathbf{u}\cdot\nabla w + w\frac{\partial w}{\partial z}).\end{aligned} \tag{II.2.9}$$

For estimates let us take the typical values of Lake Okeechobee, $h_0 = 4$ m, $\omega = 7.27\cdot 10^{-5}$ s^{-1}, $\nu_0 = 0.008 \sim 0.02$ m^2/s (from Equation (I.2.2), Soulsby), then $\epsilon = 0.058 \sim 0.145$, namely, $h_0 \ll \delta$. The physical meaning of ϵ can be clearly seen: it signifies how shallow the system is regarding to the thickness of the boundary layer induced by the oscillatory wind forcing. By rewriting

$$\epsilon = \frac{h_0^2/\nu_0}{1/\omega} = \frac{h_0^2/\nu_0}{T/2\pi} \tag{II.2.10}$$

with T being the wind cycle, we can view this small parameter as an indication of how fast it takes for momentum to be transported across the whole depth comparing to the wind period of oscillation. The smallness of ϵ just says that the lake is so shallow that the vertical structure forms before any significant change of the driving force takes place. Owing to this feature, we achieve a lot of simplication in analyzing the problem for we now come up with ordinary differential equations at various orders, as we see later in this chapter. It is readily seen from Equation (II.2.6) that the temporal variation and Coriolis effect are secondary to the balance between the net shear stress and the pressure gradient. Typically, the aspect ratio, h_0/L, is extremely small (for $h_0 = 4$ m, $L = 10^4$ m, $h_0/L = 4\cdot 10^{-4}$). Assuming $h_0/L \lesssim O(\epsilon^2)$, then the horizontal diffusion term drops out from equation (II.2.6) with an error of $O(\epsilon^4)$.

For a shallow water the dynamic boundary condition on the free surface reads

$$-p\mathbf{n} + \rho\nu[(\mathbf{n}\cdot\nabla)\mathbf{u} + n_z\frac{\partial \mathbf{u}}{\partial z} + \mathbf{n}\cdot\nabla\mathbf{u} + n_z\nabla u_z] = \vec{\tau}e^{-it} \quad \text{at } z = \zeta \tag{II.2.11}$$

and in the vertical direction

$$-pn_z + \rho\nu[(\mathbf{n}\cdot\nabla)u_z + \mathbf{n}\cdot\frac{\partial \mathbf{u}}{\partial z} + 2n_z\frac{\partial u_z}{\partial z}] = 0, \quad \text{at } z = \zeta \tag{II.2.12}$$

where $i = \sqrt{-1}$ and ζ is the surface displacement, and $(\mathbf{n}, n_z)$ the unit normal vector at the free surface. The real part of the complex quantities is taken unless otherwise specified. With shallow water assumption $h_0 << L$,

$$\nu\frac{\partial \mathbf{u}}{\partial z} = \frac{\vec{\tau}e^{-it}}{\rho}, \quad \text{at } z = \zeta, \tag{II.2.13}$$

to the leading order. This suggests that the velocity scale is related to the wind stress scale τ_0 by

$$U \equiv \frac{\tau_0 h_0}{\rho\nu_0}, \tag{II.2.14}$$

in which $\tau_0 = \iint_S |\vec{\tau}(x,y)|dxdy/S$ is the typical magnitude of the wind stress. Let us now estimate the dimensionless parameter in front of the nonlinear inertia. Suggested by Csanady (1982, pp.11), $\tau_0/\rho = 10^{-4}$ m^2/s^2 (or $\tau_0 = 0.1$ Pa for the typical wind speed of 7 m/s, which is typical for Lake Okeechobee, see Sheng et al, p 62). Therefore, $U = 10^{-4}\times 4/(0.008 \sim 0.02) = 0.02 \sim 0.05$ m/s and

$$\frac{Uh_0^2}{L\nu_0} = \frac{\tau_0 h_0^3}{\rho L\nu_0^2} = \frac{10^{-4}\times 4^3}{10^4\times(0.008\sim 0.02)^2} = 0.0016 \sim 0.01 = O(\epsilon^2), \tag{II.2.15}$$

It is easy to show that in (II.2.9) the next most significant term to the pressure gradient and the gravitational acceleration is the component of the Coriolis force and

$$\frac{2\Omega}{\omega}\frac{\omega h_0^2}{\nu_0}\frac{h_0}{L} \le O(1)\cdot\epsilon\cdot O(\epsilon^2) = O(\epsilon^3). \tag{II.2.16}$$

Owing to this fact, the vertical momentum equation simply implies a hydrostatic

pressure distribution:

$$\frac{\partial p}{\partial z} = -\frac{\rho g h_0}{P} + O(\epsilon^3) = -\frac{g h_0^3}{L \nu_0 U} + O(\epsilon^3). \tag{II.2.17}$$

Making use of (II.2.5), the dimensionless form of (II.2.12) reads,

$$-p + (h_0/L)[(h_0/L)^2(\frac{\mathbf{n}}{n_z} \cdot \nabla) u_z + \frac{\mathbf{n}}{n_z} \cdot \frac{\partial \mathbf{u}}{\partial z} + 2(h_0/L)^2 \frac{\partial u_z}{\partial z}] = 0. \quad \text{at } z = \zeta \tag{II.2.18}$$

As long as the surface is reasonably flat, namely, $\mathbf{n}/n_z \leq O(h_0/L)$ (we will check this later), we have

$$p = O(h_0/L)^2 \quad z = (A/h_0)\zeta \tag{II.2.19}$$

with ζ being the surface displacement and A its amplitude. Using this boundary condition we obtain

$$p = \frac{g h_0^3}{L \nu_0 U}(\frac{A}{h_0}\zeta - z). \tag{II.2.20}$$

With this Equation (II.2.1) becomes

$$\frac{\partial}{\partial z}(\nu \frac{\partial \mathbf{u}}{\partial z}) - g \nabla \zeta = \frac{\partial \mathbf{u}}{\partial t} + \mathbf{f} \times \mathbf{u} + \mathbf{u} \cdot \nabla \mathbf{u} + w \frac{\partial \mathbf{u}}{\partial z}, \tag{II.2.21}$$

The balance between the two terms on the left side of the above equation suggests

$$A \sim \frac{\nu_0 U L}{g h_0^2} \equiv \frac{\tau_0 L}{\rho g h_0}, \tag{II.2.22}$$

showing that the amplitude of surface displacement, A, is also linearly proportional to the wind stress. With $\tau_0/\rho = 10^{-4}$ m^2/s^2, $L = 10^4$ m, $g = 9.8$ m/s and $h_0 = 4$ m, the typical value of A is therefore 0.026 m.

Consider now the kinematic boundary condition at the free surface,

$$w = \frac{\partial \zeta}{\partial t} + \mathbf{u} \cdot \nabla \zeta, \quad z = \zeta, \tag{II.2.23}$$

which can be written in dimensionless form, with primes omitted again,

$$w = \frac{A\omega L}{h_0 U}\frac{\partial \zeta}{\partial t} + \frac{A}{h_0}\mathbf{u}\cdot\nabla\zeta, \quad z = (A/h_0)\zeta. \tag{II.2.24}$$

We now estimate the parameter in front of the time derivative by the typical physical scales,

$$\frac{A\omega L}{h_0 U} = \frac{0.026 \times 0.727 \cdot 10^{-4} \times 10^4}{4 \times (0.02 \sim 0.05)} = 0.09 \sim 0.23 = O(\epsilon). \tag{II.2.25}$$

It is seen that

$$w = O(\epsilon) \quad z = (A/h_0)\zeta, \tag{II.2.26}$$

which says that the vertical velocity on the free surface is zero at the leading order. Hence,

$$\frac{A}{h_0} = \frac{A\omega L}{h_0 U}\cdot\frac{U h_0^2}{L\nu_0}\cdot\frac{\nu_0}{\omega h_0^2} = O(\epsilon)\cdot O(\epsilon^2)\cdot O(\epsilon^{-1}) = O(\epsilon^2), \tag{II.2.27}$$

and

$$\frac{A}{L} = \frac{A}{h_0}\cdot\frac{h_0}{L} \leq O(\epsilon^4). \tag{II.2.28}$$

This implies that the surface slope is $O(\epsilon^4)$ small, which implies, in turn, that the unit normal vector at the surface will be

$$(\mathbf{n}, n_z) = \frac{(-\partial\zeta/\partial x,\ -\partial\zeta/\partial y,\ 1)}{\sqrt{(\partial\zeta/\partial x)^2 + (\partial\zeta/\partial y)^2 + 1}} \approx (O(\epsilon^4),\ O(\epsilon^4),\ 1). \tag{II.2.29}$$

Indeed, $\mathbf{n}/n_z \leq O(\epsilon^2)$. The dimensionless form of (II.2.11) reads

$$-p\frac{\mathbf{n}}{n_z} + \nu[(\frac{\mathbf{n}}{n_z}\cdot\nabla)\mathbf{u} + \frac{\partial \mathbf{u}}{\partial z} + \frac{\mathbf{n}}{n_z}\cdot\nabla\mathbf{u} + \nabla u_z] = \vec{\tau}e^{-it} \quad \text{at } z = \zeta \tag{II.2.30}$$

Therefore,

$$\nu\frac{\partial \mathbf{u}}{\partial z} = \vec{\tau}e^{-it} + O(\epsilon^4), \quad \text{at } z = (A/h_0)\zeta, \tag{II.2.31}$$

After Taylor expansion about $z = 0$, we write down the dynamic boundary condition at the mean surface

$$\nu \frac{\partial \mathbf{u}}{\partial z} = \vec{\tau} e^{-it} - \alpha \epsilon^2 \zeta \frac{\partial}{\partial z}(\nu \frac{\partial \mathbf{u}}{\partial z}) + O(\epsilon^4), \quad \text{at } z = 0, \tag{II.2.32}$$

where

$$\alpha = \frac{A}{h_0}/\epsilon^2 = \frac{\tau_0 L \nu_0^2}{\rho g \omega^2 h_0^6} = O(1), \tag{II.2.33}$$

indicating the nonlinearity is at $O(\epsilon^2)$. Integrating the local mass conservation equation for an incompressible fluid

$$\nabla \cdot \mathbf{u} + \frac{\partial w}{\partial z} = 0 \tag{II.2.34}$$

and making use of the exact kinematic boundary conditions at the free surface and at the bed, the integral form of continuity equation results

$$\frac{\partial \zeta}{\partial t} + \nabla \cdot \mathbf{Q} = 0, \tag{II.2.35}$$

in which

$$\mathbf{Q} = \int_{-h}^{\zeta} \mathbf{u} dz = \mathbf{Q}_0 + \int_0^{\zeta} \mathbf{u} dz \tag{II.2.36}$$

is the total flux across the water depth, with $\mathbf{Q}_0 = \int_{-h}^{0} \mathbf{u} dz$ being the discharge beneath the static surface. In dimensionless terms, we have

$$\mathbf{Q} = \mathbf{Q}_0 + \int_0^{\alpha \epsilon^2 \zeta} \mathbf{u} dz, \tag{II.2.37}$$

and

$$\int_0^{\alpha \epsilon^2 \zeta} \mathbf{u} dz = \alpha \epsilon^2 (\zeta \mathbf{u}|_{z=0}) + O(\epsilon^4), \tag{II.2.38}$$

by Taylor expansion. Now the dimensionless continuity equation (II.2.35) reads

$$S_t \epsilon \frac{\partial \zeta}{\partial t} + \alpha \epsilon^2 \nabla \cdot (\zeta \mathbf{u}|_{z=0}) + \nabla \cdot \mathbf{Q}_0 = O(\epsilon^4), \tag{II.2.39}$$

where

$$S_t = \frac{A\omega L}{Uh_0}/\epsilon = \frac{L^2\nu_0^2}{gh_0^5} = O(1) \tag{II.2.40}$$

is a modified Strouhal number.

Let us now consider the lateral boundary condition. We point out here that our theory is good only for the flow field far from the bank. In the vicinity of the lateral boundary, the horizontal length scale is much smaller than L and the shallow water assumption fails. The complete solution of this physical problem should be a combination of near field and far field with a matching in between. However, the three dimensional near field is beyond the scope of current research. We will restrict our interest to the far-field, which is the majar portiion in a shallow lake. A lateral boundary condition of integral form is given at the outer edge of the lateral boundary layer of thickness $O(h_0)$:

$$Q_n = 0, \quad \text{at the outer edge of lateral boundary layer,} \tag{II.2.41}$$

where subscript n denotes the component of the flux along the direciton, $\mathbf{n}$, normal to the bank. To estimate the accuracy of the above condition we examine the lateral boundary layer. The thickness of this layer δ_l should be at the order of the water depth since the horizontal diffusion must be equally important to the vertical one within the layer. Therefore, in nondimensional quantities,

$$\begin{aligned} Q_n &= \int_{-h}^{\alpha\epsilon^2\zeta} u_n|_{n=\delta/L} dz \\ &= \int_{-h}^{\alpha\epsilon^2\zeta} [u_n|_{n=0} + \frac{\partial u_n}{\partial n}|_{n=0}\frac{\delta_l}{L} + O(\frac{\delta_l^2}{L^2})]dz. \end{aligned} \tag{II.2.42}$$

Clearly

$$u_n|_{n=0} = 0. \tag{II.2.43}$$

To avoid dealing with the complex run-up phenomenon we assume that there is a vertical wall at the bank where $n = 0$. On the wall all velocity components vanish

and by continuity,

$$\frac{\partial u_n}{\partial n}|_{n=0} = 0. \tag{II.2.44}$$

Consequently,

$$Q_n = \int_{-h}^{\alpha\epsilon^2\zeta} O(\frac{\delta^2}{L^2})dz = O(\frac{\delta_l^2}{L^2}) \leq O(\epsilon^4). \tag{II.2.45}$$

In summary, we now have the equation of motion

$$\frac{\partial}{\partial z}(\nu\frac{\partial \mathbf{u}}{\partial z}) - \nabla\zeta = \epsilon[\frac{\partial \mathbf{u}}{\partial t} + (\mathbf{f}/\omega) \times \mathbf{u}] + Re\epsilon^2(\mathbf{u}\cdot\nabla\mathbf{u} + w\frac{\partial \mathbf{u}}{\partial z}) + O(\epsilon^3) \tag{II.2.46}$$

with Reynolds number

$$Re = \frac{Uh_0^2}{L\nu_0}/\epsilon^2 = \frac{\tau_0/\rho}{L\omega^2 h_0} = O(1), \tag{II.2.47}$$

the surface dynamic boundary condition

$$\nu\frac{\partial \mathbf{u}}{\partial z} = \vec{\tau}e^{-it} - \alpha\epsilon^2\zeta\frac{\partial}{\partial z}(\nu\frac{\partial \mathbf{u}}{\partial z}) + O(\epsilon^4), \quad \text{at } z = 0, \tag{II.2.48}$$

the bottom boundary condition

$$\mathbf{u} = 0, \quad w = 0, \quad z = -h(x,y), \tag{II.2.49}$$

and the depth-integrated mass conservation

$$S_t\epsilon\frac{\partial\zeta}{\partial t} + \nabla\cdot\mathbf{Q}_0 + \alpha\epsilon^2\nabla\cdot(\zeta\mathbf{u}|_{z=0}) + O(\epsilon^4) = 0. \tag{II.2.50}$$

Along the bank of the lake the normal flux vanishes,

$$Q_n = (Q_0)_n + \alpha\epsilon^2\zeta u_n|_{z=0} = O(\epsilon^4), \quad \text{along the bank, B} \tag{II.2.51}$$

where the subscript n denotes the component in the direction normal to the bank. Since this leads to a Neumann boundary value problem we add a global law of mass

conservation for a unique solution,

$$\iint_S \zeta dxdy = 0, \tag{II.2.52}$$

where S is the total surface area of the lake.

It is clear that the above equation set is accurate up to $O(\epsilon^2)$ and the assumptions of the magnitudes of the nondimensional parameters are so far consistent. Taking advantage of the fact that the time dependency and the effect of earth rotation appear at $O(\epsilon)$ and that the nonlinear inertia at $O(\epsilon^2)$, we can apply the perturbation analysis and obtain quasi-steady linear equations at various orders of ϵ. Then, the vertical structure of the flow field can be readily worked out by integrating the momentum equation twice and making use of the dynamic boundary conditions at the surface and the bottom. The horizontal velocity is then written in terms of the surface slope. Substituting into the integral continuity equation, we will end up a single equation with single unknown, ζ. With the lateral boundary condition of no normal flux at the bank, the surface elevation can be determined at each order, and so can the flow field, accordingly. The vertical velocity component is then determined through mass conservation

$$w = -\int_{-h(x,y)}^{z} \nabla \cdot \mathbf{u} dz'. \tag{II.2.53}$$

2.2 Solution

We now proceed to implement the approach stated above. Expanding the velocity components and surface displacement with respect to ϵ,

$$\mathbf{u} = \mathbf{u}^{(0)} + \epsilon \mathbf{u}^{(1)} + \epsilon^2 \mathbf{u}^{(2)} + \cdots, \tag{II.2.54}$$

$$w = w^{(0)} + \epsilon w^{(1)} + \epsilon^2 w^{(2)} + \cdots, \tag{II.2.55}$$

$$\zeta = \zeta^{(0)} + \epsilon \zeta^{(1)} + \epsilon^2 \zeta^{(2)} + \cdots, \tag{II.2.56}$$

we collect terms at the leading order,

$$\frac{\partial}{\partial z}(\nu\frac{\partial \mathbf{u}^{(0)}}{\partial z}) - \nabla\zeta^{(0)} = 0, \tag{II.2.57}$$

$$\mathbf{u}^{(0)} = 0, \quad \text{at } z = -h, \tag{II.2.58}$$

$$\nu\frac{\partial \mathbf{u}^{(0)}}{\partial z} = \vec{\tau}e^{-it}, \quad \text{at } z = 0, \tag{II.2.59}$$

$$\nabla \cdot \mathbf{Q_0}^{(0)} = 0, \tag{II.2.60}$$

$$(Q_0^{(0)})_n = 0, \quad \text{at the bank.} \tag{II.2.61}$$

The Coriolis factor $\mathbf{f}$ does not show up at all at this order. We, therefore, expect that no effect of earth rotation will be found in the response of the system to the wind at the leading order. Integrating (II.2.57) with respect to z and making use of the dynamic boundary condition at the surface,

$$\nu\frac{\partial \mathbf{u}^{(0)}}{\partial z} = \vec{\tau}e^{-it} + \nabla\zeta^{(0)}z, \tag{II.2.62}$$

and integrating once again with the no slip condition on the bottom,

$$\mathbf{u}^{(0)} = f_1\vec{\tau}e^{-it} + f_2\nabla\zeta^{(0)}, \tag{II.2.63}$$

where

$$f_1 = \int_{-h}^{z} \frac{1}{\nu(z')}dz', \tag{II.2.64}$$

$$f_2 = \int_{-h}^{z} \frac{z'}{\nu(z')}dz', \tag{II.2.65}$$

Therefore, the flux is

$$\mathbf{Q_0}^{(0)} = \vec{\tau}e^{-it}\int_{-h}^{0} f_1 dz + \int_{-h}^{0} f_2 dz \nabla\zeta^{(0)}, \tag{II.2.66}$$

Equation (II.2.60) then gives the governing equation for $\zeta^{(0)}$.

$$e^{-it}\nabla \cdot (\vec{\tau}\int_{-h}^{0} f_1 dz) + \nabla \cdot (\int_{-h}^{0} f_2 dz \nabla\zeta^{(0)}) = 0, \tag{II.2.67}$$

with the lateral boundary condition

$$e^{-it}(\tau_n \int_{-h}^{0} f_1 dz) + \frac{\partial \zeta^{(0)}}{\partial n} \int_{-h}^{0} f_2 dz = 0, \quad \text{at the bank,} \tag{II.2.68}$$

and the constraint of mass conservation

$$\iint_S \zeta^{(0)} dx dy = 0. \tag{II.2.69}$$

The above three equations will determine uniquely the solution for $\zeta^{(0)}$. Subsequently, the leading order velocity can be obtained from (II.2.63). And

$$w^{(0)} = -\int_{-h(x,y)}^{z} \nabla \cdot \mathbf{u}^{(0)} dz'. \tag{II.2.70}$$

At the next order $O(\epsilon)$,

$$\frac{\partial}{\partial z}(\nu \frac{\partial \mathbf{u}^{(1)}}{\partial z}) - \nabla \zeta^{(1)} = \frac{\partial \mathbf{u}^{(0)}}{\partial t} + \frac{\mathbf{f}}{\omega} \times \mathbf{u}^{(0)}, \tag{II.2.71}$$

$$\mathbf{u}^{(1)} = 0, \quad \text{at } z = -h, \tag{II.2.72}$$

$$\nu \frac{\partial \mathbf{u}^{(1)}}{\partial z} = 0, \quad \text{at } z = 0, \tag{II.2.73}$$

$$\nabla \cdot \mathbf{Q}_0^{(1)} = -S_t \frac{\partial \zeta^{(0)}}{\partial t}, \tag{II.2.74}$$

$$(Q_0^{(1)})_n = 0, \quad \text{along the bank, B,} \tag{II.2.75}$$

where the subscript n denotes the component in the direction normal to the bank. The flow field at this order starts to be affected by the Coriolis force. Integrating once from $z' = z$ to $z' = 0$ and making use of the dynamic boundary condition,

$$\nu \frac{\partial \mathbf{u}^{(1)}}{\partial z} = z \nabla \zeta^{(1)} - \frac{\partial}{\partial t} \mathbf{Q}_*^{(0)} - \frac{\mathbf{f}}{\omega} \times \mathbf{Q}_*^{(0)}, \tag{II.2.76}$$

where

$$\mathbf{Q}_*^{(0)} = \int_z^0 \mathbf{u}^{(0)} dz, \tag{II.2.77}$$

which is the flux between the mean sea level and an arbitrary depth z. Integrating once more, we get

$$\mathbf{u}^{(1)} = f_2 \nabla \zeta^{(1)} - \frac{\partial}{\partial t} \int_{-h}^{z} \frac{1}{\nu} \mathbf{Q}_*^{(0)} dz' - \frac{\mathbf{f}}{\omega} \times \int_{-h}^{z} \frac{1}{\nu} \mathbf{Q}_*^{(0)} dz', \tag{II.2.78}$$

hence,

$$\mathbf{Q}_0{}^{(1)} = \int_{-h}^{0} f_2 dz \nabla \zeta^{(1)} - \frac{\partial}{\partial t} \int_{-h}^{0} dz \int_{-h}^{z} \frac{1}{\nu} \mathbf{Q}_*^{(0)} dz' - \frac{\mathbf{f}}{\omega} \times \int_{-h}^{0} dz \int_{-h}^{z} \frac{1}{\nu} \mathbf{Q}_*^{(0)} dz', \tag{II.2.79}$$

Substituting (II.2.79) in Equation (II.2.74) gives

$$\begin{aligned} &\nabla \cdot (\int_{-h}^{0} f_2 dz \nabla \zeta^{(1)}) - \frac{\partial}{\partial t} \nabla \cdot (\int_{-h}^{0} dz \int_{-h}^{z} \frac{1}{\nu} \mathbf{Q}_*^{(0)} dz') \\ &-\nabla \cdot (\frac{\mathbf{f}}{\omega} \times \int_{-h}^{0} dz \int_{-h}^{z} \frac{1}{\nu} \mathbf{Q}_*^{(0)} dz') = -S_t \frac{\partial \zeta^{(0)}}{\partial t}, \quad \text{in S} \end{aligned} \tag{II.2.80}$$

From (II.2.75) we get

$$\begin{aligned} &\int_{-h}^{0} f_2 dz \frac{\partial \zeta^{(1)}}{\partial n} - \frac{\partial}{\partial t} \int_{-h}^{0} dz \int_{-h}^{z} \frac{1}{\nu} \int_{z'}^{0} u_n^{(0)} dz'' dz' \\ &-(\frac{\mathbf{f}}{\omega} \times \int_{-h}^{0} dz \int_{-h}^{z} \frac{1}{\nu} \mathbf{Q}_*^{(0)} dz')_n = 0, \quad \text{on B} \end{aligned} \tag{II.2.81}$$

and from (II.2.52) the constraint

$$\iint_S \zeta^{(1)} dx dy = 0. \tag{II.2.82}$$

These three equations will give $\zeta^{(1)}$ and subsequently the velocity at this order is found. In addition,

$$w^{(1)} = -\int_{-h(x,y)}^{z} \nabla \cdot \mathbf{u}^{(1)} dz'. \tag{II.2.83}$$

At the next order $O(\epsilon^2)$,

$$\frac{\partial}{\partial z}(\nu\frac{\partial \mathbf{u}^{(2)}}{\partial z}) - \nabla\zeta^{(2)} = \frac{\partial \mathbf{u}^{(1)}}{\partial t} + \frac{\mathbf{f}}{\omega} \times \mathbf{u}^{(1)} + Re(\mathbf{u}^{(0)} \cdot \nabla\mathbf{u}^{(0)} + w^{(0)}\frac{\partial \mathbf{u}^{(0)}}{\partial z}), \quad \text{(II.2.84)}$$

and

$$\mathbf{u}^{(2)} = 0, \quad \text{at } z = -h, \quad \text{(II.2.85)}$$

$$\nu\frac{\partial \mathbf{u}^{(2)}}{\partial z} = -\alpha\zeta^{(0)}\frac{\partial}{\partial z}(\nu\frac{\partial \mathbf{u}^{(0)}}{\partial z}), \quad \text{at } z = 0, \quad \text{(II.2.86)}$$

$$\nabla \cdot \mathbf{Q}_0{}^{(2)} = -S_t\frac{\partial \zeta^{(1)}}{\partial t} - \alpha\nabla \cdot (\zeta^{(0)}\mathbf{u}^{(0)}|_{z=0}), \quad \text{(II.2.87)}$$

$$(Q_0^{(2)})_n = -\alpha\zeta^{(0)}u_n^{(0)}|_{z=0}, \quad \text{along the bank.} \quad \text{(II.2.88)}$$

The vertical structure of horizontal flow at this order are affected by the transient and Coriolis terms associated with the flow at $O(\epsilon)$.

Integrating once with respect to z from z to 0 and making use of the dynamic boundary condition,

$$\begin{aligned} \nu\frac{\partial \mathbf{u}^{(2)}}{\partial z} &= \nabla\zeta^{(2)}z - \frac{\partial}{\partial t}\mathbf{Q}_*^{(1)} - \frac{\mathbf{f}}{\omega} \times \mathbf{Q}_*^{(1)} - Re\int_z^0 \mathbf{R}^{(0)}dz' \\ &- \alpha\zeta^{(0)}\frac{\partial}{\partial z}(\nu\frac{\partial \mathbf{u}^{(0)}}{\partial z})|_{z=0}, \end{aligned} \quad \text{(II.2.89)}$$

where

$$\mathbf{Q}_*^{(1)} = \int_z^0 \mathbf{u}^{(1)}dz, \quad \text{(II.2.90)}$$

$$\mathbf{R}^{(0)} = \mathbf{u}^{(0)} \cdot \nabla\mathbf{u}^{(0)} + w^{(0)}\frac{\partial \mathbf{u}^{(0)}}{\partial z}. \quad \text{(II.2.91)}$$

Integrating one more time, we get

$$\begin{aligned} \mathbf{u}^{(2)} &= f_2\nabla\zeta^{(2)} - \frac{\partial}{\partial t}\int_{-h}^z \frac{1}{\nu}\mathbf{Q}_*^{(1)}dz' - \frac{\mathbf{f}}{\omega} \times \int_{-h}^z \frac{1}{\nu}\mathbf{Q}_*^{(1)}dz' \\ &- Re\int_{-h}^z dz'\int_{z'}^0 \mathbf{R}^{(0)}dz''dz' - \alpha f_1\zeta^{(0)}\frac{\partial}{\partial z}(\nu\frac{\partial \mathbf{u}^{(0)}}{\partial z})|_{z=0}, \end{aligned} \quad \text{(II.2.92)}$$

hence,

$$\begin{aligned}\mathbf{Q}_0{}^{(2)} &= \int_{-h}^{0} f_2 dz \nabla\zeta^{(2)} - \frac{\partial}{\partial t}\int_{-h}^{0} dz \int_{-h}^{z} \frac{1}{\nu}\mathbf{Q}_*^{(1)} dz' \\ &- \frac{\mathbf{f}}{\omega} \times \int_{-h}^{0} dz \int_{-h}^{z} \frac{1}{\nu}\mathbf{Q}_*^{(1)} dz' - Re \int_{-h}^{0} dz \int_{-h}^{z} dz' \int_{z'}^{0} \mathbf{R}^{(0)} dz'' dz' \\ &- \alpha \int_{-h}^{0} f_1 dz \zeta^{(0)} \frac{\partial}{\partial z}(\nu \frac{\partial \mathbf{u}^{(0)}}{\partial z})|_{z=0}. \end{aligned} \tag{II.2.93}$$

It then follows Equation (II.2.87) that

$$\begin{aligned}\nabla \cdot (\int_{-h}^{0} f_2 dz \nabla\zeta^{(2)}) &- \frac{\partial}{\partial t}\nabla \cdot (\int_{-h}^{0} dz \int_{-h}^{z} \frac{1}{\nu}\mathbf{Q}_*^{(1)} dz') \\ &- \nabla \cdot (\frac{\mathbf{f}}{\omega} \times \int_{-h}^{0} dz \int_{-h}^{z} \frac{1}{\nu}\mathbf{Q}_*^{(1)} dz') \\ &- Re\nabla \cdot (\int_{-h}^{0} dz \int_{-h}^{z} dz' \int_{z'}^{0} \mathbf{R}^{(0)} dz'' dz') \\ &- \alpha\nabla \cdot (\int_{-h}^{0} f_1 dz \zeta^{(0)} \frac{\partial}{\partial z}(\nu \frac{\partial \mathbf{u}^{(0)}}{\partial z})|_{z=0}) + St\frac{\partial \zeta^{(1)}}{\partial t} \\ &+ \alpha\nabla \cdot (\zeta^{(0)}\mathbf{u}^{(0)})|_{z=0} = 0, \qquad \text{in S} \end{aligned} \tag{II.2.94}$$

with the boundary condition

$$\begin{aligned}\frac{\partial \zeta^{(2)}}{\partial n}\int_{-h}^{0} f_2 dz &- \frac{\partial}{\partial t}\int_{-h}^{0} dz \int_{-h}^{z} \frac{1}{\nu}\int_{z'}^{0} u_n^{(1)} dz'' dz' \\ &- (\frac{\mathbf{f}}{\omega} \times \int_{-h}^{0} dz \int_{-h}^{z} \frac{1}{\nu}\int_{z'}^{0} \mathbf{u}^{(1)} dz'' dz')_n \\ &- Re \int_{-h}^{0} dz \int_{-h}^{z} dz' \int_{z'}^{0} R_n{}^{(0)} dz'' dz' \\ &- \alpha \int_{-h}^{0} f_1 dz \zeta^{(0)} \frac{\partial}{\partial z}(\nu \frac{\partial u_n{}^{(0)}}{\partial z}) \\ &+ \alpha\zeta^{(0)} u_n{}^{(0)}|_{z=0} = 0, \qquad \text{on B} \end{aligned} \tag{II.2.95}$$

and

$$\iint_S \zeta^{(2)} dx dy = 0. \tag{II.2.96}$$

The three equations (II.2.94), (II.2.95) and (II.2.96) will be solved for $\zeta^{(2)}$. Consequently the instantaneous horizontal velocity can be determined through Equa-

tion (II.2.92). In addition,

$$w^{(2)} = -\int_{-h}^{z} \nabla \cdot \mathbf{u}^{(2)} dz'. \tag{II.2.97}$$

Let us limit our inquiries to steady streaming only, and take time averages over a wind period. With angle brackets denoting time-averages, we get from (II.2.84)-(II.2.88)

$$\frac{\partial}{\partial z}(\nu \frac{\partial \langle \mathbf{u}^{(2)} \rangle}{\partial z}) - \nabla \langle \zeta^{(2)} \rangle = Re(\langle \mathbf{u}^{(0)} \cdot \nabla \mathbf{u}^{(0)} \rangle + \langle w^{(0)} \frac{\partial \mathbf{u}^{(0)}}{\partial z} \rangle), \tag{II.2.98}$$

$$\langle \mathbf{u}^{(2)} \rangle = 0, \quad \text{at } z = -h, \tag{II.2.99}$$

$$\nu \frac{\partial \langle \mathbf{u}^{(2)} \rangle}{\partial z} = -\alpha \langle \zeta^{(0)} \frac{\partial}{\partial z}(\nu \frac{\partial \mathbf{u}^{(0)}}{\partial z}) \rangle, \quad \text{at } z = 0, \tag{II.2.100}$$

$$\nabla \cdot \langle \mathbf{Q}_0{}^{(2)} \rangle = -\alpha \nabla \cdot \langle \zeta^{(0)} \mathbf{u}^{(0)}|_{z=0} \rangle, \tag{II.2.101}$$

$$\langle (Q_0^{(2)})_n \rangle = -\alpha \langle \zeta^{(0)} u_n^{(0)} \rangle, \quad \text{at the bank.} \tag{II.2.102}$$

In the forcing terms in the above equation set, only the leading order flow quantities play a role in the steady streaming at $O(\epsilon^2)$. Since the solutions at $O(1)$ are independent of the Coriolis force, earth rotation plays no role on the time-averaged flow quantities at this order. For a lake with constant depth, the averaged mass transport will therefore be confined in vertical planes (characteristic planes) parallel to the wind stress.

Integrating once and making use of the dynamic boundary condition (II.2.100), we get

$$\begin{aligned} \nu \frac{\partial \langle \mathbf{u}^{(2)} \rangle}{\partial z} &= \nabla \langle \zeta^{(2)} \rangle z - Re \int_z^0 \langle \mathbf{R}^{(0)} \rangle dz' \\ &- \alpha \langle \zeta^{(0)} \frac{\partial}{\partial z}(\nu \frac{\partial \mathbf{u}^{(0)}}{\partial z})|_{z=0} \rangle, \end{aligned} \tag{II.2.103}$$

where

$$\langle \mathbf{R}^{(0)} \rangle = \langle \mathbf{u}^{(0)} \cdot \nabla \mathbf{u}^{(0)} \rangle + \langle w^{(0)} \frac{\partial \mathbf{u}^{(0)}}{\partial z} \rangle. \tag{II.2.104}$$

Integrating once again, we get

$$\begin{aligned}\langle \mathbf{u}^{(2)} \rangle &= f_2 \nabla \langle \zeta^{(2)} \rangle - Re \int_{-h}^{z} dz' \int_{z'}^{0} \langle \mathbf{R}^{(0)} \rangle dz'' dz' \\ &- \alpha f_1 \langle \zeta^{(0)} \frac{\partial}{\partial z} (\nu \frac{\partial \mathbf{u}^{(0)}}{\partial z})|_{z=0} \rangle, \end{aligned} \tag{II.2.105}$$

and hence,

$$\begin{aligned}\langle \mathbf{Q}_0{}^{(2)} \rangle &= \int_{-h}^{0} f_2 dz \nabla \langle \zeta^{(2)} \rangle - Re \int_{-h}^{0} dz \int_{-h}^{z} dz' \int_{z'}^{0} \langle \mathbf{R}^{(0)} \rangle dz'' dz' \\ &- \alpha \int_{-h}^{0} f_1 dz \langle \zeta^{(0)} \frac{\partial}{\partial z} (\nu \frac{\partial \mathbf{u}^{(0)}}{\partial z})|_{z=0} \rangle, \end{aligned} \tag{II.2.106}$$

it then follows Equation (II.2.101) that

$$\begin{aligned}\nabla \cdot (\int_{-h}^{0} f_2 dz \nabla \langle \zeta^{(2)} \rangle) &- Re \nabla \cdot (\int_{-h}^{0} dz \int_{-h}^{z} dz' \int_{z'}^{0} \langle \mathbf{R}^{(0)} \rangle dz'' dz') \\ &- \alpha \nabla \cdot (\int_{-h}^{0} f_1 dz \langle \zeta^{(0)} \frac{\partial}{\partial z} (\nu \frac{\partial \mathbf{u}^{(0)}}{\partial z})_{z=0} \rangle) \\ &+ \alpha \nabla \cdot \langle \zeta^{(0)} \mathbf{u}^{(0)}|_{z=0} \rangle = 0, \qquad \text{in S} \end{aligned} \tag{II.2.107}$$

with

$$\begin{aligned}\frac{\partial \langle \zeta^{(2)} \rangle}{\partial n} \int_{-h}^{0} f_2 dz &- Re \int_{-h}^{0} dz \int_{-h}^{z} dz' \int_{z'}^{0} \langle R_n{}^{(0)} \rangle dz'' dz' \\ &- \alpha \int_{-h}^{0} f_1 dz \langle \zeta^{(0)} \frac{\partial}{\partial z} (\nu \frac{\partial u_n{}^{(0)}}{\partial z})|_{z=0} \rangle \\ &+ \alpha \langle \zeta^{(0)} u_n{}^{(0)}|_{z=0} \rangle = 0, \qquad \text{on B} \end{aligned} \tag{II.2.108}$$

and

$$\iint_S \langle \zeta^{(2)} \rangle dx dy = 0. \tag{II.2.109}$$

The three equations (II.2.107)-(II.2.109) will give $\langle \zeta^{(2)} \rangle$. And then the steady mass transport can be determined through Equation (II.2.105). The vertical steady stream-

ing can be found from mass balance

$$\langle w^{(2)} \rangle = - \int_{-h}^{z} \langle \nabla \cdot \mathbf{u}^{(2)} \rangle dz'. \tag{II.2.110}$$

Since the equation sets at various orders deal with general depth variation $h(x, y)$, shape of the lake, wind stress field $\vec{\tau}(x, y)$ and vertical eddy viscosity distribution $\nu(z)$ remain general, the solutions for surface elevation and velocity field have to be obtained through numerical methods. Nevertheless, analytical solutions are achievable for simple geometry with constant depth and eddy viscosity.

Chapter 3

Analytical Solution for a Constant-Depth Lake Forced by Uniform Wind

Consider a constant depth lake of arbitrary shape forced by uniform wind, namely $h = 1$ and $\nabla\tau_x = \nabla\tau_y = 0$ anywhere within S. At the leading order,

$$F_1 = \int_{-1}^{0} f_1(z)dz \tag{II.3.1}$$

and

$$F_2 = \int_{-1}^{0} f_2(z)dz \tag{II.3.2}$$

are both positive constant, the governing equation (II.2.67) reduces to the Laplace equation:

$$\nabla^2\zeta^{(0)} = 0, \tag{II.3.3}$$

and the lateral boundary condition (II.2.61) can be written as

$$\mathbf{n}\cdot[\nabla\zeta^{(0)}F_2] = -\mathbf{n}\cdot[\vec{\tau}e^{-it}F_1)], \quad \text{at the bank.} \tag{II.3.4}$$

Obviously

$$\nabla\zeta^{(0)} = -\vec{\tau}e^{-it}\frac{F_1}{F_2} \tag{II.3.5}$$

satisfies both (II.3.3) and (II.3.4). Therefore, the surface slope is a constant vector and the surface is simply a plane, regardless of the shape of the lake:

$$\zeta^{(0)} = -e^{-it}\frac{F_1}{F_2}(\tau_x x + \tau_y y + C). \tag{II.3.6}$$

C is an integration constant which can be fixed with the mass constraint (I.2.94), i.e.,

$$-e^{-it}\frac{F_1}{F_2}[\iint_S(\tau_x x + \tau_y y)dxdy + C \cdot S] = 0, \tag{II.3.7}$$

thus

$$\zeta^{(0)} = -e^{-it}\frac{F_1}{F_2}[\tau_x x + \tau_y y - \frac{\iint_S(\tau_x x + \tau_y y)dxdy}{S}]. \tag{II.3.8}$$

It is shown in Appendix B that (II.3.8) is the unique for the equation set in this case. In addition, we have, from (II.2.63),

$$\mathbf{u}^{(0)} = f_1(z)\vec{\tau}e^{-it} - f_2(z)\vec{\tau}e^{-it}\frac{F_1}{F_2} = \vec{\tau}e^{-it}[f_1(z) - \frac{F_1}{F_2}f_2(z)]. \tag{II.3.9}$$

Moreover, $\mathbf{u}^{(0)}$ depends only on z and t and therefore $\nabla \cdot \mathbf{u}^{(0)} = 0$. As a result,

$$w^{(0)} = 0, \tag{II.3.10}$$

by continuity, taking account of the impermeable condition at the bottom. Hence, in a constant-depth shallow lake forced by a uniform sinusoidal low-frequency wind, the leading order flow response is quasi-steady, one dimensional flow exactly parallel to the direction of forcing, regardless of either the shape of the lake or the vertical variation of eddy viscosity. Nevertheless, the eddy viscosity distribution affects the vertical flow profile. It is seen from (II.3.9) that

$$\mathbf{Q}_0^{(0)} = \int_{-1}^{0}\mathbf{u}^{(0)}dz = \vec{\tau}e^{-it}(F_1 - F_2\frac{F_1}{F_2}) = 0. \tag{II.3.11}$$

So there is no flux anywhere at $O(1)$. Since we only specify zero-normal-flux condition at the bank which is satisfied by the above solution regardless of the configuration of the bank, the shape of the lake does not affect the flow response but the value of constant C.

Welander (1957) derived a theory on the steady circulation in a shallow lake with depth variation based on constant eddy viscosity. The Coriolis force was of leading order importance in his study. For a constant-depth basin forced by a uniform wind-stress, he pointed out, as discussed by Ekman (1923) and Schalkwijk (1947), that "the surface slope will be independent of the horizontal extensions of the sea."With effect of earth rotation being at the leading order, this slope will make an angle with the direction of the wind.

At $O(\epsilon)$, using (II.3.9) we have

$$\mathbf{Q}_*^{(0)} = \vec{\tau} e^{-it}\left(\int_z^0 f_1 dz' - \int_z^0 f_2 dz' \frac{F_1}{F_2}\right) \tag{II.3.12}$$

and thus

$$\int_{-1}^0 dz \int_z^{-1} \frac{\mathbf{Q}_*^{(0)}}{\nu} dz' = C_Q \vec{\tau} e^{-it}, \tag{II.3.13}$$

where

$$C_Q = \int_{-1}^0 dz \int_z^{-1} \frac{1}{\nu}\left(\int_{z'}^0 f_1 dz'' - \int_{z'}^0 f_2 dz'' \frac{F_1}{F_2}\right) dz' = \text{constant}. \tag{II.3.14}$$

Hence, (II.2.80) and (II.2.75) become

$$\nabla^2 \zeta^{(1)} = -iS_t e^{-it} \frac{F_1}{F_2^2}(\tau_x + \tau_y + C), \tag{II.3.15}$$

and

$$\frac{\partial \zeta^{(1)}}{\partial n} = \frac{C_Q}{F_2} e^{-it}\left[-i\tau_n + \left(\frac{\mathbf{f}}{\omega} \times \vec{\tau}\right)_n\right]. \tag{II.3.16}$$

Let us first rewrite

$$\zeta^{(1)} = {\zeta^{(1)}}_1 + {\zeta^{(1)}}_2 \tag{II.3.17}$$

with

$$\nabla\zeta^{(1)}{}_2 = \frac{C_Q}{F_2}e^{-it}[-i\vec{\tau} + \frac{\mathbf{f}}{\omega} \times \vec{\tau}]. \tag{II.3.18}$$

It is easy to see that the problem reduces to one with homogeneous boundary condition:

$$\nabla^2\zeta^{(1)}{}_1 = -iS_t e^{-it}\frac{F_1}{F_2^2}(\tau_x + \tau_y + C), \tag{II.3.19}$$

with

$$\frac{\partial\zeta^{(1)}{}_1}{\partial n} = 0. \tag{II.3.20}$$

Unfortunately, the set of (II.3.19) and (II.3.20) can not be solved analytically unless a simple geometry of the basin is given.

Because $\nabla\mathbf{u}^{(0)} = 0$ and $w^{(0)} = 0$, the nonlinear convective inertia vanishes:

$$\mathbf{R}^{(0)} = 0 \tag{II.3.21}$$

at the leading order. As a result, at $O(\epsilon^2)$ the steady streaming is not forced by the Reynolds stress. The governing equation (II.2.107) becomes

$$\begin{aligned} F_2\nabla^2\langle\zeta^{(2)}\rangle - \alpha F_1\nabla\cdot\langle\zeta^{(0)}\frac{\partial}{\partial z}(\nu\frac{\partial\mathbf{u}^{(0)}}{\partial z})|_{z=0}\rangle \\ +\alpha\nabla\cdot\langle\zeta^{(0)}\mathbf{u}^{(0)}|_{z=0}\rangle = 0. \end{aligned} \tag{II.3.22}$$

Now,

$$\langle\zeta^{(0)}\mathbf{u}^{(0)}|_{z=0}\rangle = -\frac{1}{2}\frac{F_1}{F_2}(\tau_x x + \tau_y y + C)[f_1(0) - f_2(0)\frac{F_1}{F_2}]\vec{\tau}. \tag{II.3.23}$$

So

$$\nabla\cdot\langle\zeta^{(0)}\mathbf{u}^{(0)}|_{z=0}\rangle = -\frac{1}{2}\frac{F_1}{F_2}[f_1(0) - f_2(0)\frac{F_1}{F_2}]. \tag{II.3.24}$$

We calculate from (II.3.9) to get the forcing function for (II.3.22)

$$\begin{aligned} &\frac{\partial}{\partial z}(\nu\frac{\partial\mathbf{u}^{(0)}}{\partial z})|_{z=0} \\ =\ &\frac{\partial}{\partial z}\{\nu(z)\vec{\tau}e^{-it}[f_1'(z) - f_2'(z)\frac{F_1}{F_2}]\}|_{z=0} \\ =\ &\vec{\tau}e^{-it}\Gamma, \end{aligned} \tag{II.3.25}$$

where primes denote differentiation regarding z and the constant

$$\Gamma = \nu'(0)[f_1'(0) - f_2'(0)\frac{F_1}{F_2}] + \nu(0)[f_1''(0) - f_2''(0)\frac{F_1}{F_2}]. \tag{II.3.26}$$

Therefore,

$$\langle \zeta^{(0)} \frac{\partial}{\partial z}(\nu \frac{\partial \mathbf{u}^{(0)}}{\partial z})|_{z=0} \rangle = -\frac{1}{2}\frac{F_1}{F_2}(\tau_x x + \tau_y y + C)\Gamma \vec{\tau}. \tag{II.3.27}$$

and

$$\nabla \cdot \langle \zeta^{(0)} \frac{\partial}{\partial z}(\nu \frac{\partial \mathbf{u}^{(0)}}{\partial z})|_{z=0} \rangle = -\frac{1}{2}\frac{F_1}{F_2}\Gamma, \tag{II.3.28}$$

Thus (II.3.22) becomes

$$\nabla^2 \langle \zeta^{(2)} \rangle = \frac{\alpha}{2}\frac{F_1}{F_2^2}[f_1(0) - f_2(0)\frac{F_1}{F_2} - F_1\Gamma] = \text{const.} \tag{II.3.29}$$

The lateral boundary condition (II.2.108) now reads

$$\frac{\partial \langle \zeta^{(2)} \rangle}{\partial n} - \frac{\alpha}{2}\frac{F_1}{F_2^2}[f_1(0) - f_2(0)\frac{F_1}{F_2} - F_1\Gamma](\tau_x x + \tau_y y + C)\tau_n = 0. \tag{II.3.30}$$

It is readily seen that a $\langle \zeta^{(2)} \rangle$ satisfy the following equation will be a solution of (II.3.29) and (II.3.30):

$$\nabla \langle \zeta^{(2)} \rangle - \frac{\alpha}{2}\frac{F_1}{F_2^2}[f_1(0) - f_2(0)\frac{F_1}{F_2} - F_1\Gamma](\tau_x x + \tau_y y + C)\vec{\tau} = 0. \tag{II.3.31}$$

Therefore, the x-component is

$$\frac{\partial \langle \zeta^{(2)} \rangle}{\partial x} - \frac{\alpha}{2}\frac{F_1}{F_2^2}[f_1(0) - f_2(0)\frac{F_1}{F_2} - F_1\Gamma](\tau_x x + \tau_y y + C)\tau_x = 0. \tag{II.3.32}$$

Integrating once

$$\langle \zeta^{(2)} \rangle = \frac{\alpha}{2}\frac{F_1}{F_2^2}\gamma\tau_x(\tau_x \frac{x^2}{2} + \tau_y xy + Cx) + C^*(y) \tag{II.3.33}$$

with

$$\gamma = [f_1(0) - f_2(0)\frac{F_1}{F_2} - F_1\Gamma]. \tag{II.3.34}$$

Taking derivative with respect to y,

$$\frac{\partial\langle\zeta^{(2)}\rangle}{\partial y} = \frac{\alpha}{2}\frac{F_1}{F_2^2}\gamma\tau_x\tau_y x + \frac{dC^*(y)}{dy}. \tag{II.3.35}$$

From (II.3.31)

$$\frac{\partial\langle\zeta^{(2)}\rangle}{\partial y} - \frac{\alpha}{2}\frac{F_1}{F_2^2}[f_1(0) - f_2(0)\frac{F_1}{F_2} - F_1\Gamma](\tau_x x + \tau_y y + C)\tau_y = 0. \tag{II.3.36}$$

By comparison with (II.3.35)

$$\frac{dC^*(y)}{dy} = \frac{\alpha}{2}\frac{F_1}{F_2^2}\gamma\tau_y(\tau_y y + C), \tag{II.3.37}$$

and then

$$C^* = \frac{\alpha}{2}\frac{F_1}{F_2^2}\gamma\tau_y(\tau_y\frac{y^2}{2} + Cy) + \tilde{C}. \tag{II.3.38}$$

Using the mass constraint (II.2.109)

$$\tilde{C} = -\frac{\alpha}{2S}\frac{F_1}{F_2^2}\gamma\iint_S[\frac{1}{2}(\tau_x^2x^2 + \tau_y^2y^2) + C(\tau_x x + \tau_y y) + \tau_x\tau_y xy]dxdy. \tag{II.3.39}$$

Consequently,

$$\begin{aligned}\langle\zeta^{(2)}\rangle = \frac{\alpha}{2}\frac{F_1}{F_2^2}\gamma\{&\frac{1}{2}(\tau_x^2x^2 + \tau_y^2y^2) + C(\tau_x x + \tau_y y) + \tau_x\tau_y xy \\ -\frac{1}{S}&\iint_S[\frac{1}{2}(\tau_x^2x^2 + \tau_y^2y^2) + C(\tau_x x + \tau_y y) + \tau_x\tau_y xy]dxdy\}.\end{aligned} \tag{II.3.40}$$

It follows (II.2.105) that

$$\langle\mathbf{u}^{(2)}\rangle = \frac{\alpha}{2}\frac{F_1}{F_2}\vec{\tau}(\tau_x x + \tau_y y + C)[\frac{\gamma f_2(z)}{F_2} + \Gamma f_1(z)]. \tag{II.3.41}$$

We find that the horizontal mass transport is linear in x and y. Owing to this fact,

the vertical streaming is purely dependent on z:

$$\langle w^{(2)} \rangle = \frac{\alpha}{2} \frac{F_1}{F_2} [\frac{\gamma}{F_2} \int_{-1}^{z} f_2(z')dz' - \Gamma \int_{-1}^{z} f_1(z')dz']. \tag{II.3.42}$$

Due to the uniqueness of solution as shown in Appendix B, the above results are the only solution for this problem. We note that the vertical distribution of eddy viscosity is yet general and will determine the vertical profile of the flow field.

Chapter 4

Rectanglar Lake with Uniform Depth

To give some more explicit results, we consider the flow field in a rectangular lake with constant depth ($h = 1$). The direction of sinusoidal wind forcing is general in the horizontal plane, namely $\vec{\tau} = (\tau_x, \tau_y) =$ constant vector and

$$\tau_x^2 + \tau_y^2 = 1. \tag{II.4.1}$$

In addition, we adopt a constant eddy viscosity across the depth,

$$\nu = 1. \tag{II.4.2}$$

Now at the leading order,

$$\frac{\partial^2 \mathbf{u}^{(0)}}{\partial z^2} - \nabla \zeta^{(0)} = 0, \tag{II.4.3}$$

$$\mathbf{u}^{(0)} = 0, \quad \text{at } z = -1, \tag{II.4.4}$$

$$\frac{\partial \mathbf{u}^{(0)}}{\partial z} = \vec{\tau} e^{-it}, \quad \text{at } z = 0. \tag{II.4.5}$$

The real parts of the complex quantities are implied. Intergrating twice and making use of boundary conditions at the surface and the bottom, the formal solution of the

velocity at this order reads

$$\mathbf{u}^{(0)} = \frac{1}{2}\nabla\zeta^{(0)}(z^2-1) + \vec{\tau}(z+1)e^{-it}, \tag{II.4.6}$$

and consequently,

$$\begin{aligned} \mathbf{Q_0}^{(0)} &= \int_{-1}^{0} \mathbf{u}^{(0)} dz \\ &= -\frac{1}{3}\nabla\zeta^{(0)} + \frac{\vec{\tau}}{2}e^{-it}. \end{aligned} \tag{II.4.7}$$

The integrated continuity equation (II.2.60) and the lateral boundary condition (II.2.61) then give

$$\nabla^2\zeta^{(0)} = 0, \tag{II.4.8}$$

$$\frac{\partial\zeta^{(0)}}{\partial x} = \frac{3}{2}\tau_x e^{-it}, \quad x = 0, a/L, \tag{II.4.9}$$

$$\frac{\partial\zeta^{(0)}}{\partial y} = \frac{3}{2}\tau_y e^{-it} \quad y = 0, b/L, \tag{II.4.10}$$

where a and b are the length and width of the lake, respectively. The solution of leading order surface elevation, with the global mass constraint (II.2.69), is obtained readily

$$\zeta^{(0)} = \frac{3}{2}[\tau_x(x - \frac{a}{2L}) + \tau_y(y - \frac{b}{2L})]e^{-it}, \tag{II.4.11}$$

and it follows that

$$\mathbf{u}^{(0)} = \frac{\vec{\tau}}{4}(z+1)(3z+1)e^{-it}, \tag{II.4.12}$$

and

$$w^{(0)} = 0. \tag{II.4.13}$$

With a constant eddy viscosity and uniform depth we have

$$\begin{aligned} f_1 &= z+1, \\ f_2 &= (z^2-1)/2, \end{aligned}$$

$$
\begin{aligned}
F_1 &= 1/2, \\
F_2 &= -1/3 \\
C &= -(\tau_x a + \tau_y b)/2L,
\end{aligned} \tag{II.4.14}
$$

which follow from (II.3.8) and (II.3.9). The solutions shows that the leading order surface set-up is indeed planar and the flow response truly uniform horizontally and parallel to the wind forcing. The spatial dependency is uncoupled with the temporal one owing to the small frequency. More precisely, the wind varies so slowly that the vertical structure of flow forms before it "feels" any change in the forcing. The velocity is exactly in phase with the surface slope, as will be shown later. This will lead to an interesting phenomenon for the steady streaming at $O(\epsilon^2)$. The spatial dependency of the flow is identical to the steady response of the lake to a constant wind field. This is a quasi-steady situation. The vertical profile of $\mathbf{u}^{(0)}$ at a given time, say, $t = 0$, is plotted in Figure II-4-1. The total flux across the depth is zero at any cross-section. It is heuristicly expected that near the bank opposing the wind the top layer fluid will go down and flows back in the lower layer again the wind. In the other end of the lake, an up-welling flow results and a circulation pattern forms in the vertical plane. Therefore near the bank the vertical flow is as significant as the horizontal flow, hence neither shallow water or hydrostatic assumption holds in the lateral boundary layer.

At the next order $O(\epsilon)$,

$$
\frac{\partial^2 \mathbf{u}^{(1)}}{\partial z^2} - \nabla \zeta^{(1)} = \frac{\partial \mathbf{u}^{(0)}}{\partial t} + \frac{\mathbf{f}}{\omega} \times \mathbf{u}^{(0)}, \tag{II.4.15}
$$

$$
\mathbf{u}^{(1)} = 0, \quad \text{at } z = -1, \tag{II.4.16}
$$

$$
\frac{\partial \mathbf{u}^{(1)}}{\partial z} = 0, \quad \text{at } z = 0. \tag{II.4.17}
$$

Clearly the flow field at this order are forced by the transient and Coriolis terms of $\mathbf{u}^{(0)}$. We can tell as a result the solution will show contribution from both of these two sources. Moreover, due to the horizontal uniformity of leading order flow field,

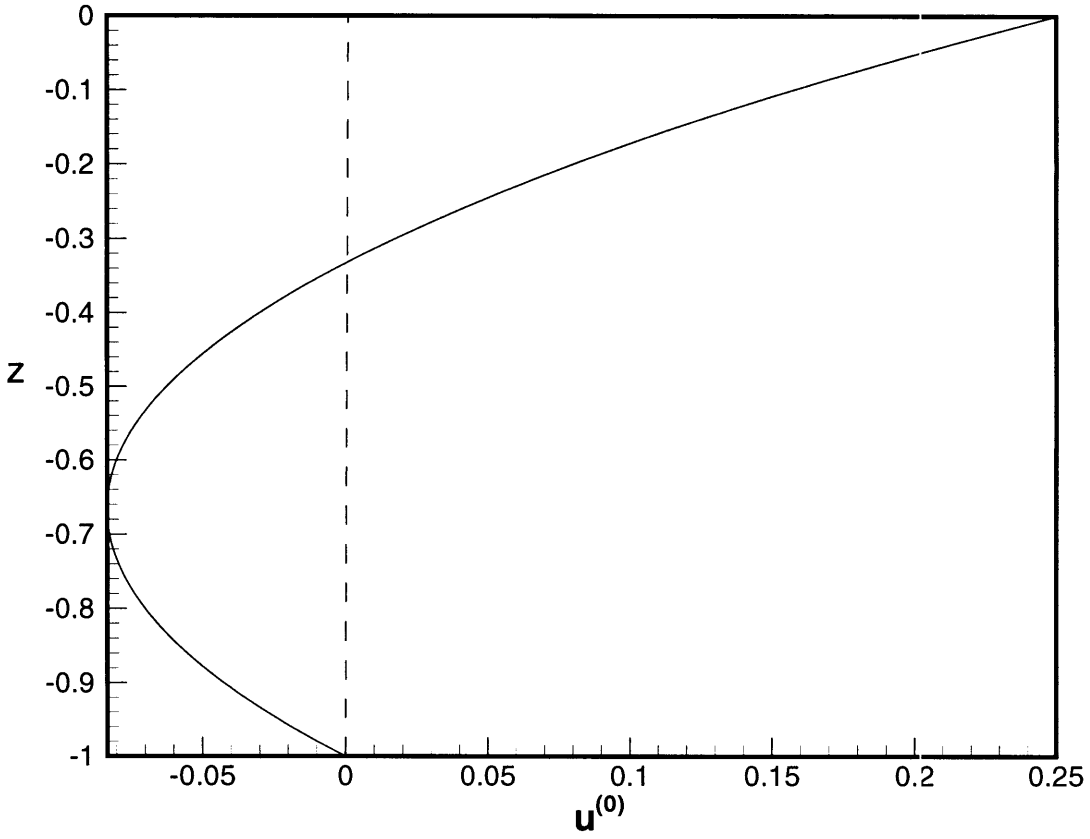

Figure II-4-1: Vertical profile of $\mathbf{u}^{(0)}$ along the wind forcing direction at $t = 0$

the Coriolis force is invariant horizontally. Using the solution at the previous order we can write the forcing term in an explicit form,

$$\frac{\partial^2 \mathbf{u}^{(1)}}{\partial z^2} - \nabla\zeta^{(1)} = \frac{e^{-it}}{4}(z+1)(3z+1)[-i\vec{\tau} + \frac{\mathbf{f}}{\omega} \times \vec{\tau}], \tag{II.4.18}$$

The solution is

$$\mathbf{u}^{(1)} = \frac{1}{2}\nabla\zeta^{(1)}(z^2-1) + \frac{e^{-it}}{48}(3z^4+8z^3+6z^2-1)[-i\vec{\tau} + \frac{\mathbf{f}}{\omega} \times \vec{\tau}]. \tag{II.4.19}$$

It is readily seen that

$$\mathbf{Q}_0{}^{(1)} = -\frac{1}{3}\nabla\zeta^{(1)} + \frac{1}{120}[i\vec{\tau} - \frac{\mathbf{f}}{\omega} \times \vec{\tau}]e^{-it}. \tag{II.4.20}$$

From the continuity equation (II.2.74) we realize that the other driven source besides the forcing associated with $\mathbf{u}^{(0)}$ is due to the oscillation of the surface at the leading order. Recalling Equation (II.2.74) and (II.2.75), the governing equation and boundary conditions for $\zeta^{(1)}$ are as follows:

$$\nabla^2\zeta^{(1)} = -\frac{9iS_t}{2}[\tau_x(x - \frac{a}{2L}) + \tau_y(y - \frac{b}{2L})]e^{-it}, \tag{II.4.21}$$

$$\frac{\partial\zeta^{(1)}}{\partial x} = \frac{1}{40}(i\tau_x + \frac{f}{\omega}\tau_y)e^{-it}, \quad x = 0, a/L, \tag{II.4.22}$$

$$\frac{\partial\zeta^{(1)}}{\partial y} = \frac{1}{40}(i\tau_y - \frac{f}{\omega}\tau_x)e^{-it} \quad y = 0, b/L, \tag{II.4.23}$$

where $f = |\mathbf{f}|$. The effect of earth rotation come into play through the boundary conditions. Worth attention is that the forcing term in (II.4.21) (associated with $\zeta^{(0)}$) is much greater than those in the boundary conditions (associated with $\mathbf{u}^{(0)}$). Because of linearity, we write

$$\zeta^{(1)} = [\zeta_1(x) + \zeta_2(y)]e^{-it}, \tag{II.4.24}$$

it is seen then

$$\frac{\partial^2 \zeta_1}{\partial x^2} = -\frac{9iS_t\tau_x}{2}(x - \frac{a}{2L}), \tag{II.4.25}$$

$$\frac{\partial \zeta_1}{\partial x} = \frac{1}{40}(i\tau_x + \frac{f}{\omega}\tau_y), \quad x = 0, a/L, \tag{II.4.26}$$

and

$$\frac{\partial^2 \zeta_2}{\partial y^2} = -\frac{9iS_t\tau_y}{2}(y - \frac{b}{2L}), \tag{II.4.27}$$

$$\frac{\partial \zeta_2}{\partial y} = \frac{1}{40}(i\tau_y - \frac{f}{\omega}\tau_x) \quad y = 0, b/L. \tag{II.4.28}$$

Simply integrating twice and and using the Neumann condition, we find

$$\zeta_1 = -\frac{9iS_t\tau_x}{4}(\frac{x^3}{3} - \frac{ax^2}{2L}) + \frac{1}{40}(i\tau_x + \frac{f}{\omega}\tau_y)x + C_1, \tag{II.4.29}$$

and the solution for ζ_2 is, similarly,

$$\zeta_2 = -\frac{9iS_t\tau_y}{4}(\frac{y^3}{3} - \frac{by^2}{2L}) + \frac{1}{40}(i\tau_y - \frac{f}{\omega}\tau_x)y + C_2, \tag{II.4.30}$$

Adding (II.4.29) and (II.4.30) together, the two integration constants are combined into one constant which is then fixed by the mass constraint at this order. Therefore, the solution reads

$$\begin{aligned}
\zeta^{(1)} &= \{-\frac{9iS_t}{4}[\tau_x(\frac{x^3}{3} - \frac{ax^2}{2L} + \frac{a^3}{12L^3}) \\
&+ \tau_y(\frac{y^3}{3} - \frac{by^2}{2L} + \frac{b^3}{12L^3})] \\
&+ \frac{1}{40}[(i\tau_x + \frac{f}{\omega}\tau_y)(x - \frac{a}{2L}) \\
&+ (i\tau_y - \frac{f}{\omega}\tau_x)(y - \frac{b}{2L})]\}e^{-it},
\end{aligned} \tag{II.4.31}$$

Since the surface displacement at this order is governed by a Poisson equation with a forcing linearly varying in the horizontal plane (or mathematically, the curvature of the surface varies linearly in x and y), it is reasonable that $\zeta^{(1)}$ has a cubic dependency upon the horizontal extensions. In addition, the cumulative response corresponding to earth rotation is linearly dependent on x and y due to the horizontal uniformity of

Coriolis force at this order. Noting also that there is an antisymmetry with respect to the geometric center of the lake ($x = a/2L, y = b/2L$), namely,

$$\zeta^{(1)}(x_0, y_0) = -\zeta^{(2)}(\frac{a}{L} - x_0, \frac{b}{L} - y_0), \tag{II.4.32}$$

the global mass conservation indeed holds. Surface and equal-elevation line plots at $t = 0, \pi/4, \pi/2, 3\pi/4$ are shown in figures II-4-2-II-4-5.

The parameters are taken as: $h_0 = 4$ m, $\nu_0 = 0.015$ m^2/s, $a/L = 1$, $b/L = 0.8$, $L = 10000$ m, $\omega = 7.27 \cdot 10^{-5}$ s^{-1}, $\tau_0/\rho = 10^{-4}$ m^2/s^2, and $\phi = 40°$. In this case, $S_t = 2.24$, $f/\omega = 1.3$ and $\epsilon = 0.08$. $\vec{\tau} = (1, 0)$ is specified so that the Coriolis effect is more distinguishable from the transient effect. At $t = 0$, because of the $\pi/2$ phase lag of the transient response, the surface displacement is purely due to Coriolis effect of $\mathbf{u}^{(0)}$ and thus the surface slope is perpendicular to x. Since $\mathbf{u}^{(0)}$ at this moment is along positive x, the Coriolis force is then pointing to the right of the velocity and consequently results in a set-up at the south bank. The constant surface corresponds to the horizontal uniformity of $\mathbf{u}^{(0)}$. At $t = \pi/4$, the transient effect is obviously seen; the Coriolis effect together with the transient effect makes the elevation at (1,0) the maximum. We see that the contribution of $\zeta^{(0)}$ is much greater than that of $\mathbf{u}^{(0)}$ for now the resulting displacement is much more significant. At $t = \pi/2$, the transient effect reaches the maximum (with the $\pi/2$ lag) while Coriolis effect disappear as $\mathbf{u}^{(0)} = 0$ at the moment. At $t = 3\pi/4$, the transient effect due to $\zeta^{(0)}$ and $\mathbf{u}^{(0)}$ is exactly the same as that at $t = \pi/4$ (noting the phase lag) while Coriolis effect is just the opposite as $\mathbf{u}^{(0)}$ now goes toward west. This can be seen perfectly if we compare Figure II-4-3 with II-4-5.

Substituting (II.4.31) into the formal solution of velocity generates

$$\begin{aligned} \mathbf{u}^{(1)} &= e^{-it}\{\frac{1}{240}(15z^4 + 40z^3 + 27z^2 - 2)(\frac{\mathbf{f}}{\omega} \times \vec{\tau} - i\vec{\tau}) \\ &- \frac{9iS_t}{8}(z^2 - 1)\begin{bmatrix} \tau_x(x^2 - \frac{ax}{L}) \\ \tau_y(y^2 - \frac{by}{L}) \end{bmatrix}\}, \end{aligned} \tag{II.4.33}$$

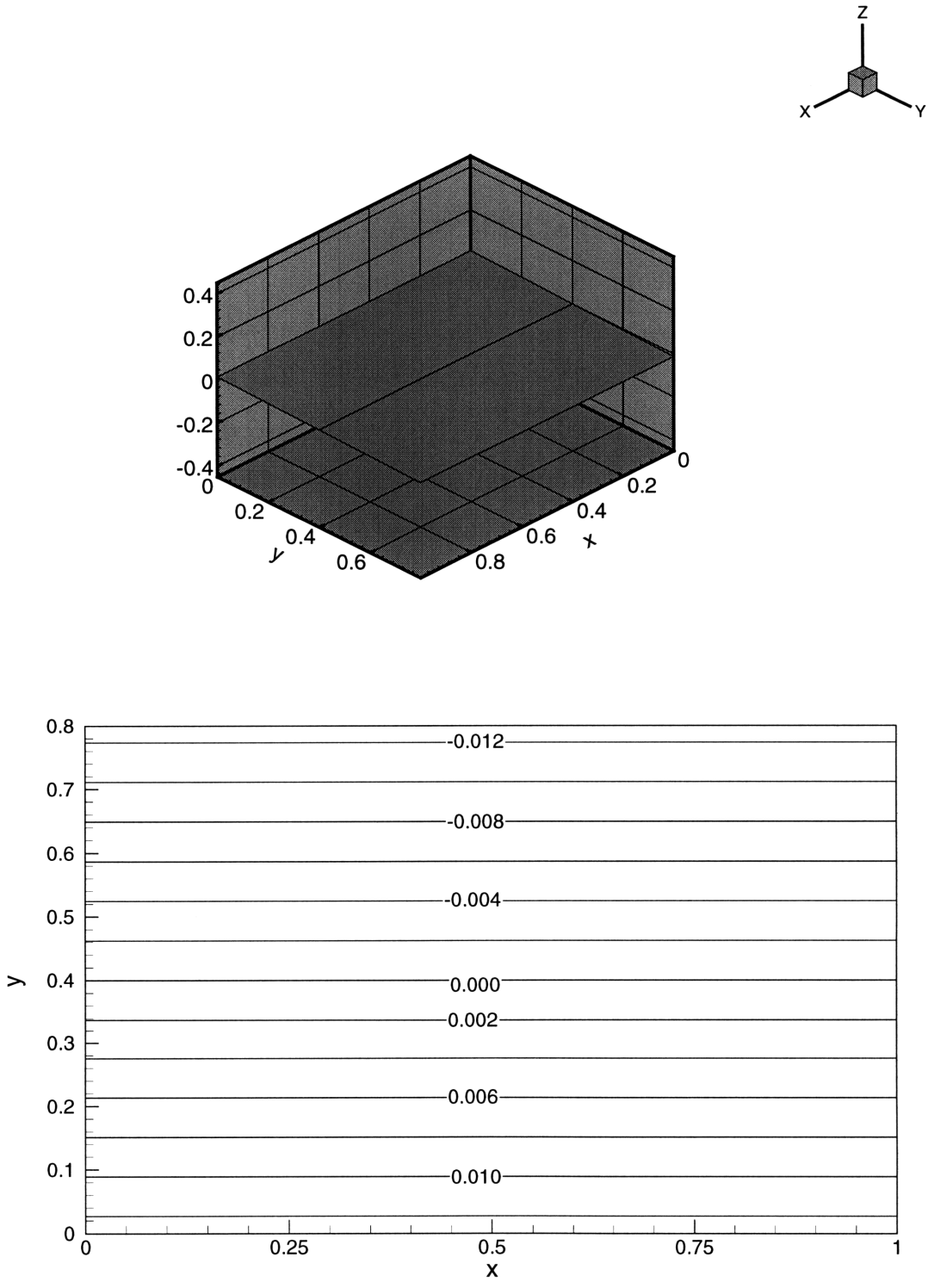

Figure II-4-2: Snapshot of $\zeta^{(1)}$ at $t = 0$. Upper: surface plot; lower: equal-elevation lines.

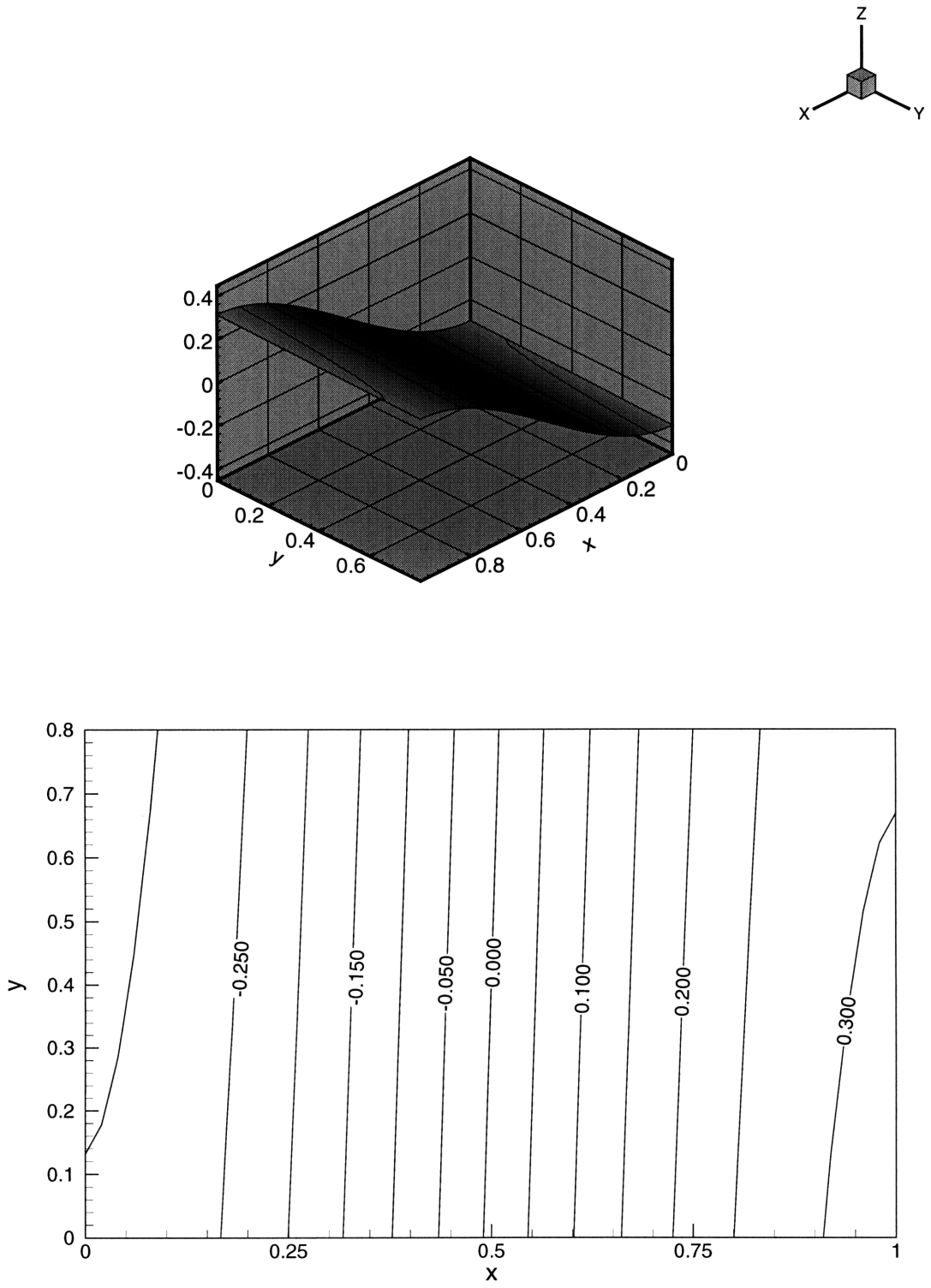

Figure II-4-3: Snapshot of $\zeta^{(1)}$ at $t = \pi/4$. Upper: surface plot; lower: equal-elevation lines.

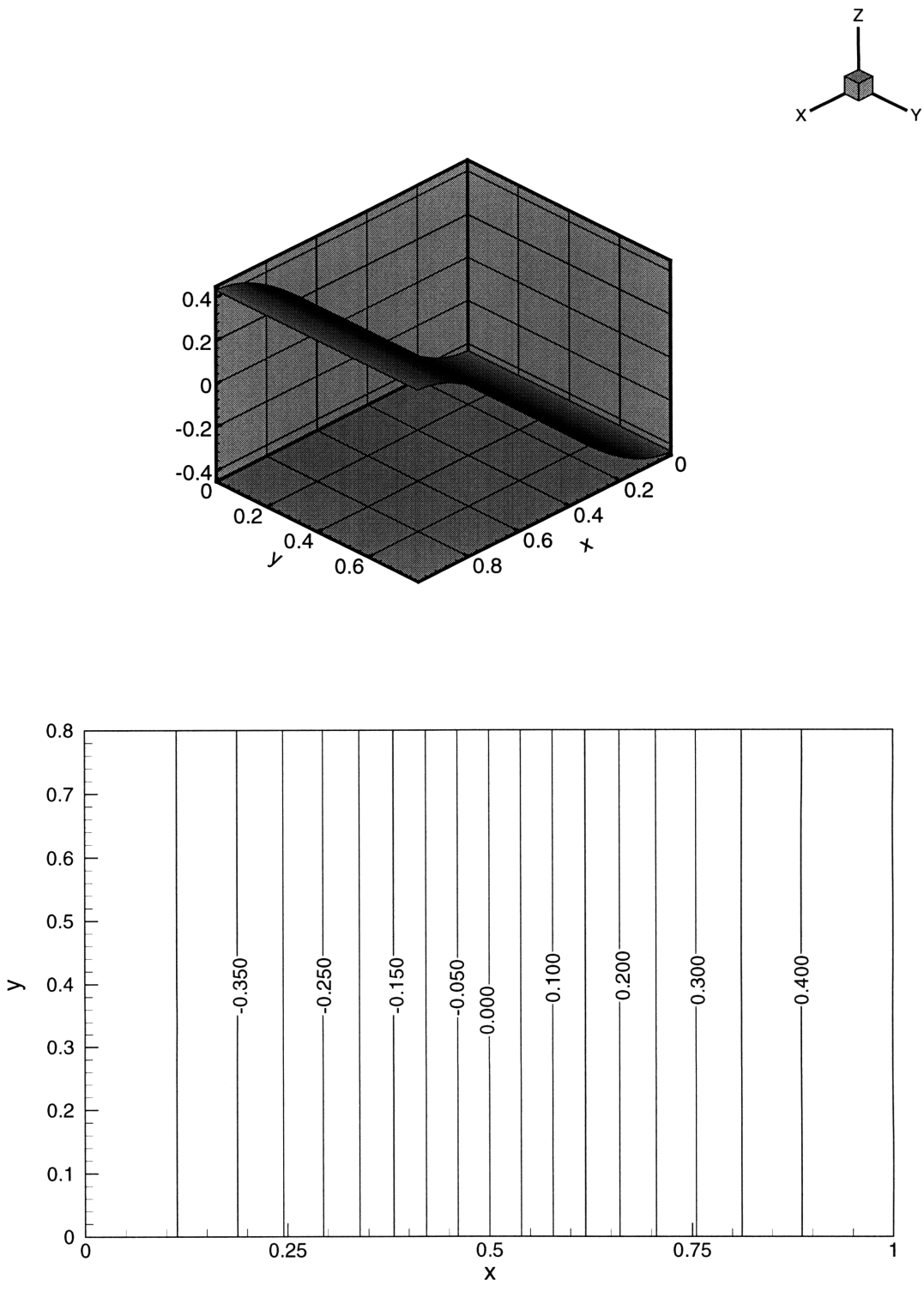

Figure II-4-4: Snapshot of $\zeta^{(1)}$ at $t = \pi/2$. Upper: surface plot; lower: equal-elevation lines.

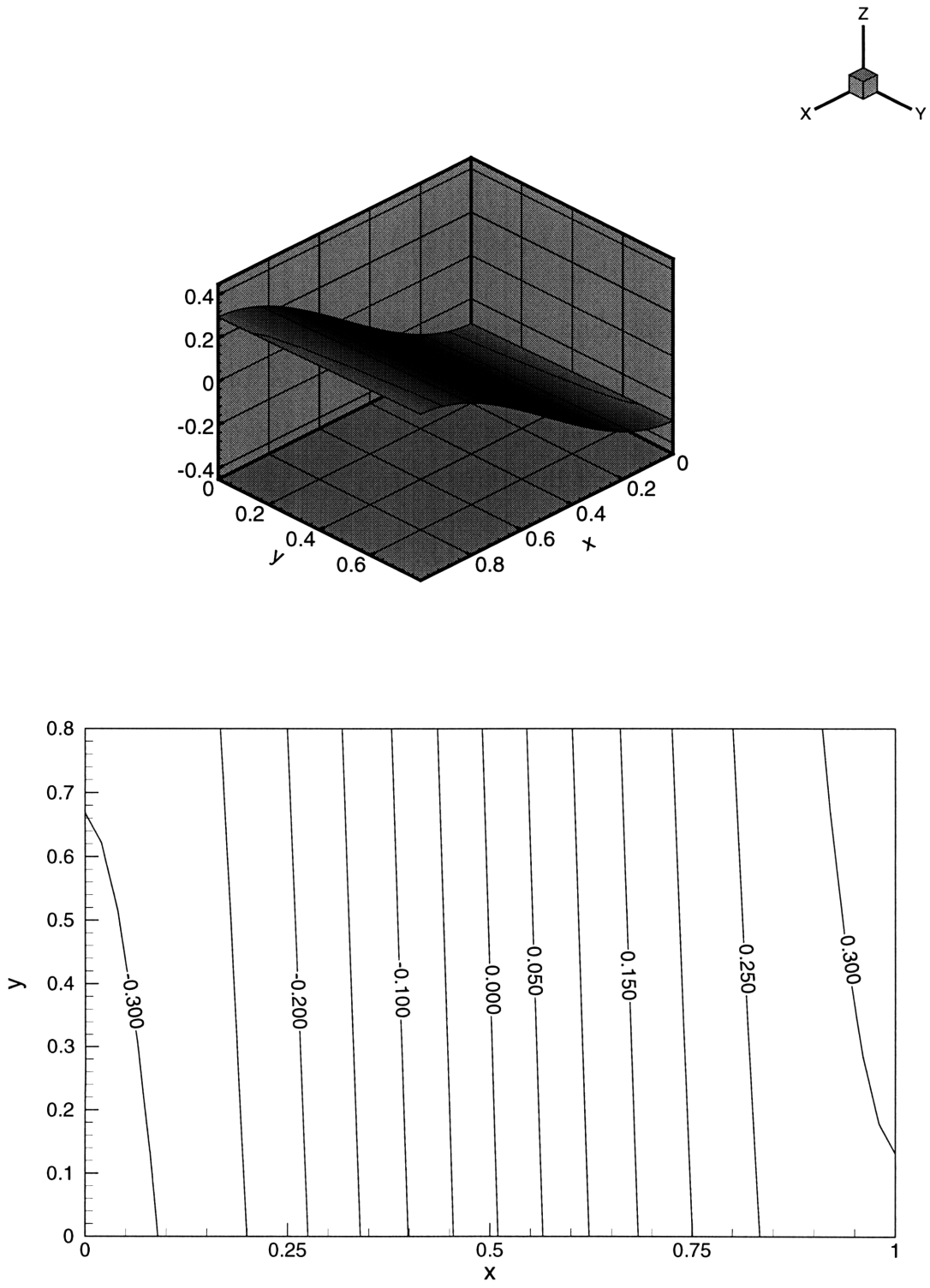

Figure II-4-5: Snapshot of $\zeta^{(1)}$ at $t = 3\pi/4$. Upper: surface plot; lower: equal-elevation lines.

and

$$\begin{aligned} w^{(1)} &= -\int_{-1}^{z} \nabla \cdot \mathbf{u}^{(2)} dz' \\ &= -e^{-it} \int_{-1}^{z} (z'^2 - 1)(-\frac{9iS_t}{8})[\tau_x(2x - \frac{a}{L}) + \tau_y(2y - \frac{b}{L})]dz' \\ &= \frac{3iS_t}{4}(z^3 - 3z - 2)[\tau_x(x - \frac{a}{2L}) + \tau_y(y - \frac{b}{2L})]e^{-it}. \end{aligned} \tag{II.4.34}$$

To check the correctness of above results we verify whether the solution satisfies the free surface kinematic boundary condition. Making a Taylor expansion of the kinematic boundary condition at the free surface, Equation (II.2.24), we find an approximate condition applied at the static surface,

$$w + \alpha\epsilon^2\zeta\frac{\partial w}{\partial z} = S_t\epsilon\frac{\partial \zeta}{\partial t} + \alpha\epsilon^2(\mathbf{u} \cdot \nabla\zeta) + O(\epsilon^4), \quad z = 0. \tag{II.4.35}$$

Grouping terms at $O(\epsilon)$ after the perturbation expansion gives

$$w^{(1)} = S_t\frac{\partial \zeta^{(0)}}{\partial t}. \tag{II.4.36}$$

It follows (II.4.34) that

$$w^{(1)}|_{z=0} = \frac{3iS_t}{4}(-2)[\tau_x(x - \frac{a}{2L}) + \tau_y(y - \frac{b}{2L})]e^{-it} = S_t\frac{\partial \zeta^{(0)}}{\partial t}. \tag{II.4.37}$$

The solution indeed passes the checking.

The flow field at this order is indeed, as we anticipate, affected by the earth rotation and there is velocity component in the direction perpendicular to the characteristic plane. More precisely, the results consist of two types of terms: one is tagged with i indicating the temporal effect and also a $\pi/2$ lag in phase behind the wind forcing; the other is marked by f showing the contribution of Coriolis force.

The response now becomes three dimensional. It is the effect of earth rotation that leads to the horizontal component along the direction perpendicular to the wind. Yet the vertical velocity component is still free of Coriolis effect since it is seen from

(II.2.16) that the Coriolis terms in the vertical momentum equation does not play any role until $O(\epsilon^3)$. The oscillation of the planar surface at the leading order causes a vertical velocity at the static surface and therefore the third velocity component starts to appear. The temporal dependency is still periodic since no nonlinear effect shows up yet. The Strouhal number indicates the contribution of mass accumulation over time due to the net flux beneath the static surface.

In plotting the results we only focus on the first half cycle due to the periodicity of the flow. The value of any flow quantity after half period will differ from the current value by a minus sign. The transient term due to $\zeta^{(0)}$ is dominant. This can be see clearly in Figures II-4-6 and II-4-7.

At $t = 0$ the flow is purely due to Coriolis effect of $\mathbf{u}^{(0)}$. The flow is along negative y axis while the speed is tiny. $\pi/4$ later, noting that in (II.4.19) the pressure gradient term is dominanting, the flow is essentially going westward (see Figure II-4-3 for the pressure gradient which is opposite to $\nabla\zeta^{(1)}$). At $t = \pi/2$ the largest surface slope occurs and leads to the largest leftward flow accordingly. (II.3.20) in last section implies that no normal surface slope at the bank is due to the forcing associated with $\zeta^{(0)}$, and thus the normal velocity at the bank is purely due to $\mathbf{u}^{(0)}$ and very small. FiguresII-4-8 shows the verticle dependency of the Coriolis effect on $\mathbf{u}^{(1)}$.

A plot for $z = -0.7$ and $t = \pi/4$ in figure II-4-9, comparing with the lower plot in figure II-4-6 shows that although Coriolis force changes direction the flow is dominated by the transient response of $\zeta^{(0)}$.

The flow pattern does not change much except the speed drops according to $(1 - z^2)^{-1}$. More interesting is the circulation pattern in xz plane. Figure II-4-10 shows snapshots of flow field in the cross-section $y = b/2L$ at $t = 0.25\pi$ and $t = 0.5\pi$.

Clearly the flow pattern is caused by the oscillation of $\zeta^{(0)}$. Recall in this case

$$\zeta^{(0)} = \frac{3}{2}(x - 1/2)e^{-it} \tag{II.4.38}$$

With the right half surface sweeping down during $t = 0$ to $t = 0.5\pi$, the flow is forced

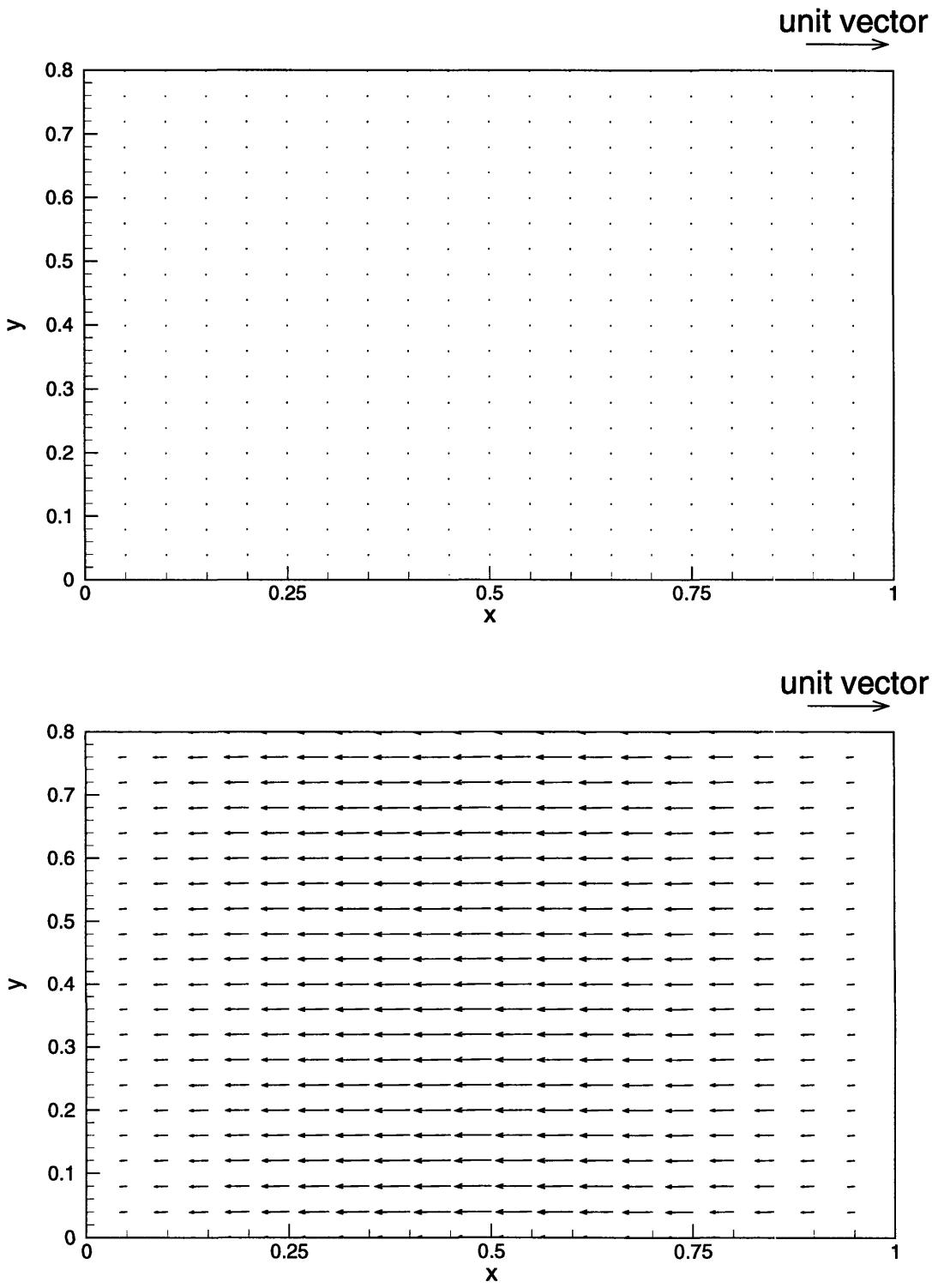

Figure II-4-6: Snapshots of $\mathbf{u}^{(1)}$ at $z = 0$. Upper: $t = 0$; lower: $t = \pi/4$.

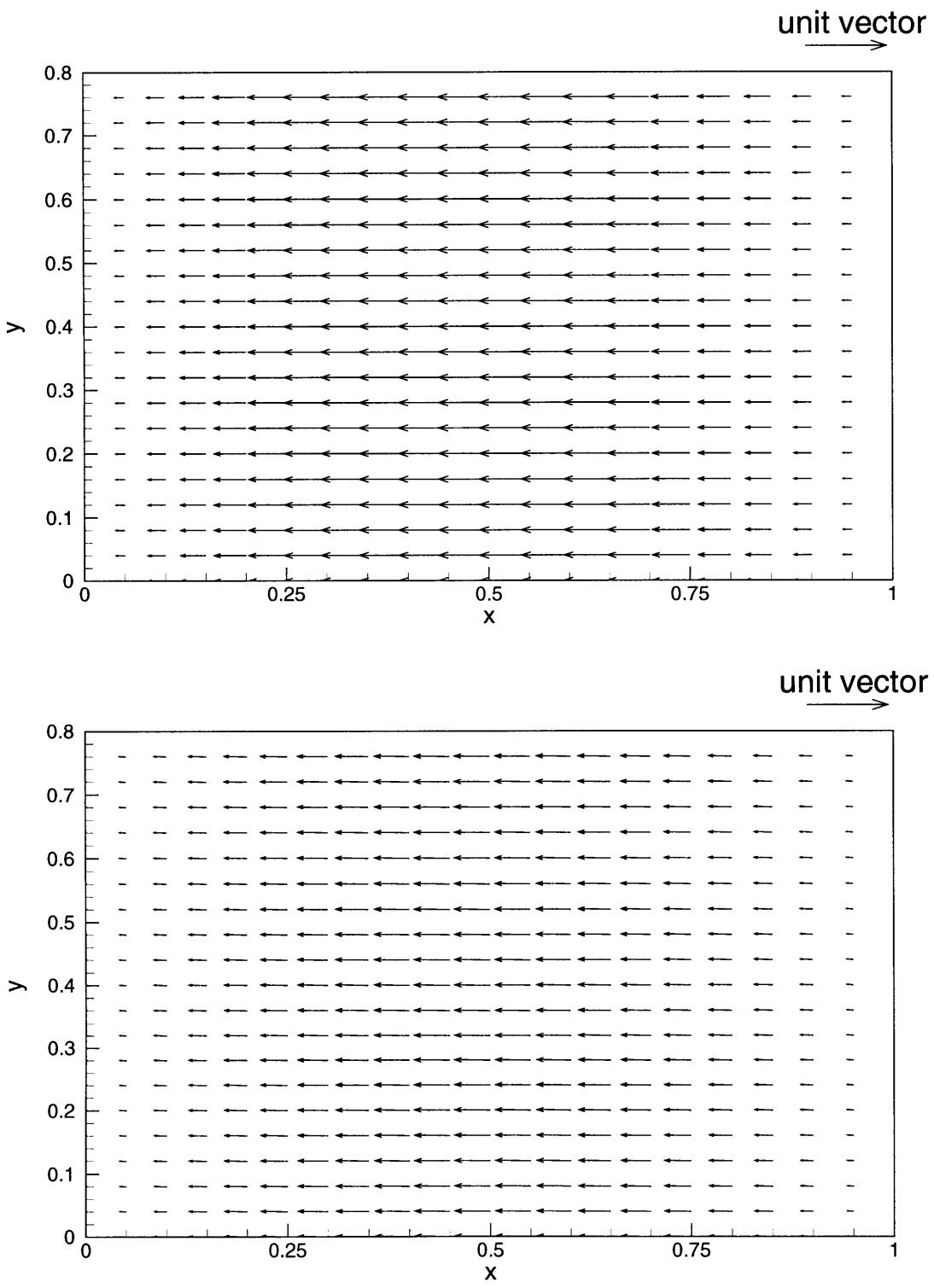

Figure II-4-7: Snapshots of $\mathbf{u}^{(1)}$ at $z = 0$. Upper: $t = \pi/2$; lower: $t = 3\pi/4$.

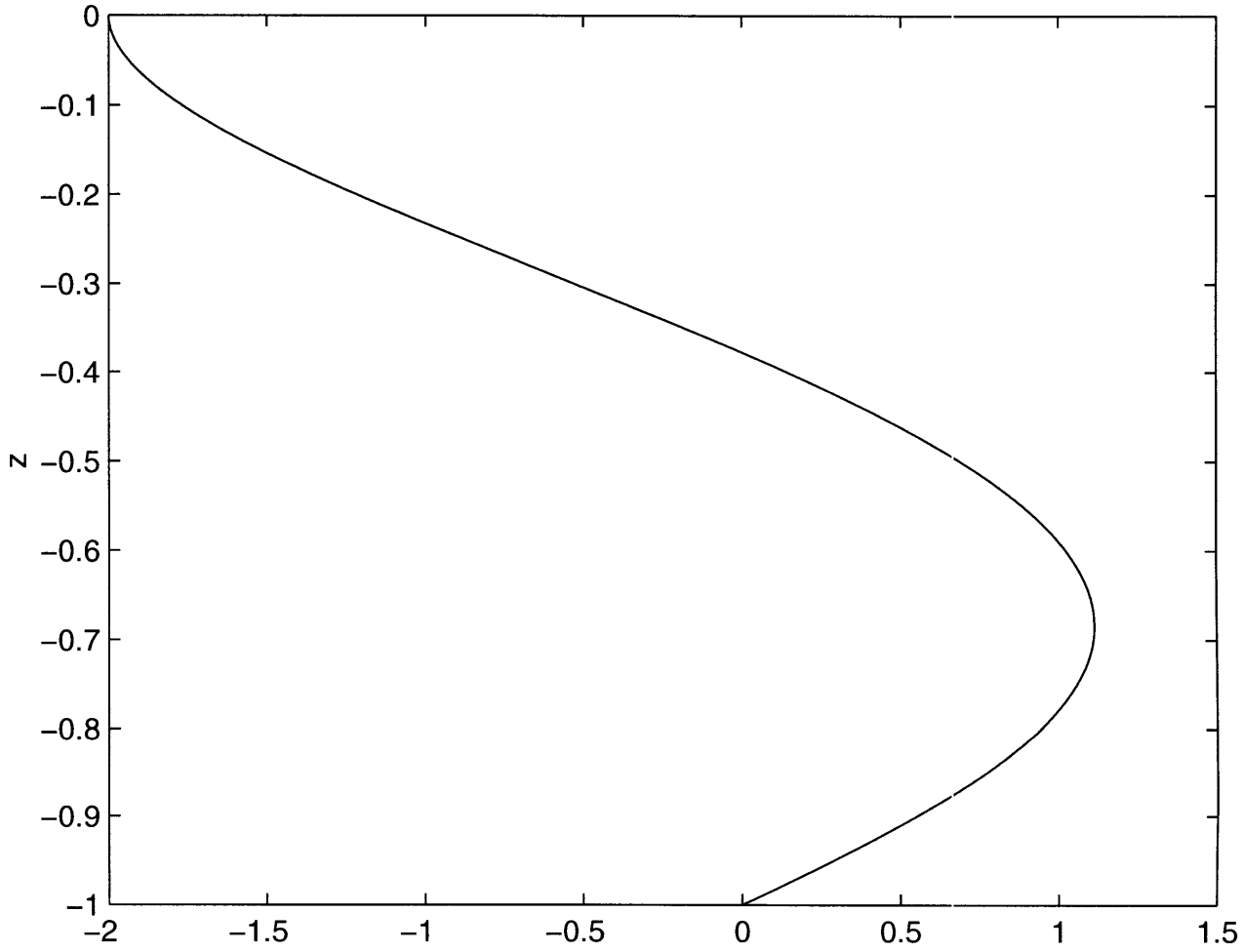

Figure II-4-8: z-dependency of the term in $\mathbf{u}^{(1)}$ associated with $\mathbf{u}^{(0)}$.

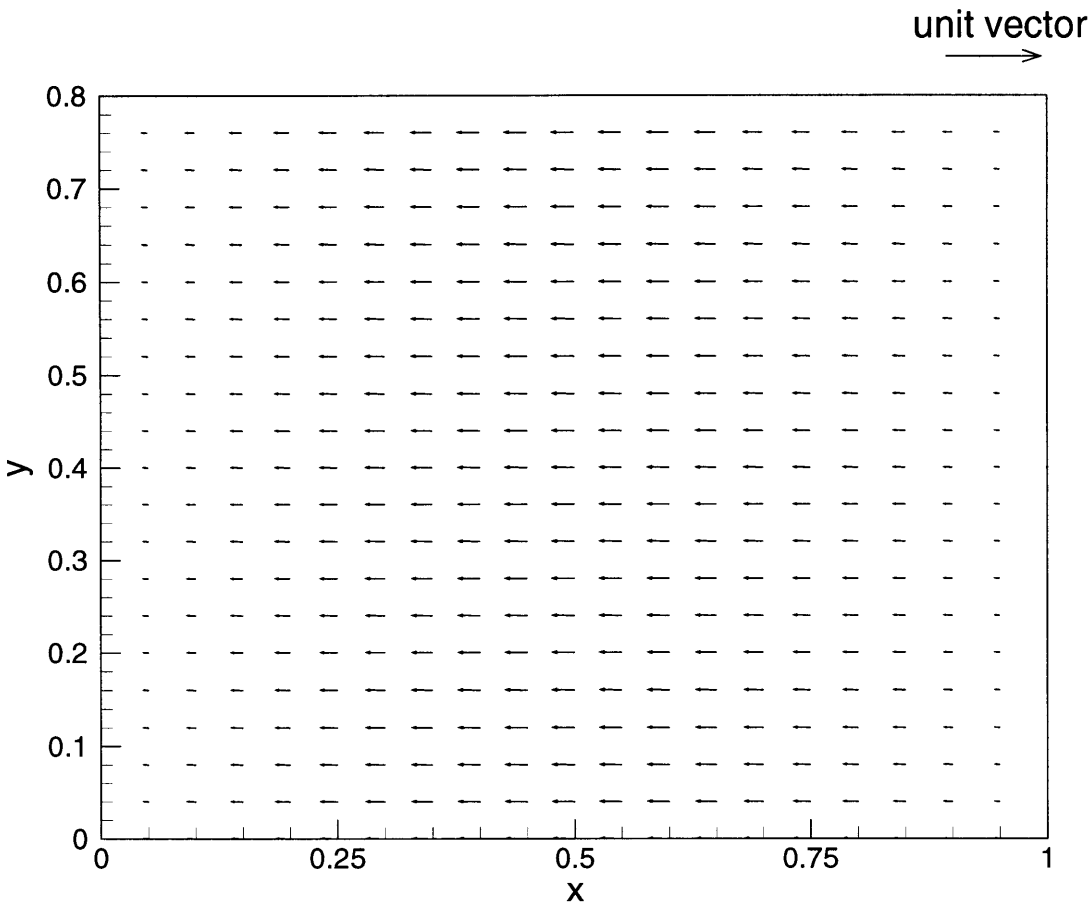

Figure II-4-9: Flow pattern of $\mathbf{u}^{(1)}$ at $z = -0.7$ and $t = \pi/4$.

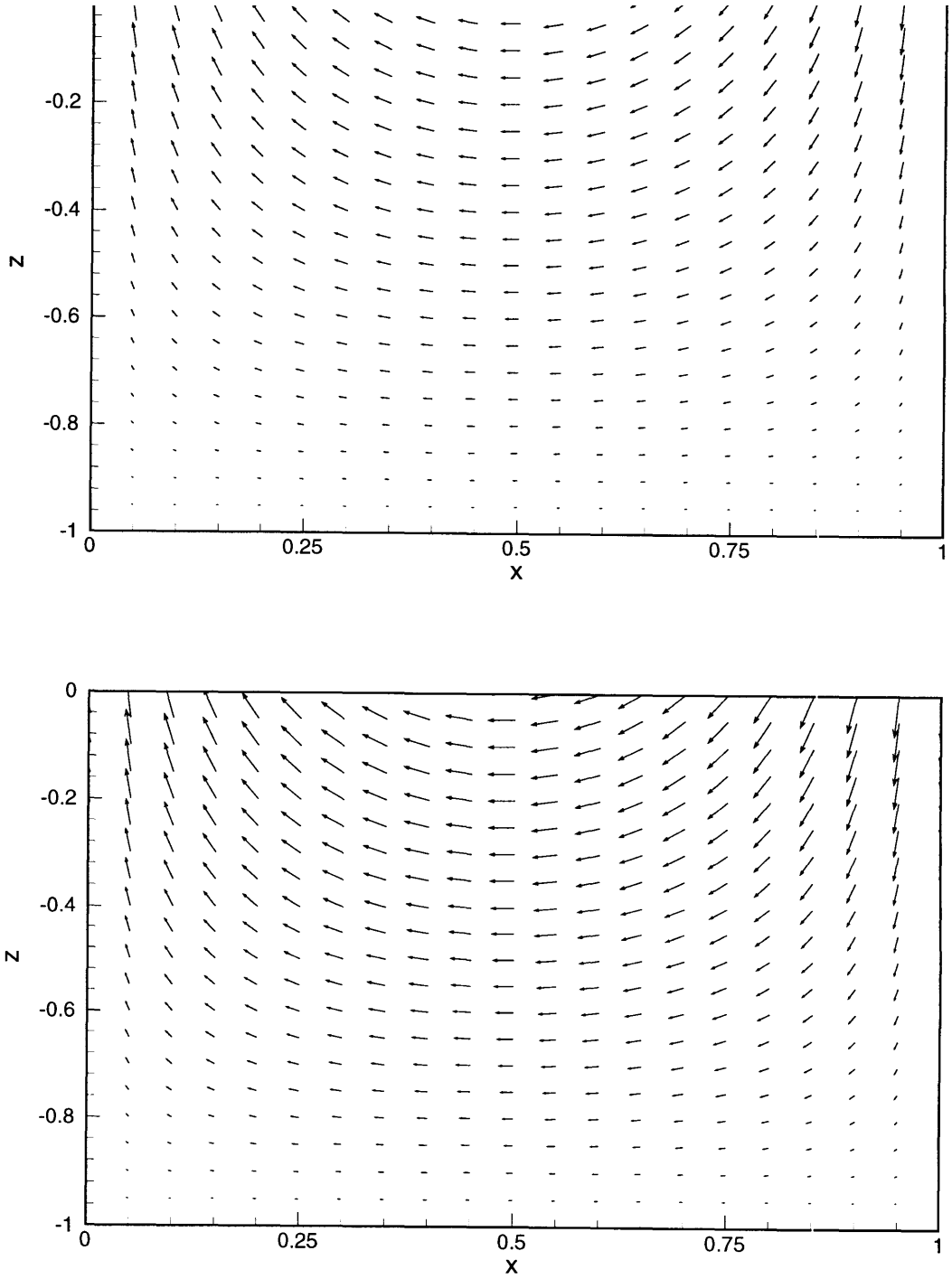

Figure II-4-10: Snapshots of circulation in xz plane at $y = h/2L$. Upper: $t = T/2$;

to move, following the streaming shown in the figure, toward the left region under the left half surface which is rising. At $t = 0$ the fluid starts to be pushed to the left region and at $t = 0.5\pi$ the vertical velocity reaches its maximum. Then the flow slows down till it stops moving in this plane at $t = \pi$. After that the process reverses and the fluid goes back to the right region as the left half surface drops and the right half rises.

In summary, the transient effect due to the oscillation of $\zeta^{(0)}$ plays the mojor role in driving the flow at this order. Due to the small aspect ratio, the real flow is mainly oscillating in x direction with a phase lag of $3\pi/2$ behind the forcing $\zeta^{(0)}$, which is exactly in phase with $\mathbf{u}^{(0)}$. The transient and Coriolis effect due to $\mathbf{u}^{(0)}$ is minor and hence the flow perpendicular to $\vec{\tau}$ is relatively trivial.

At $O(\epsilon^2)$,

$$\frac{\partial^2 \mathbf{u}^{(2)}}{\partial z^2} - \nabla \zeta^{(2)} = \frac{\partial \mathbf{u}^{(1)}}{\partial t} + \frac{\mathbf{f}}{\omega} \times \mathbf{u}^{(1)} + Re(\mathbf{u}^{(0)} \cdot \nabla \mathbf{u}^{(0)} + w \frac{\partial \mathbf{u}^{(0)}}{\partial z}), \tag{II.4.39}$$

With $\mathbf{u}^{(0)}$ being horizontally uniform and $w^{(0)}$, the nonlinear forcing terms vanish in this particular example. To obtain the steady streaming, we take time average over a wind period.

$$\frac{\partial^2 \langle \mathbf{u}^{(2)} \rangle}{\partial z^2} - \nabla \langle \zeta^{(2)} \rangle = 0, \tag{II.4.40}$$

with the boundary conditions

$$\langle \mathbf{u}^{(2)} \rangle = 0, \quad z = -1, \tag{II.4.41}$$

and

$$\begin{aligned}\frac{\partial\langle\mathbf{u}^{(2)}\rangle}{\partial z} &= -\alpha\langle\zeta^{(0)}\frac{\partial^2\mathbf{u}^{(0)}}{\partial z^2}|_{z=0}\rangle \\ &= -\alpha\langle\{\frac{3}{4}[\tau_x(x-\frac{a}{2L})+\tau_y(y-\frac{b}{2L})]e^{-it}+\ *\} \\ &\quad\times[\frac{3\vec{\tau}}{4}e^{-it}+\ *]\rangle \\ &= -\frac{9\alpha\vec{\tau}}{8}[\tau_x(x-\frac{a}{2L})+\tau_y(y-\frac{b}{2L})],\quad z=0, \qquad \text{(II.4.42)}\end{aligned}$$

in which asterisks denote the complex conjugates. The solution is

$$\frac{\partial\langle\mathbf{u}^{(2)}\rangle}{\partial z} = z\nabla\langle\zeta^{(2)}\rangle - \frac{9\alpha\vec{\tau}}{8}[\tau_x(x-\frac{a}{2L})+\tau_y(y-\frac{b}{2L})], \qquad \text{(II.4.43)}$$

and

$$\langle\mathbf{u}^{(2)}\rangle = \frac{1}{2}\nabla\langle\zeta^{(2)}\rangle(z^2-1) - \frac{9\alpha\vec{\tau}}{8}(z+1)[\tau_x(x-\frac{a}{2L})+\tau_y(y-\frac{b}{2L})]. \qquad \text{(II.4.44)}$$

Integrating from the bottom to the static water surface,

$$\langle\mathbf{Q}_0{}^{(2)}\rangle = -\frac{1}{3}\nabla\langle\zeta^{(2)}\rangle - \frac{9\alpha\vec{\tau}}{16}[\tau_x(x-\frac{a}{2L})+\tau_y(y-\frac{b}{2L})]. \qquad \text{(II.4.45)}$$

The time average continuity equation at this order

$$\nabla\cdot\langle\mathbf{Q}_0{}^{(2)}\rangle + \alpha\nabla\cdot\langle\zeta^{(0)}\mathbf{u}^{(0)}|_{z=0}\rangle = 0, \qquad \text{(II.4.46)}$$

with

$$\langle Q_{0x}^{(2)}\rangle + \alpha\langle\zeta^{(0)}u^{(0)}|_{z=0}\rangle = 0,\quad x=0,a/L, \qquad \text{(II.4.47)}$$

and

$$\langle Q_{0y}^{(2)}\rangle + \alpha\langle\zeta^{(0)}v^{(0)}|_{z=0}\rangle = 0,\quad y=0,b/L. \qquad \text{(II.4.48)}$$

Making use of Equation (II.4.45), we have the governing equation for the time-averaged surface set-up

$$\nabla^2\langle\zeta^{(2)}\rangle = -\frac{9\alpha}{8}, \qquad \text{(II.4.49)}$$

which is simply a Poisson equation with the following lateral boundary conditions:

$$\frac{\partial\langle\zeta^{(2)}\rangle}{\partial x} = -\frac{9\alpha\tau_x}{8}[\mp\tau_x\frac{a}{2L} + \tau_y(y - \frac{b}{2L})], \quad x = 0, a/L, \tag{II.4.50}$$

and

$$\frac{\partial\langle\zeta^{(2)}\rangle}{\partial y} = -\frac{9\alpha\tau_y}{8}[\tau_x(x - \frac{a}{2L}) \mp \tau_y\frac{b}{2L}], \quad y = 0, b/L. \tag{II.4.51}$$

Noting that the above equation set is linear, we rewrite

$$\langle\zeta^{(2)}\rangle = \zeta^* + \overline{\zeta_1}(x) + \overline{\zeta_2}(y), \tag{II.4.52}$$

with

$$\zeta^* = -\frac{9\alpha}{8}\tau_x\tau_y(x - \frac{a}{2L})(y - \frac{b}{2L}), \tag{II.4.53}$$

satisfying Laplace equation. It is readily seen that

$$\frac{d^2\overline{\zeta_1}}{dx^2} = -\frac{9\alpha\tau_x^2}{8}, \tag{II.4.54}$$

subjecting to

$$\frac{d\overline{\zeta_1}}{dx} = \pm\frac{9\alpha\tau_x^2 a}{16L}, \quad x = 0, a/L, \tag{II.4.55}$$

and

$$\frac{d^2\overline{\zeta_2}}{dy^2} = -\frac{9\alpha\tau_y^2}{8}, \tag{II.4.56}$$

subjecting to

$$\frac{d\overline{\zeta_2}}{dy} = \pm\frac{9\alpha\tau_y^2 b}{16L}, \quad y = 0, b/L. \tag{II.4.57}$$

We readily get

$$\overline{\zeta_1} = -\frac{9\alpha\tau_x^2}{16}(x - \frac{a}{2L})^2 + C_x, \tag{II.4.58}$$

and,

$$\overline{\zeta_2} = -\frac{9\alpha\tau_y^2}{16}(y - \frac{b}{2L})^2 + C_y, \tag{II.4.59}$$

where by substituting (II.4.58) and (II.4.59) back to (II.4.52) C_x and C_y add up to a constant which is fixed with the mass constraint (II.2.109). Hence,

$$\begin{aligned}\langle\zeta^{(2)}\rangle &= -\frac{9\alpha}{8}\tau_x\tau_y(x-\frac{a}{2L})(y-\frac{b}{2L}) \\ &+ \frac{3\alpha}{16}\{\tau_x^2[-3(x-\frac{a}{2L})^2+\frac{(a/L)^2}{4}] \\ &+ \tau_y^2[-3(y-\frac{b}{2L})^2+\frac{(b/L)^2}{4}]\}. \end{aligned} \tag{II.4.60}$$

Clearly,

$$\nabla\langle\zeta^{(2)}\rangle = -\frac{9\alpha}{8}[\tau_x(x-\frac{a}{2L})+\tau_y(y-\frac{b}{2L})]\vec{\tau}. \tag{II.4.61}$$

The surface slope is parallel to the wind stress and linear in x and y. The free surface is a parabola. A contour distribution and surface plot are displayed in Figure II-4-11 and Figure II-4-12 for a wind inclined at 22.5° with respect to the positive x axis. The physical parameters are taken as $h_0 = 4$ m, $L = 10000$ m, $\omega = 7.27\cdot 10^{-5}$ s^{-1}, $\tau_0/\rho = 10^{-4}$ m^2/s^2, $a/L = 1$ and $b/L = 0.8$. Along the wind direction the surface rises in the middle and drops at both ends. The surface elevation remains the same along the straight line perpendicular to the wind direction.

Therefore, the steady mass transport is found from (II.4.44) to be

$$\langle\mathbf{u}^{(2)}\rangle = -\frac{9\alpha\vec{\tau}}{16}(z+1)^2[\tau_x(x-\frac{a}{2L})+\tau_y(y-\frac{b}{2L})], \tag{II.4.62}$$

and

$$\begin{aligned}\langle w^{(2)}\rangle &= -\int_{-1}^{z}\nabla\cdot\langle\mathbf{u}^{(2)}\rangle dz' \\ &= \frac{3\alpha}{16}(z+1)^3. \end{aligned} \tag{II.4.63}$$

A plot of the surface steady streaming pattern corresponding to the above plotted steady surface displacement is shown in Figure II-4-13.

It shows that the surface steady streaming is along the forcing direction, flowing towards the line with maximum elevation and the magnitude of speed reduces linearly

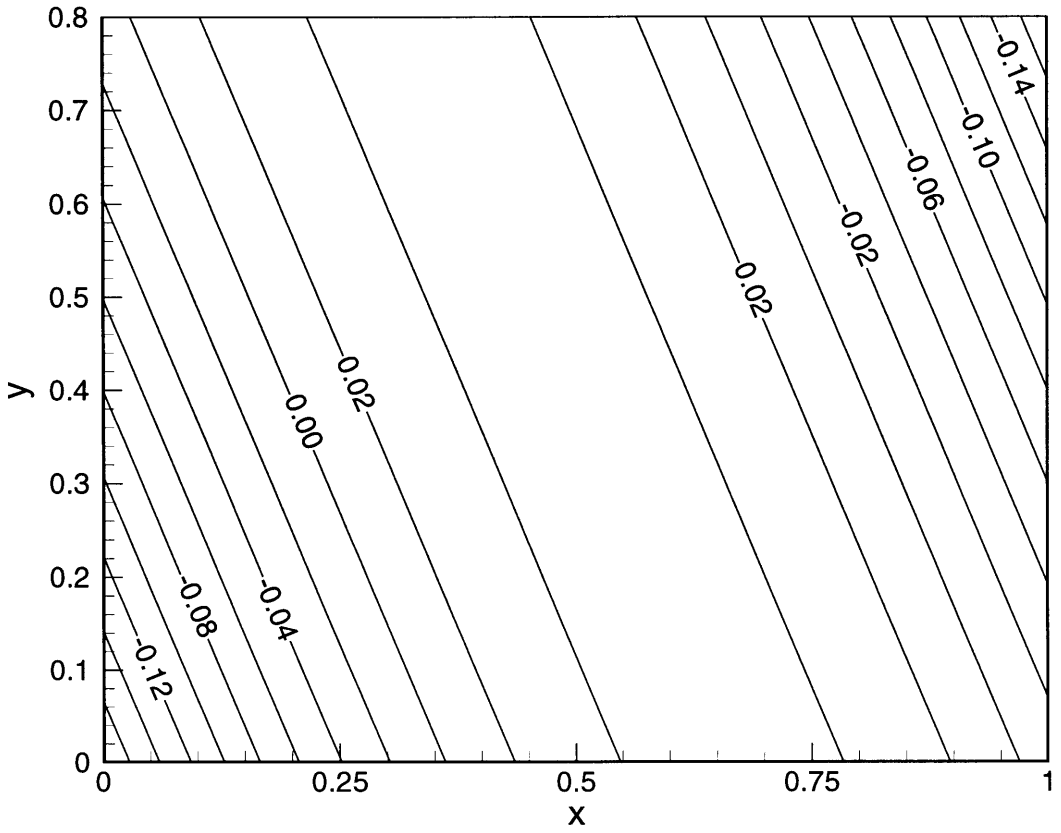

Figure II-4-11: Contours of steady surface set-up $\langle \zeta^{(2)} \rangle$ with a wind inclined at 22.5° with respect to the positive x axis.

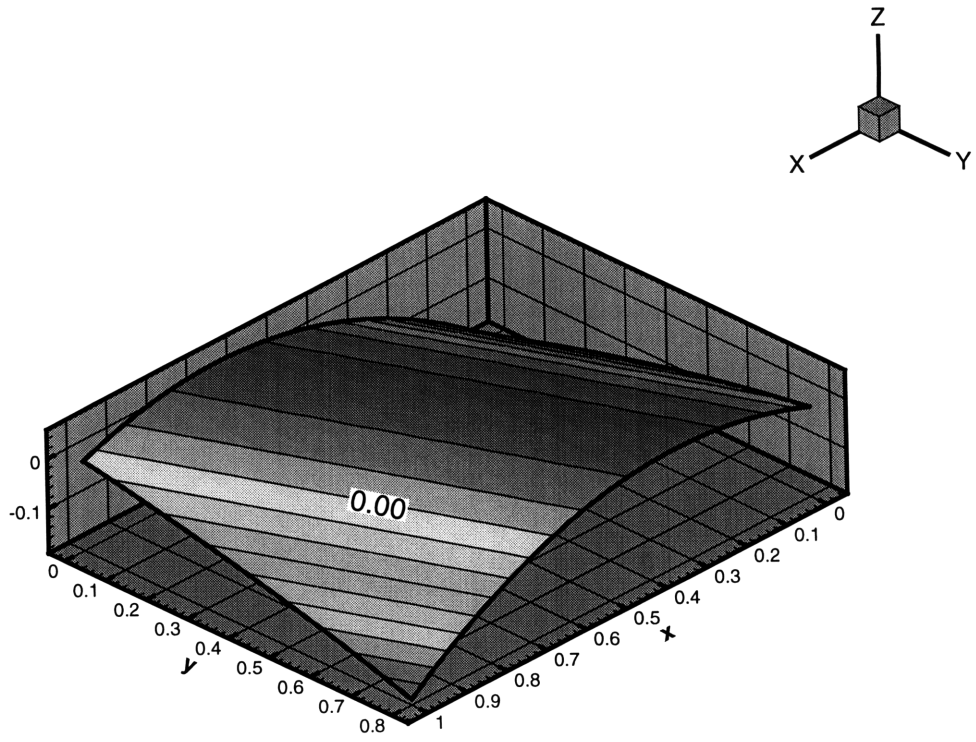

Figure II-4-12: Surface plot of steady surface set-up $\langle \zeta^{(2)} \rangle$

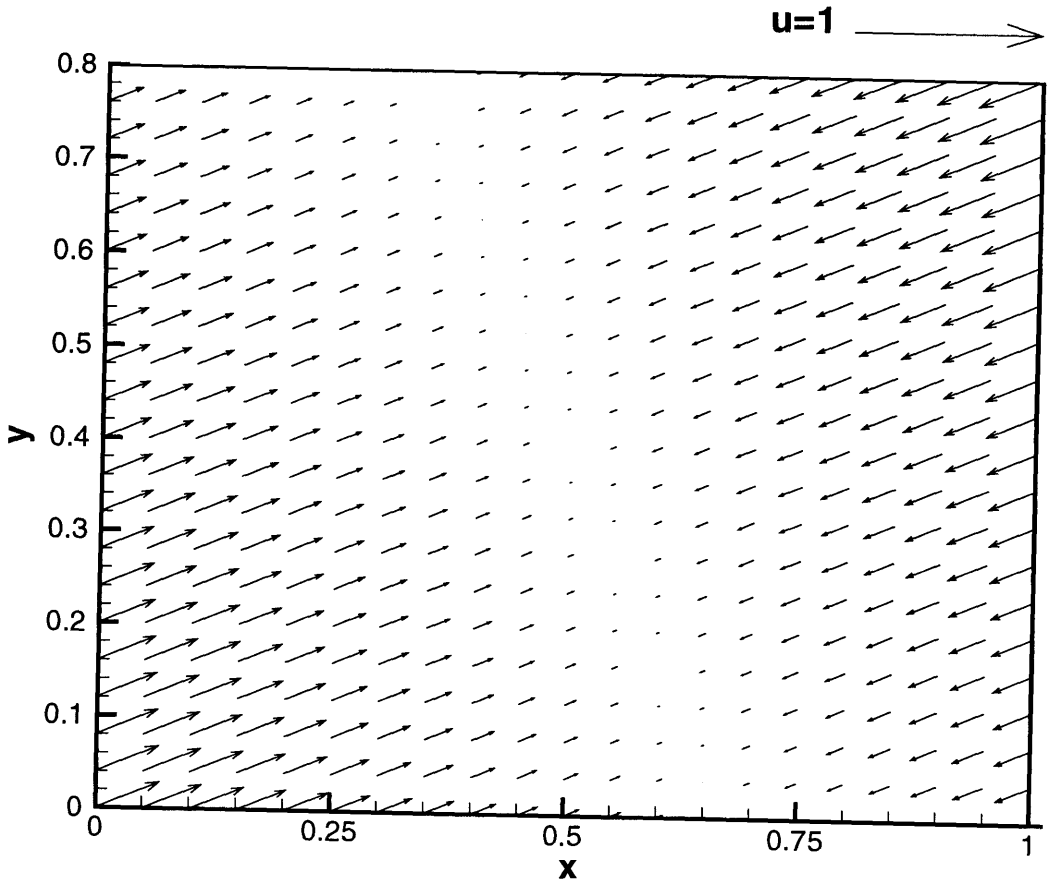

Figure II-4-13: Surface mass transport pattern with the wind making a 22.5° angle with $+x$ axis

and vanishes at the crestline. The flow pattern at lower level should be the same except that the speed of streaming drops quadraticly with z, described by (II.4.62). Since $\mathbf{u}^{(0)}$ varies linearly in x and y, we understand that $w^{(2)}$ will be constant in any horizontal plane.

To verify the correctness of the above result, let us check with mean mass transport at the surface through an different approach. Collecting terms from (II.4.35) at $O(\epsilon^2)$,

$$w^{(2)} + \alpha\zeta\frac{\partial w^{(0)}}{\partial z} = S_t\frac{\partial \zeta^{(1)}}{\partial t} + \alpha\mathbf{u}^{(0)}\cdot\nabla\zeta^{(0)}, \quad z = 0. \tag{II.4.64}$$

Recalling Equation (II.4.13) and taking time average over a wind period, we can see that, at $z = 0$,

$$\begin{aligned}\langle w^{(2)}\rangle &= \alpha\langle\mathbf{u}^{(0)}\cdot\nabla\zeta^{(0)}\rangle \\ &= \alpha\langle(\frac{\vec{\tau}}{8}e^{-it} + \ *)\cdot(\frac{3}{4}\vec{\tau}e^{-it} + \ *)\rangle \\ &= \frac{3\alpha}{16},\end{aligned} \tag{II.4.65}$$

which agrees with Equation (II.4.63) at $z = 0$. From the results for a general shaped lake, we put $\Gamma = 3/2$ and $\gamma = -1/2$, and get perfect agreement. From Equation (II.4.62), the horizontal steady streaming is always parallel to the wind stress vector $\vec{\tau}$. That is to say, the steady mass transport is confined within a vertical plane parallel to the wind forcing.

To make more sense of the results let us take another look. It is clear from (II.4.65) that the vertical streaming at the surface is determined by the interaction between the leading order sinusoidal velocity and the sinusoidal surface slope over a wind period. Unless $\mathbf{u}^{(0)}$ and $\zeta^{(0)}$ have a phase difference of $\pi/2$, the vertical mass transport should not be zero. Now,

$$\nabla\zeta^{(0)} = \frac{3}{2}\vec{\tau}e^{-it}, \tag{II.4.66}$$

which is perfectly in phase with $\mathbf{u}^{(0)}$ due to the quasi-steady behavior at the leading order, we can infer that $\langle w^{(2)}\rangle$ is positive. In addition, both $\mathbf{u}^{(0)}$ and the leading order surface slope are uniform in horizontal plane. As a result, $\langle w^{(2)}\rangle$, remains invariant

horizontally. From (II.4.63) we expect that $\langle \mathbf{u}^{(2)} \rangle$ varies linearly in x. Due to the geometrical and the forcing symmetry with respect to $x = a/2L$, it is natural that along this line $\langle \mathbf{u}^{(2)} \rangle$ ought to be zero. Consider the integrated continuity equation (II.4.46). The second term is actually the vertical transport at the surface. In fact,

$$\alpha \nabla \cdot \langle \zeta^{(0)} \mathbf{u}^{(0)}|_{z=0} \rangle = \alpha \langle \mathbf{u}^{(0)}|_{z=0} \nabla \cdot \zeta^{(0)} \rangle = \langle w^{(2)} \rangle \tag{II.4.67}$$

Think of a water column stemming from the bottom to the static water surface. The above equation simply states that the net inflow across the four sides flows out of the top.

From the steady momentum conservation (II.4.40) we see the balance between the net shear stress and the net pressure force, the same as that at the leading order. This implies a parabolic profile of the horizontal transport. The surface shear stress in (II.4.42), different from that at the leading order where the stress is spatially uniform wind, now becomes spatially variable as a result of interaction of the surface oscillation and the oscillatory vertical gradient of shear stress at the static surface level.

From Equation (II.4.62) we see that the horizontal steady streaming is always parallel to the wind stress vector $\vec{\tau}$. That is to say, the steady mass transport is confined within a vertical plane parallel to the wind. Taking advantage of this property we consider a case with the wind blowing along x, without loss of generality. Now, $\tau_x = 1$ and $\tau_y = 0$. As we have found the equal-elevation lines are all perpendicular to the wind direction, the problem reduces to one dimensional, independent of y. With this simplification, the distribution of steady surface shear stress becomes

$$\frac{\partial \langle u^{(2)} \rangle}{\partial z} = -\frac{9\alpha}{8}(x - \frac{a}{2L}), \quad z = 0 \tag{II.4.68}$$

It is obvious that the stress decreases linearly from positive value (along x) to negative value, vanishing at the plane of symmetry at $x = a/2L$. This explains the surface

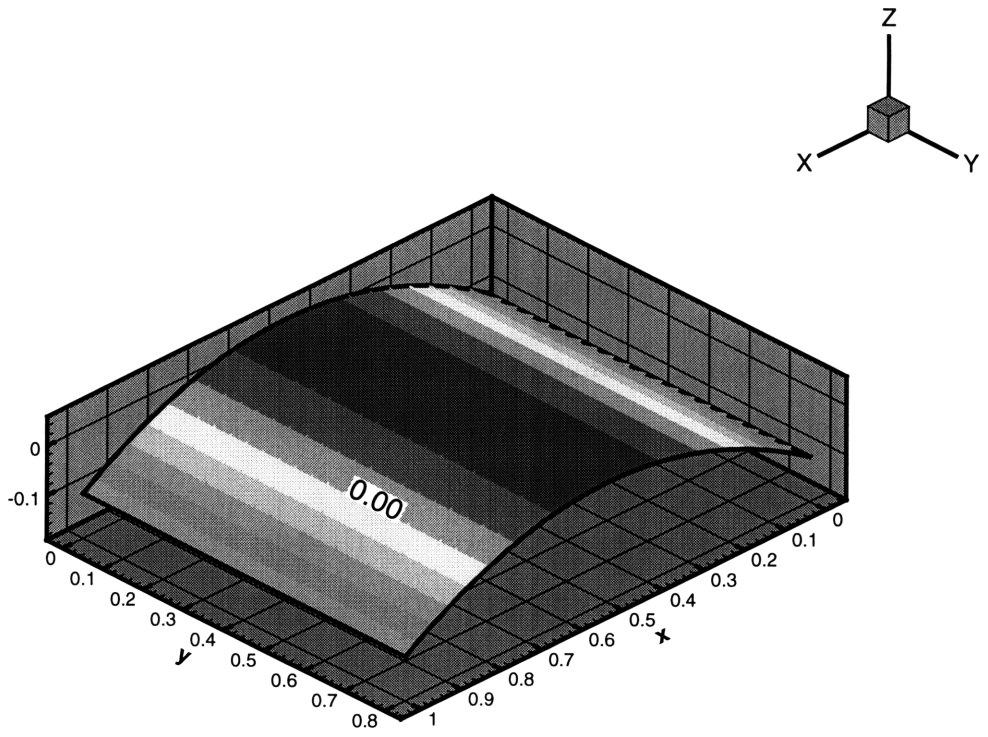

Figure II-4-14: Steady surface set-up due to oscillatory wind along x axis.

rise in the middle and depression at both ends. Also, (II.4.49) reduces to

$$\frac{\partial^2 \langle \zeta^{(2)} \rangle}{\partial x^2} = -\frac{9\alpha}{8}, \tag{II.4.69}$$

implying a constant negative surface curvature, as is seen in Figure II-4-14.

In this case, the transport pattern in xz is plotted in Figure II-4-15. Keeping in mind that the plot is for dimensionless quantities and that the scale for vertical velocity is two orders ($h_0/L \leq O(\epsilon^2)$) smaller than the horizontal velocity, the physical mass transport is essentially horizontal as we expect in shallow water system.

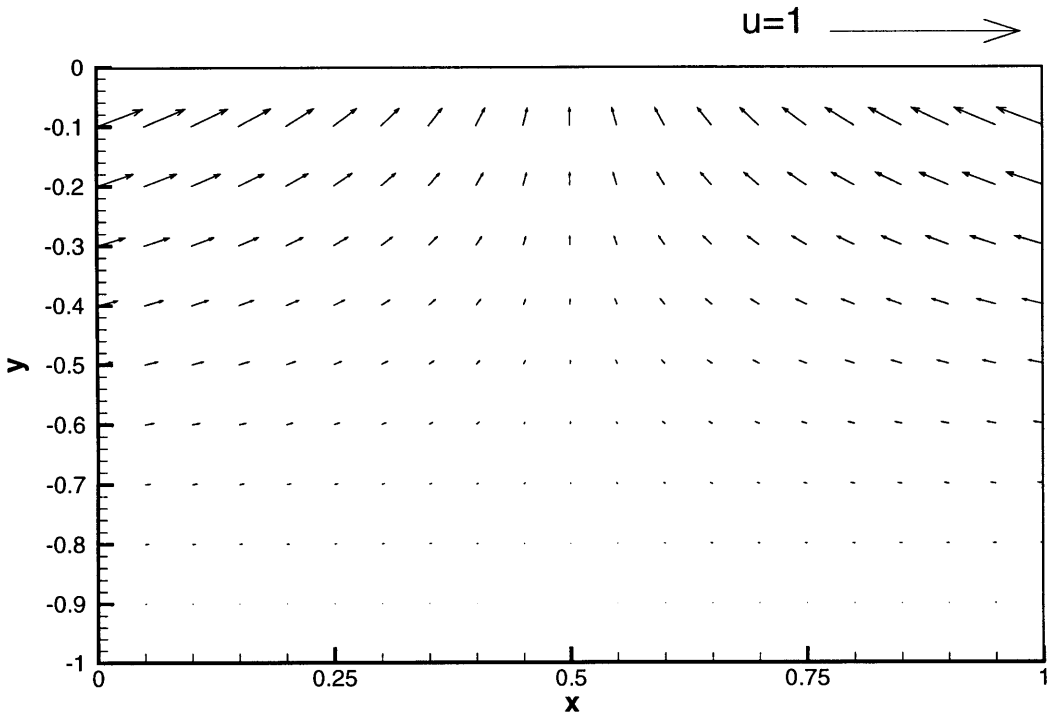

Figure II-4-15: Mass transport pattern in xz due to oscillatory wind along x axis.

Chapter 5

Conclusion

The shallow water response to a surface sinusoidal wind in a basin with topographic variation is studied. Due to the shallowness of the lake and the low frequency of wind the vertical structure of the flow establishes before any significant change of forcing happens. Consequently we have a quasi-steady problem and the vertical direction is decoupled with the horizontal direction. This simply allows us to solve an odinary differential equation at various orders for the vertical flow profile in terms of surface slope. With the small parameter ϵ which stands for the ratio of the time it takes for momentum to be transported across the layer to the wind period, a perturbation theory is presented and leads to an elliptic governing equation and a Neumann boundary condition for the surface displacement at each order. With an eddy viscosity of vertical dependency, the solution of surface movement and the velocity field can be determined straightforwardly.

In a lake of constant depth but arbitrary shore configuration, analytical results are obtained for the leading order flow field, the steady streaming and surface set-up at $O(\epsilon^2)$ for a spatially uniform wind. At $O(1)$ the surface remains as a plane at any moment and the surface slope is parallel to the wind. The flow field is one dimensional (along the wind direction) and independent of x or y. The surface oscillation is exactly in phase with the oscillatory flow velocity. The steady surface at $O(\epsilon^2)$ is found to be a concave parabola with equal-elevation lines perpendicular to the wind. The mass transport converges toward the crestline. In these two situations fluxes across the

depth are universally zero. This implies that the no-penetration lateral boundary condition can be satisfied regardless of the location of the bank. These solutions are valid for a general eddy viscosity distribution across the depth. Nevertheless, different eddy viscosity models will result in different vertical structures of the flow field. We have not worked out the analytical solution for the oscillatory flow field at $O(\epsilon)$ due to the spatially varying source term associated with oscillation of the leading order surface level in the governing equation.

A more special case of rectangular lake with constant eddy viscosity is discussed to show more explicit results. The solutions at the leading order and the steady streaming are shown to be reducible from the more general results in the arbitrary-shaped lake with general $\nu(z)$. At $O(\epsilon)$, the transient effect of $\zeta^{(0)}$ dominates the contribution from $\mathbf{u}^{(0)}$ and thus Coriolis effect is relatively trivial.

The immediate further work will be the numerical solution of the pertubation equations at various orders for a basin with topographic variation. .

Appendix A

Fortran program solving the effective transport equation

```
ccccccccccccccccccccccccccccccccccccccccccccccccccccccccccccccccccccccc
c     Solving Advection-Diffusion Equation with ADI Method
c     Polar Coordinates with Stretching
c     Dispersion of Particles near a Circular Peninsula
c     ----------by Feng Ye, Summer, 1997----------
ccccccccccccccccccccccccccccccccccccccccccccccccccccccccccccccccccccccc

      parameter(mm=201,nn=201,PI=3.1415927)

      real a1x(mm),a2x(mm),a3x(mm),b1x(mm,nn),b1y(mm,nn)                    10
      real b2(mm,nn),b3x(mm,nn),b3y(mm,nn),b3xy(mm,nn)
      real a1y(nn),a2y(nn),a3y(nn),c(mm,nn),rr(mm),c15(mm,nn)
      real a1y0(nn),a2y0(nn),a3y0(nn),c5(mm,nn),c10(mm,nn)
      real tht(nn),ccx(mm),ccy(nn),rx(mm),ry(nn),xx(mm,nn),yy(mm,nn)
      real rx0(mm,nn),ry0(mm,nn),drr1(nn),dtt1(mm),dttnn(mm)
      real ax1r(mm),ax1l(mm),ax3r(mm),ax3l(mm),ax2r(mm),ax2l(mm)
      complex z,ii,dwdz,uv,h1,wpp,udu
      real ih1

      open(51, file='bump.inp', status='old')                               20
      read(51,*)nt,rc,thtc,totalt,t0
```

```
      close(51)

      ii=(0.,1.)
      r41=0.017
      r42=0.0022
      r43=0.0435
      r44=-0.0345
      rh1=0.0833
      ih1=-0.089                                                    30
      h1=rh1+ii*ih1
      d0=0.001
      thtc=pi*thtc
      ximax=0.2
      nxi=mm-1
      ne=nn-1
      ntht=ne
      rmax=exp(2.*pi*ximax)
      r0=1.
      dt=totalt/float(nt)                                           40
      dxi=ximax/float(nxi)
      dtht=PI/float(ntht)
      de=1./float(ne)
      c0=1.
      xc=rc*cos(thtc)
      yc=rc*sin(thtc)
      b0=2.*dxi*de/dt

      open(11,file='eij.out')
      write(11,*)'title="dispersion coef"'                          50
      write(11,*)'variables="x","y","exy","eyx"'
      write(11,*)'zone i=',nn,', j=',mm,', f=point'
      write(*,*)'coef iter starts'
1000  format(1x,3f12.7)

      do 101 i=1,nxi+1
        xi=(i-1)*dxi
```

```
      r=exp(2.*PI*xi)
      rr(i)=r
      s0=1./2./pi/r                                                    60
     do 101 j=1,ne+1
      tht(j)=(j-1)*dtht
      tht1=tht(j)
      x=r*cos(tht1)
      xx(i,j)=x
      y=r*sin(tht1)
      yy(i,j)=y
      c(i,j)=c0*exp(-((x-xc)**2+(y-yc)**2)/0.01)

c---------parameters in xi, eta coordinates--------                    70

      z=x+ii*y
      dwdz=1.-1./z**2
      wpp=2./z**3
      uv=h1*dwdz*conjg(wpp)
      udu=dwdz*conjg(wpp)
      udur=real(udu)
      udui=aimag(udu)
      dax=(r44-r43)*udui
      day=-(r44-r43)*udur                                              80
      u=real(uv)
      v=aimag(uv)
      u0=real(dwdz)
      v0=-aimag(dwdz)
      u0dx=2.*cos(3*tht1)/r/r/r
      v0dy=-u0dx
      u0dy=2.*sin(3*tht1)/r/r/r
      v0dx=u0dy
      gamma=rh1*2.*(u0dx**2+v0dx**2)
      dxx=r41*u0*u0+r42*v0*v0+(r43+r44)*u0*v0+d0                       90
      dyy=r42*u0*u0+r41*v0*v0-(r43+r44)*u0*v0+d0
      dxy=0.5*(r44+r43)*(v0*v0-u0*u0)+(r41-r42)*u0*v0
      ut=u+dax
```

```
      vt=v+day
      exy=-r43*u0*u0+r44*v0*v0+(r41-r42)*u0*v0
      eyx=r43*v0*v0-r44*u0*u0+(r41-r42)*u0*v0
      write(11,4000)x,y,exy,eyx
      ddx=v0*u0dx+u0*v0dx
      ddy=v0*u0dy+u0*v0dy
      dxxdx=2.*r41*u0*u0dx+r42*2.*v0*v0dx+(r43+r44)*ddx                    100
      dyydy=2*r42*u0*u0dy+2*r41*v0*v0dy-(r43+r44)*ddy
      dxydx=(r43+r44)*(v0*v0dx-u0*u0dx)+(r41-r42)*ddx
      dxydy=(r43+r44)*(v0*v0dy-u0*u0dy)+(r41-r42)*ddy
      up=ut-dxxdx-dxydy
      vp=vt-dxydx-dyydy
      drr=dxx*cos(tht1)**2+dxy*sin(2*tht1)+dyy*sin(tht1)**2
      dtt=dxx*sin(tht1)**2-dxy*sin(2*tht1)+dyy*cos(tht1)**2
      dtr=(dyy-dxx)*sin(2.*tht1)/2.+dxy*cos(2.*tht1)
      urp=up*cos(tht1)+vp*sin(tht1)-dxx*sin(tht1)**2/r-dyy*cos(tht1)
     $     **2/r+dxy*sin(2.*tht1)/r                                      110
      utp=-up*sin(tht1)+vp*cos(tht1)-dxx*sin(2*tht1)/r+dyy
     $     *sin(2*tht1)/r+2*dxy*(2*cos(tht1)**2-1)/r

      if(i.eq.1) then
        ert=(dyy-dxx)*cos(tht1)*sin(tht1)+exy*cos(tht1)**2
     $       -eyx*sin(tht1)**2
        err=dxx*cos(tht1)**2+dyy*sin(tht1)**2
     $       +cos(tht1)*sin(tht1)*(exy+eyx)
        a1y0(j)=2.*ert*dxi
        a3y0(j)=-a1y0(j)                                                  120
        ure=u*cos(tht1)+v*sin(tht1)
        a2y0(j)=4.*pi*r0*ure*dxi*de+3.*err*de
        drr1(j)=err

        if (j.eq.1) then
          drt11=ert
          ur1=ure
        endif
```

```
      if (j.eq.nn) then                                                  130
        drt1nn=ert
        urnn=ure
      endif
    endif

    if(j.eq.1) then
      dtr=(-dxx+dyy)*cos(tht1)*sin(tht1)-exy*sin(tht1)**2
     $     +eyx*cos(tht1)**2
      ax1r(i)=dtr*de
      ax3r(i)=-ax1r(i)                                                   140
      utht=v
      dtt=dxx*sin(tht1)**2+dyy*cos(tht1)**2
     $     -(exy+eyx)*cos(tht1)*sin(tht1)
      dtt1(i)=dtt
      ax2r(i)=4.*pi*r*dxi*de*utht+6.*dtt*dxi

  endif

  if(j.eq.nn) then
    dtr=(-dxx+dyy)*cos(tht1)*sin(tht1)-exy*sin(tht1)**2                  150
     $     +eyx*cos(tht1)**2
    ax1l(i)=-dtr*de
    ax3l(i)=-ax1l(i)
    utht=-v
    dtt=dxx*sin(tht1)**2+dyy*cos(tht1)**2
     $     -(exy+eyx)*cos(tht1)*sin(tht1)
    dttnn(i)=dtt
    ax2l(i)=-4.*pi*dxi*de*r*utht+6.*dtt*dxi

    if(ax2l(i).le.0.and.i.ne.1.and.i.ne.mm) then                         160
      write(*,*)'ax2l(',i,')=',ax2l(i)
    endif
  endif

  gxi=urp*s0+2.*PI*drr*s0*s0
```

```
      ge=utp*s0*2.
      gxx=drr*s0*s0
      gee=dtt*s0*s0*4.
      gxe=dtr*s0*s0*2.
                                                                      170
      b1x(i,j)=gxi*de/2.
      b1y(i,j)=ge*dxi/2.
      b2(i,j)=gamma*dxi*de/2.
      b3x(i,j)=gxx*de/dxi
      b3y(i,j)=gee*dxi/de
      b3xy(i,j)=gxe/2.

101   continue

3000  format(1x,5f12.5)                                               180

      close(11)
4000  format(1x,4f12.4)

      open(46,file='monit1.out')

      vol=0.

      do 550 i=1,nxi
        ds=dxi*de*(PI*(rr(i)+rr(i+1)))**2/2.                          190
      do 550 j=1,ne

550     vol=vol+ds*0.25*(c(i,j)+c(i,j+1)+c(i+1,j)+c(i+1,j+1))

      vol0=vol
      write(*,*)'vol0',vol0,'vol/vol0',vol/vol0

      do 201 j=1,nn
201     c(mm,j)=0.
                                                                      200
      write(*,*)'opening "out1.dat"'
```

```
      open(12,file='out1.dat',status='unknown')

      t=t0
      write(*,*)'time marching begins'
      open(32,file='masscons.out')

      do 100 k=1,nt
        t=t+dt                                                          210
        cm=0.
        do 504 i=2,nxi
        do 504 j=2,ne
          alpha=b3xy(i,j)*(c(i+1,j+1)-c(i-1,j+1)-c(i+1,j-1)+c(i-1,j-1))
504       rx0(i,j)=(b0-b2(i,j)-2*b3y(i,j))*c(i,j)+(b3y(i,j)-b1y(i,j))*
     $       c(i,j+1)+(b1y(i,j)+b3y(i,j))*c(i,j-1)+alpha

        do 10 j=2,ne
          do 20 i=1,nxi
            a1x(i)=-b1x(i,j)-b3x(i,j)                                   220
            a2x(i)=b0+b2(i,j)+2*b3x(i,j)

            if(a2x(i).lt.0.) write(*,*)i,j,'a2x(i)=',a2x(i)
            a3x(i)=b1x(i,j)-b3x(i,j)

            rx(i)=rx0(i,j)
20        continue
          rx(2)=rx(2)-a1x(2)*c(1,j)

          call solve(a1x,a3x,a2x,rx,mm,ccx)                             230
          do 15 i=2,nxi
            c(i,j)=ccx(i)

            if(c(i,j).lt.-1.0e-3) then
              write(*,*)'c<e-3 at',i,j,c(i,j),'k=',k
              ac=abs(c(i,j))
```

```
            if(ac.gt.cm) cm=ac
          endif
15        continue                                                    240
10        continue

      do 45 j=2,ne
45      ry(j)=drr1(j)*de*(4.*c(2,j)-c(3,j))

      ry(2)=ry(2)-a1y0(2)*c(1,1)
      ry(ne)=ry(ne)-a3y0(ne)*c(1,nn)
      call  solve(a1y0,a3y0,a2y0,ry,nn,ccy)

      do 6 j=2,ne                                                     250
        c(1,j)=ccy(j)

        if(c(1,j).lt.-1.0e-5) then
          write(*,*)'c=',c(1,j),'at i=1,j)=',j
          read(*,*)k2
        endif
6     continue

      do 145 i=2,nxi
145     rx(i)=2.*dtt1(i)*dxi*(4.*c(i,2)-c(i,3))                       260

      rx(2)=rx(2)-ax1r(2)*c(1,1)
      call solve(ax1r,ax3r,ax2r,rx,mm,ccx)

      do 106 i=2,nxi
        c(i,1)=ccx(i)
106   continue

      do 146 i=2,nxi
146     rx(i)=2.*dttnn(i)*dxi*(4.*c(i,ne)-c(i,ne-1))                  270

      rx(2)=rx(2)-ax1l(2)*c(1,nn)
      call solve(ax1l,ax3l,ax2l,rx,mm,ccx)
```

```
      do 107 i=2,nxi
        c(i,nn)=ccx(i)
107   continue

      c(1,1)=(4.*c(2,1)-c(3,1))/3.
      c(1,nn)=(4.*c(2,nn)-c(3,nn))/3.                                    280

      do 505 i=2,nxi
      do 505 j=2,ne
        alpha=b3xy(i,j)*(c(i+1,j+1)-c(i-1,j+1)-c(i+1,j-1)+c(i-1,j-1))
505   ry0(i,j)=(b0-b2(i,j)-2*b3x(i,j))*c(i,j)+(b3x(i,j)-b1x(i,j))*
     $      c(i+1,j)+(b1x(i,j)+b3x(i,j))*c(i-1,j)+alpha

      do 30 i=2,nxi
        do 35 j=1,nn
          a1y(j)=-b1y(i,j)-b3y(i,j)                                      290
          a2y(j)=b0+b2(i,j)+2*b3y(i,j)
          a3y(j)=b1y(i,j)-b3y(i,j)
          ry(j)=ry0(i,j)
35       continue
        ry(2)=ry(2)-a1y(2)*c(i,1)
        ry(ne)=ry(ne)-a3y(ne)*c(i,nn)

        do 40 j=2,ne
          c(i,j)=ccy(j)
40       continue                                                        300

30    continue

      do 240 j=2,ne
240      ry(j)=drr1(j)*de*(4.*c(2,j)-c(3,j))

      ry(2)=ry(2)-a1y0(2)*c(1,1)
      ry(ne)=ry(ne)-a3y0(ne)*c(1,nn)
      call solve(a1y0,a3y0,a2y0,ry,nn,ccy)
```

```
                                                                      310
      do 205 j=2,ne
        c(1,j)=ccy(j)
205    continue

      do 245 i=2,nxi
245      rx(i)=2.*dtt1(i)*dxi*(4.*c(i,2)-c(i,3))

      rx(2)=rx(2)-ax1r(2)*c(1,1)
      call solve(ax1r,ax3r,ax2r,rx,mm,ccx)
                                                                      320
      do 206 i=2,nxi
        c(i,1)=ccx(i)
206    continue

      do 246 i=2,nxi
246      rx(i)=2.*dttnn(i)*dxi*(4.*c(i,ne)-c(i,ne-1))

      rx(2)=rx(2)-ax1l(2)*c(1,nn)
      call solve(ax1l,ax3l,ax2l,rx,mm,ccx)
                                                                      330
      do 207 i=2,nxi
        c(i,nn)=ccx(i)
207    continue

      c(1,1)=(4.*c(2,1)-c(3,1))/3.
      c(1,nn)=(4.*c(2,nn)-c(3,nn))/3.
      vol=0.

      do 50 i=1,nxi
        ds=dxi*de*(PI*(rr(i)+rr(i+1)))**2/2.                          340
      do 50 j=1,ne
50       vol=vol+ds*0.25*(c(i,j)+c(i,j+1)+c(i+1,j)+c(i+1,j+1))

      if (mod(k,100).eq.0) then
        write(*,*)k,vol/vol0
```

```
        write(32,*)k,vol/vol0
      endif

      if(float(k).eq.float(nt)/4.) then
        do 360 i=1,mm                                              350
        do 360 j=1,nn
360         c5(i,j)=c(i,j)
      end if

      if(float(k).eq.float(nt)/2.) then
        do 370 i=1,mm
        do 370 j=1,nn
370      c10(i,j)=c(i,j)
      end if
                                                                   360
      if(float(k).eq.float(nt)*.75) then
        do 380 i=1,mm
        do 380 j=1,nn
380         c15(i,j)=c(i,j)
      endif

100   continue

      open(13,file='final.out',status='unknown')
      write(12,*)'title=" concentration"'                          370
      write(12,*)'variables="x","y","c1","c2","c3"'
      write(12,*)'zone i=',nn,', j=',mm,', f=point'
      write(13,*)'title=" concentration"'
      write(13,*)'variables="x","y","c4"'
      write(13,*)'zone i=',nn,', j=',mm,', f=point'

      do 400 i=1,mm
        do 400 j=1,nn
          write(13,1000)xx(i,j),yy(i,j),c(i,j)
400   write(12,3000)xx(i,j),yy(i,j),c5(i,j),c10(i,j),c15(i,j)      380
2000  format(1x,6f11.5)
```

```
      close(12)
      close(13)
      close(32)

      end

c---------Solution for tridiagonal system-----------------
                                                                      390
      subroutine solve(b,a,d,r,m,cc)

      real a(m),b(m),d(m),cc(m),r(m),diag(1000)

      do 1 j1=2,m-1
        diag(j1)=d(j1)
1     continue

      do 2 j1=3,m-1
2       diag(j1)=diag(j1)-b(j1)*a(j1-1)/diag(j1-1)                    400

      do 3 j1=3,m-1
3       r(j1)=r(j1)-b(j1)*r(j1-1)/diag(j1-1)

      cc(m-1)=r(m-1)/diag(m-1)

      do 4 j1=m-2,2,-1
        cc(j1)=(r(j1)-a(j1)*cc(j1+1))/diag(j1)
4     continue
                                                                      410
      return
      end

c---------End of Code-------------------------------------
```

Appendix B

Proof of the uniqueness

Consider a two dimensional Poisson equation

$$\nabla^2\zeta(x,y) = f(x,y), \tag{II.2.1}$$

with a Neumann boundary condition

$$\frac{\partial\zeta}{\partial n} = g(x,y), \quad \text{on the boundary, B,} \tag{II.2.2}$$

and a mass constraint

$$\iint_S \zeta dxdy = C, \tag{II.2.3}$$

where f and g are given functions and C is a constant.

Let us show that this equation set has a unique solution. Assume that $\zeta_1(x,y)$ and $\zeta_2(x,y)$ are two solutions of the set so that

$$\nabla^2\zeta_1(x,y) = f(x,y), \tag{II.2.4}$$

$$\frac{\partial\zeta_1}{\partial n} = g(x,y), \quad \text{on B,} \tag{II.2.5}$$

$$\iint_S \zeta_1 dxdy = C, \tag{II.2.6}$$

and

$$\nabla^2\zeta_2(x,y) = f(x,y), \tag{II.2.7}$$

$$\frac{\partial \zeta_2}{\partial n} = g(x,y), \quad \text{on B,} \tag{II.2.8}$$

$$\iint_S \zeta_2 dxdy = C. \tag{II.2.9}$$

Now since both ζ_1 and ζ_2 are arbitrary solutions, we can show the uniqueness of solution as long as ζ_1 is shown to be equal to ζ_2. The diffence between the equation set for ζ_2 and that for ζ_1 gives

$$\nabla^2(\zeta_1 - \zeta_2) = 0, \tag{II.2.10}$$

$$\frac{\partial(\zeta_1 - \zeta_2)}{\partial n} = 0, \quad \text{on B,} \tag{II.2.11}$$

$$\iint_S (\zeta_1 - \zeta_2) dxdy = 0. \tag{II.2.12}$$

This is simply a set of equation governing the steady distribution of any diffusive quantity with no flux across the boundary of the domain. No gradient of $(\zeta_1 - \zeta_2)$ is allowed to exist anywhere. The only solution for (II.2.10) and (II.2.11) is

$$\zeta_1 - \zeta_2 = C' = \text{const.} \tag{II.2.13}$$

With (II.2.12) $C' = 0$. Thus,

$$\zeta_1 = \zeta_2. \tag{II.2.14}$$

Uniqueness of the solution is proved.

Appendix C

Bibliography

Bibliography

[1] AWAJI, T., IMASATO, N. AND KUNISHI, H. (1980) Tidal exchange through a strait: A numerical experiment using a simple model basin. *J. Phys. Oceanogr.* **10**, 1499-1508.

[2] AWAJI, T. (1982) Water mixing in a tidal current and the effect of turbulence on tidal exchange through a strait. *J. Physical Oceanography* **12**, 501-514.

[3] BAGNOLD, R.A. (1951) The movement of a cohesionless granular bed by fluid flow over it. *Brit. J. Applied Physics* **2**, 29.

[4] BOWDEN, K.F. (1965) Horizontal mixing in the sea due to a shearing current. *J. Fluid Mech.* **21**, 83-95.

[5] BOWDEN, K.F. (1967) Stability effects on mixing in tidal currents. *Phys. Fluids*, Suppliment, **10**, S278-S280.

[6] CARTER, H. H. AND OKUBO, A. (1965) *A study of the physical processes of movement and dispersion in the Cape Kennedy area.* Chesapeake Bay Inst., Johns Hopkins Univ., Rep. Ref. 65-2, 150 pp.

[7] CHIAN, C. (1993) *Dispersion of Heavy Particles in Water Waves.* MIT thesis.

[8] CSANADY, G. T. (1973) *Turbulent Diffusion in the Environment.* D. Reidel, Dordrecht, Holland.

[9] CSANADY, G.T. (1982) *Circulation in the Coastal Ocean.* D. Reidel, Dordrecht, Holland.

[10] FANG, G. AND ICHIYE, T. (1983) One the vertical structure of tidal currents in a homogeneous sea. *Geophys. J. R. astr. Soc.* **73**, 65-82.

[11] FUKUOKA, S. (1974) A laboratory study on longitudinal dispersion in alternating shear flows. *Res. Bull.* **No. 112**, Dept. of Eng., James Cook Univ. of North Queensland, Australia.

[12] GEYER, W.R. AND SIGNELL, R. P. (1992) A reassessment of the role of tidal dispersion in estuaries and Bays. *Estuaries* **15**, No. 2, 97-108.

[13] HOLLY, E.R. AND HARLEMAN, D.R.F. (1965) Dispersion of pollutants in estuary type flows. *MIT Hydrodyn. Lab. Rep. No. 74*, 202 pp.

[14] HUNT, J.N. AND JOHNS, B. (1963) Currents induced by tides and gravity waves. *Tellus* **15**, 4.

[15] KRONE, R.B. (1962). Flume studies of the transport of sediment in estuarial shoaling processes, 110 pp, Univ. of Calif. Hydraul. Eng. and Sanitary Eng. Res. Lab, Berkeley, Calif.

[16] KRUPITSKY, A. AND CANE, M.A. (1997) A two-layer wind-driven ocean model in a multiply connected domain with bottom topography. *J. Phys. Oceanography* **27** No.11, 2395-2404.

[17] KUNDU, P.K., BLANTON, J.O. AND JANOPAUL, M.M. (1981) Analysis of current observations on the Georgia shelf. *Journal of Physical Oceanography* **11**, No.8, 1139-1149

[18] LAMOURE, J. AND MEI, C.C. (1977) Effects of horizontally two-dimensional bodies on the mass transport near the sea bottom. *J. Fluid Mech.* **83**, 415-431.

[19] LEE, K.K. AND LIGGETT, J.A. (1970) Computation for circulation in stratified lakes. *J. Hydraulics Division, Proceedings of ASCE* **96** No. HY10, 2089-2112.

[20] LIGGETT, J.A. AND HADJITHEODOROU, C. (1969) Circulation in shallow homogeneous lakes. *J. Hydraulics Division, Proceedings of ASCE* **95** No. HY2, 609-620.

[21] LIGGETT, J.A. (1969) Unsteady circulation in shallow, homogeneous lakes. *J. Hydraulics Division, Proceedings of ASCE* **95** No. HY4, 1273-1288.

[22] LUMLEY, J.L. (1978) Two-phase and non-Newtonian flows. in *Turbulence* (Bradshaw, P. ed.), Springer-Verlag, Berlin. 289-324.

[23] MEI, C. C. (1989) *The Applied Dynamics of Ocean Surface Waves.* World Scientific.

[24] MEI, C. C. AND CHIAN, C. (1994) Dispersion of small suspended particles in a wave boundary layer. *J. Phy. Ocean.* **24**, 2479-2495.

[25] MEI, C.C., FAN, S. J. AND JIN, K. R. (1997) Resuspension and transport of fine sediments by waves. *J. Geophy. Res.* **102** No. C7, 15807-15821.

[26] MEI, C.C., CHIAN, C. AND YE, F. (1998) Transport and resuspension of fine particles in a tidal boundary layer near a small peninsula. *J. Physical Oceanography* Submitted.

[27] OKUBO, A. (1967) The effect of shear in an oscillatory current on horizontal diffusion from an instantaneous source. *Int. J. Oceanol. Limnol.* **1**, 194-204.

[28] OKUBO, A. (1971) Oceanic diffusion diagrams. *Deep-Sea Res.* **18**, 789-802.

[29] PATHENIADES, E. (1965) Erosion and deposition of cohesive soils. *J. Hydraul. Div. Amer. Soc. Civ., Engrs. 91* (HY1), 105-139.

[30] PEDLOSKY, J. (1979) *Geophysical Fluid Dynamics.* Springer-Verlag New York Inc.

[31] SHENG, Y.P. AND CHEN, X.J. (1991) *Lake Okeechobee Phosphorus Dynamics Study: a Three Dimensional Numerical Model of Hydrodynamics, Sediment*

Transport, and Phosphorus Dynamics: Theory, Model Development, and Documentation.

[32] SIGNELL, R.P. AND GEYER, W.R. (1991) Transient Eddy Formation Around peninsulas. *J. Geophysical Research* **96**, No. C2, 2561-2575.

[33] TAYLOR, G.I. Dispersion of solute matter in solvent flowing slowly through a tube. *Proc. R. Soc. London* **A29** 186-203.

[34] VAN RIJN, L.C. (1994). *Principles of Sediment Transport in Rivers, Estuaries, and Coastal Seas*, Aqua Publ,. Amsterdam.

[35] WELANDER, P. (1957) Wind action on a shallow sea: some generalizations fo Ekman's theory. *Tellus* **9**, No. 1, 45-52.

[36] WELANDER, P. (1966) A two-layer frictional model of wind-driven motion in a rectangular oceanic basin. *Tellus* **18** 54-62.

[37] WELANDER, P. (1968) Wind-driven circulation in one- and two-layer oceans of variable depth. *Tellus* **20** 1-15.

[38] YASUDA, H. (1989) Longitudinal dispersion of suspended particles in oscillatory currents. *J. Marine Res.* **47**, 153-168.

[39] YOUNG, W.R, RHINES, P.B., AND GARRETT, C.J.R. (1982) Shear-flow dispersion, internal waves and horizontal mixing in the ocean. *J. Physical Oceanography* **12**, 515-527.

[40] YU, K. H. (1993) Preliminary study for the planning of Zhongshan Harbor, Jian Su Province. (in Chinese), *Internal Rep. 9406*, Rivers and Harbors Res. Inst., Nanjing, China.

[41] ZIMMERMAN, J.T.F. (1976) Mixing and flushing of tidal embayments in the western Dutch Wadden Sea. Part I: Distribution of salinity and calculation of

mixing time scales. Part II: analysis of mixing processes *Netherlands Journal of Sea Research* **10** (2), 149-191 (part I); 399-435 (Part II).

[42] ZIMMERMAN, J.T.F. (1977) Dispersion by tide-induced residual current vortices. in *Hydrodynamics in Estuaries and Fjords*, Elsevier Oceanography Series, 23 (Nihoul, J.C.J. ed.), Elsevier, Amsterdam.

[43] ZIMMERMAN, J. T. F. (1986) The tidal whirlpool: a review of horizontal dispersion by tidal and residual currents. *Netherlands J of Sea Res* **20** (2/3), 133-154.